

Srdjan Kisin  
Срђан Кисин

**Adhesion changes at metal–polymer interfaces:**  
Study of the copper–(acrylonitrile–butadiene–styrene) system

**Cover page:** The cover and the back side of the book show the front and the rear view of an equilibrium conformation of the SAN molecule, represented by its van der Waals volume, on the copper surface. Designed by Srdjan Kisin and Paul Verspaget.

**Adhesion changes at metal–polymer interfaces:  
Study of the copper–(acrylonitrile–butadiene–styrene) system**

**PROEFSCHRIFT**

ter verkrijging van de graad van doctor aan de  
Technische Universiteit Eindhoven, op gezag van de  
Rector Magnificus, prof.dr.ir. C.J. van Duijn, voor een  
commissie aangewezen door het College voor Promoties

in het openbaar te verdedigen op  
maandag 12 februari 2007 om 16.00 uur

door

Srdjan Kisin

geboren te Sombor, Servië

Dit proefschrift is goedgekeurd door de promotor:

prof.dr. G. de With

Copromotor:

dr.ir. P.G.Th. van der Varst

Kisin, Srdjan

A catalogue record is available from the Library Eindhoven University of Technology

ISBN-10: 90-386-2699-1

ISBN-13: 978-90-386-2699-4

Copyright © 2006 by Srdjan Kisin

The work described in this thesis has been carried out at the Laboratory for Materials and Interface Chemistry (SMG) within the Department of Chemical Engineering and Chemistry, Eindhoven University of Technology, The Netherlands. The research has been financially supported by the Innovation Oriented research Program Surface Technology (IOP-OT) as a part of project #IOT01008.

# **CONTENTS**

## **CHAPTER 1**

<b>THE OPENING.....</b>	<b>1</b>
1.1 In the beginning there was a word .....	1
1.2 General considerations on adhesion.....	2
1.3 Work of adhesion and mechanical adhesion tests.....	3
1.4 A challenge: Bringing polymers and metals together .....	5
1.5 Research aim, the model system and the outline of the thesis .....	6
References .....	8

## **CHAPTER 2**

<b>QUANTIFYING ADHESION .....</b>	<b>11</b>
2.1 Peel test .....	12
2.1.1 Peel test: Hardware details .....	12
2.1.2 Peel test: Theory and the energy balance .....	14
2.1.3 Peel test: Calculating the adhesive energy .....	17
2.2 Pull-off test .....	19
2.3 Adhesion on a molecular level: Molecular dynamics simulations.....	20
2.3.1 Energetic analysis of contact between a single polymer molecule and a copper surface .....	21
References .....	26

## **CHAPTER 3**

<b>SAMPLES AND SAMPLE PREPARATION .....</b>	<b>27</b>
3.1 Samples: The polymer substrate .....	28
3.2 Samples: The metallic film .....	31
3.3 Samples: Reproducibility of the preparation procedure.....	35
3.4 Delamination speed and coating thickness dependence of the adhesive energy.....	37
References .....	39

## **CHAPTER 4**

<b>INFLUENCE OF WET CHEMICAL PROCESSING ON THE ADHESIVE ENERGY AND THE INTERFACE STRUCTURE .....</b>	<b>41</b>
4.1 Introduction .....	42
4.2 Experimental .....	43
4.2.1 Peel test, adhesive energy calculations and film mechanical properties .....	43
4.2.2 Water content in the sample: Consequence of the galvanic deposition .....	46
4.2.3 Microscopy and contact angle measurements .....	46

4.3	Results and discussion.....	47
4.4	Conclusions .....	55
	References .....	56

## CHAPTER 5

### **CHEMICAL CHANGES OF THE ABS NEAR THE INTERFACE WITH COPPER..... 57**

5.1	Introduction .....	58
5.2	Experimental .....	59
5.2.1	Contact angle, infrared and SFM measurements.....	59
5.3	Results.....	60
5.4	Discussion .....	64
5.5	Proposition for of the ABS–copper interface “life line” .....	67
5.6	Conclusions .....	68
	References .....	70

## CHAPTER 6

### **ADHESION ON A MOLECULAR LEVEL: MOLECULAR DYNAMICS CALCULATIONS ..... 71**

6.1	Introduction .....	72
6.2	Molecular dynamics calculations .....	73
6.2.1	Description of the metal–polymer simulations .....	73
6.2.2	Calculations of interaction energies and work of adhesion.....	76
6.3	Results and discussion.....	78
6.4	Conclusions .....	88
	References .....	89

## CHAPTER 7

### **CORRELATING MD CALCULATIONS WITH PEEL TEST MEASUREMENTS ..... 91**

7.1	Introduction .....	92
7.2	Influence of the energy dissipation within the substrate and the substrate roughness on the adhesive energy calculated from the peel test.....	93
7.2.1	Plastic dissipation within the substrate.....	93
7.2.2	Visco-elastic dissipation within the substrate .....	93
7.2.3	Influence of the substrate roughness on the adhesive energy .....	96
7.2.4	Influence of the energy dissipation within the substrate and the substrate roughness on the adhesive energy calculated from the peel test: Conclusion .....	97
7.3	Sensitivity of the adhesive energy calculations to errors in determination of the mechanical properties of the copper film .....	97
7.4	Relation between work of adhesion and adhesive energy in the presence of plastic dissipation at the crack tip .....	99

7.5	Work of adhesion: Calculations from the MD results using a mixing rule .....	101
7.6	Discussion .....	104
7.7	Conclusions.....	106
	References .....	107
 <b>CHAPTER 8</b>		
<b>MANIPULATING THE ADHESION:</b> <b>BLOCK COPOLYMERS</b>		
<b>AS ADHESION PROMOTING LINKERS.....</b>		<b>109</b>
8.1	Introduction .....	110
8.2	Experimental procedures.....	111
8.2.1	Model copolymer synthesis and molecular characterization.....	112
8.2.1.1	Materials.....	112
8.2.2.2	Synthesis and characterization .....	113
8.2.2	Polymer film formation by spin-coating and application of block copolymer latex .....	115
8.3	Changes in adhesion.....	115
8.3.1	Influence of the solvent on the ABS surface and copper-to-ABS adhesion .....	115
8.3.2	Influence of the SAN and SMAh copolymers on the copper-to-ABS adhesion .....	118
8.3.3	Influence of the solvent borne SAN- <i>b</i> -SMAh block copolymers on the copper-to-ABS adhesion .....	119
8.3.4	Influence of the water borne latexes on copper-to-ABS adhesion.....	120
8.4	Conclusions.....	122
	References .....	123
 <b>CHAPTER 9</b>		
<b>EPILOGUE.....</b>		<b>125</b>
9.1	The lessons learned .....	125
9.2	Recommendations .....	126
<b>SUMMARY .....</b>		<b>127</b>
<b>SAMENVATTING.....</b>		<b>129</b>
<b>CURRICULUM VITAE .....</b>		<b>131</b>
<b>ACKNOWLEDGEMENTS.....</b>		<b>132</b>



# CHAPTER 1

## THE OPENING

### 1.1 In the beginning there was a word

Since the main topic of this thesis will be adhesion, logic dictates to start from explaining the origin of the word adhesion, its importation to the English language and the definition associated with it today.

As many of the words in use today, adhesion stems from Latin, originating from the word *adhaerere*, or “to stick to”<sup>[1,2]</sup>. If one is to be more precise, it has to be said that it is a compound of two words, *ad* and *haerere* with a combined meaning explained above. It was first used by Cicero in a phrase “*haerere in equo*” translating to “to stick to a horse”. The hint of scientific use comes from Lucretius (in “*De rerum natura*”) who used the term to describe iron sticking to a magnet. Finally, in 1661 Robert Boyle<sup>[3]</sup> (in “*On the spring and weight of air*”) introduced the term adhesion to modern science.

However, long before the language developed to the form known today, the phenomenon referred to as the adhesion was playing an important role. An important role in the development of life, in fighting infections, in food absorption and in helping a fly boldly defy gravity. On the other side, the lack of any stickiness kept the lotus leaves clean for centuries and is, more recently, sparing us of scraping the eggs off the pan.

Today, adhesion is defined by ASTM D 907 as “the state in which two surfaces are held together by interfacial forces which may consist of valence forces or interlocking forces or both”. Online a different, much simpler definition can be found: “Adhesion is the molecular attraction exerted between bodies in contact”<sup>[4]</sup>.

One main conclusion can be drawn. The adhesion refers to two bodies, made of different materials holding together by a range of different forces acting across their contact area on a molecular level. So, the (energetic) state of the two surfaces brought into contact will determine the magnitude of adhesion.

## 1.2 General considerations on adhesion

The energetic state of a surface is quantified by surface energy. While the surfaces of inorganic solids such as metals exhibit a high surface energy, polymer surfaces show a much lower surface energy. This brings us to the important empirical rule of adhesion: the adhesion between two surfaces will be high if they show similar surface energies and low if there is a large discrepancy between the two.

Besides the surface energies of the bodies in contact, the one other factor expected to influence the adhesion of two different surfaces is the roughness of the contact between the two. The influence of the roughness can be viewed in two different, opposite ways. On one side it is believed that roughening of one of the surfaces in contact will lead to a larger contact area and to a mechanical interlocking of the materials thus leading to a better adhesion<sup>[5,6]</sup>. This is especially the case when a liquid adhesive is applied to a solid surface. On the other side, it seems naive to believe that the roughness of the interface favors the adhesion<sup>[7]</sup>. If two atomically smooth sheets of mica are brought into contact they form a joint almost as strong as the mica itself<sup>[8]</sup>. The importance of the contact on the atomic or molecular scale and the detrimental influence of surface roughness on adhesion is very clear from this example. A close, intimate contact between the materials is an important condition for good adhesion, but is not a guarantee for it. If one takes a soft rubber ball and presses it against a rough surface, the contact along the complete surface on a molecular level will be established, but once the pressure is released the joint is broken<sup>[9]</sup>. Basically, the elastically stored energy in the ball is sufficient to disrupt the bonds as soon as the pressure is gone. The solution: avoid joints with internal stresses in either of the materials, or deform plastically both of the materials upon pressing them together.

The considerations about the influence of chemical nature (surface energy) and the roughness of the surfaces in contact is a good example of the multi-component nature of the problem of adhesion<sup>[8]</sup>. The various mechanisms should be connected in a proper way depending on the material system investigated, but none of the aspects should ever be neglected or excluded.

### 1.3 Work of adhesion and mechanical adhesion tests

A thermodynamic quantity used to quantify the adhesion is the work of adhesion. The work of adhesion between two different materials A and B in contact in equilibrium in vacuum can be defined as<sup>[10,11]</sup>:

$$W_A = \gamma_A + \gamma_B - \gamma_{AB} \quad (1.1)$$

where  $W_A$  is the work of adhesion,  $\gamma_A$  and  $\gamma_B$  are surface energies of the two separate phases in equilibrium in vacuum and  $\gamma_{AB}$  is the interface energy of the two phases in contact in equilibrium. The surface energy is connected to cleavage of the monolith bulk solid and can be defined using either Gibbs or Helmholtz energies, depending on the conditions under which the cleavage was done. If cleaving was done under constant temperature and volume, the proper definition is:

$$\gamma = \frac{H - H^b}{2A} \quad (1.2)$$

where  $\gamma$  is the surface Helmholtz energy,  $H$  is the total Helmholtz energy of the system,  $H^b$  is the value the total Helmholtz energy would have if all the constituent particles were in the same state as they are in the bulk, and  $A$  is the surface area<sup>[10]</sup>. The factor 2 is present as two surfaces of identical surface areas are created as a result of the cleaving process. Having the above consideration in mind, the surface Helmholtz energy will be referred to as just the surface energy throughout the text.

When it comes to measuring the adhesion, there are more than 350 listed adhesion tests<sup>[12]</sup>. The choice of the test depends solely on the material system investigated and the structure of the sample. For example, by the use of a surface force apparatus, adhesion of soft polymer materials with transparent substrates can be investigated. If one is dealing with sputtered metallic films on ceramic substrates the scratch<sup>[13]</sup> test is suitable while for metallic films on polymer substrates the peel test<sup>[14]</sup> is a good choice. In the case of adhesion studies for metal–polymer systems, SFM measurements can be used. In this case cantilever tips, normally used in surface force microscopy are modified with the metal of interest and its interaction with a polymeric substrate is studied<sup>[15]</sup>.

Most of the mechanical adhesion tests (non-destructive and destructive) provide a largely overestimated work of adhesion due to the large energy dissipation originating in the test samples during the measurements<sup>[10]</sup>. The dissipated work is often orders of magnitude higher than the real work of adhesion, preventing any reasonably accurate estimates of the thermodynamic quantity.

Johnson, Kendall and Roberts<sup>[16]</sup> tried to develop a theory (JKR theory) which would provide the values of the work of adhesion between two bodies based on the contact area between the two once they are pressed together. The starting point was to correct Hertz's estimate of the contact area<sup>[17]</sup> taking into account the action of surface forces. However, the JKR theory was only applicable for contact between compliant materials and accounted only for short range surface forces<sup>[18]</sup>. Contact between stiff materials was not accurately predicted by the theory. Derjaguin, Mullet and Toporov<sup>[19]</sup> investigated this further and formulated a theory, the DMT theory, which proved to be valid only to calculate the work of adhesion for stiff materials in contact and accounted only for long range surface interactions<sup>[18]</sup>. The two theories were recognized as the limiting cases of the contact problems between the elastic solids and theories connecting these two limits have also been developed<sup>[18,20-22]</sup>.

During the destructive tests only the information of the behavior of the complete system is obtained and a suitable theory is needed to process the data and eliminate, as far as possible, the influence of the sample geometry, equipment etc. Possible global plastic dissipation or small scale yielding at the crack tip can lead to discrepancies between the quantities directly measured by the destructive test and the work of adhesion. The results may also depend on temperature or the rate used for delamination, especially if polymer samples are tested since they can exhibit visco-elastic deformation. In principal, one can say that the destructive mechanical tests can only provide information about the overall energy values necessary for (possible) deformation of the system tested and breaking of the interface<sup>[23]</sup>. More involved theories are necessary if the value of the work of adhesion is to be calculated from the destructive mechanical tests. However, in everyday applications of different multimaterial systems the reliability of the joint will be solely dependent on the total energy which needs to be supplied to the system prior to the joint

failure, justifying the existence and use of the mechanical tests for adhesion quantification.

## 1.4 A challenge: Bringing polymers and metals together

Having established how to quantify the adhesion and what are the problems in doing this, a material system of interest has to be chosen. The material combination has to be, both, industrially and scientifically interesting.

Metals and polymers have played an important role in the development of mankind since the beginning of life. No life is possible without the various natural polymers, DNA and proteins and metal ions play an important role in organisms as well. Metals have also influenced human development so profoundly that the two long time periods of the human development are named according to them, the Iron and the Bronze Age.

Industrially, metallized polymer films are widely used for gas barrier applications, composite and photoconductive materials, for decorative purposes, in the automotive industry, etc. But, as already established, most synthetic polymers used as commercial materials have a surface of low surface energy and as a result these materials have a low adhesion to high surface energy metallic coatings<sup>[24]</sup>. All of the above considerations make the realization and reproducibility of good adhesion of metallic coatings on polymer substrates an important industrial and scientific problem.

The interaction between a metal and a polymer strongly depends on the type of the metal and on the functional groups present in the polymer. Oxidation of polymer substrate surfaces is one of the techniques most commonly used to promote the adhesion of polymers to metals. The oxidation can be done prior to, or during the interface formation<sup>[5,25-29]</sup>. Chemical modification of the interfacial polymer chains with polar groups, like hydroxyl, carbonyl and carboxylic acid moieties<sup>[30]</sup> is also used. Plasma treatment of the metallic surfaces seems to be favourable to adhesion as well<sup>[31,32]</sup>.

Recently the use of carefully tailored block copolymers has proven to be promising for adhesion promotion between metals and polymers<sup>[33]</sup>. A microphase separating block copolymer<sup>[34,35]</sup> which is expected to demix into a block capable of strong entanglement

formation with the polymer and a block which is free for the interaction with the applied metal coating is a very good candidate for adhesion improvement<sup>[13]</sup>. The use of such molecules is further facilitated because block copolymers are easily adsorbed onto a substrate from a dilute solution at ambient temperature as a result of their high adsorption energy<sup>[34]</sup>.

## 1.5 Research aim, the model system and the outline of the thesis

The main research goal was to gain fundamental insight into the mechanisms of adhesion of two different materials and, as an application of this knowledge, to explain the findings of a related project<sup>[33]</sup> that block copolymers can be used as adhesion promoting linkers.

The chosen model system was a sputtered and galvanically strengthened copper film on acrylonitrile–butadiene–styrene (ABS) polymer substrate. ABS is a thermoplastic polymer and a physical mixture of two phases. Two distinct incompatible phases are combined within this polymer. The *poly(butadiene)* (pBd) phase is dispersed within the continuous *poly(styrene-co-acrylonitrile)* (SAN) matrix<sup>[37]</sup>. The matrix consists of two types of SAN molecules; free SAN molecules and SAN molecules grafted onto the dispersed pBd rubber particles. The grafted molecules bind the two phases together into an excellent mixture. The continuous phase has a high rigidity and chemical resistance, while the addition of pBd introduces a good impact resistance. In addition to this, ABS has a very good thermoplastic flow behavior and heat resistance. A variety of ABS materials can be obtained from different combinations of SAN and pBd<sup>[37]</sup>.

Copper is one of the most common metals plated on several substrates<sup>[38, 39 p.61]</sup>. It is used for a variety of purposes, a few being in the automotive industry, for printing boards<sup>[40]</sup> and in the semiconductor industry where it is rapidly replacing aluminum<sup>[39 p.61]</sup> which is conventionally used. By careful tuning the deposition conditions a variety of mechanical and physical properties of deposited copper films can be achieved<sup>[41]</sup>. For the specific case of plastics metallization, copper is very useful because it is to some extent capable of absorbing the stress exerted as a result of different thermal expansion coefficients<sup>[39 p.61]</sup>.

The main adhesion quantification technique used was the 90° peel test. The peel test is one of the most extensively used adhesion quantification techniques<sup>[14]</sup>.

To get the estimates of the work of adhesion as opposed to the values measured by the peel test, molecular dynamics simulations using classical force fields will be used.

In Chapter 2 the possibilities to experimentally and theoretically quantify the adhesion will be discussed in more detail and the basics of data analysis for the peel test experiments shall be presented. The sample preparation and properties will be elaborately described in Chapter 3. In Chapter 4 the increase in adhesion as a result of the sample storage will be discussed and the structural explanation for such a behavior will be offered, while in Chapter 5 a chemical explanation of the same phenomenon will be provided. Chapter 6 aims at developing a relatively simple way for adhesion quantification using molecular dynamics. On the qualitative level the results from previous chapters will be confirmed and some ideas for adhesion manipulation are tested. As a significant gap between the peel test measured adhesive energy and the work of adhesion calculated in Chapter 6 is found, Chapter 7 presents an attempt to bridge this gap. In Chapter 8 the adhesion promoting capacity of block copolymers as linkers between the ABS substrate and the copper coating will be considered. Finally in Chapter 9, as an epilogue, the presented work will be looked onto and recommendations for further research opportunities in the field of adhesion of metals to polymers will be given.

## References

- [1] C. T. Onions, *The Oxford Dictionary of English Etymology*, Clarendon Press, Oxford, **1966**, p. 12.
- [2] D. E. Packham, *Handbook of Adhesion*, Longman Scientific & Technical, Harlow, **1992**, p. 18.
- [3] *Oxford English Dictionary: Compact Edition*, Oxford University Press, Oxford, **1980**, p. 109.
- [4] <http://en.wikipedia.org/wiki/Adhesion> accessed 25–09–2006.
- [5] J. Cognard, *C. R. Chimie*, **2006**, *9*, 13–24.
- [6] W. Brockman, *J. Adhes.* **1989**, *29*, 53–61.
- [7] K. W. Allen, *Int. J. Adhes. Adhes.* **2003**, *23*, 87–93.
- [8] K. W. Allen, *J. Adhes.* **1987**, *21*, 261–277.
- [9] N. A. de Bruyne, *Nature*, **1957**, *180*, 262–265.
- [10] D. E. Packham, *Int. J. Adhes. Adhes.* **1996**, *16*, 121–128.
- [11] D. E. Packham, *Int. J. Adhes. Adhes.* **2003**, *23*, 437–448.
- [12] K. L. Mittal, *Adhesion measurement of films and coatings*, VSP, Utrecht, **1995**, p. 5
- [13] P. Benjamin, C. Weaver, *Proc. Roy. Soc. A*, **1961**, *261*, 516–531.
- [14] A. J. Kinloch, C. C. Lau, J. G. Williams, *Int. J. Fracture*, **1994**, *66*, 45–70.
- [15] J. Božović Vukić, S. Hoeppener, D. A. Kozodaev, S. Kisin, B. Klumperman, U. S. Schubert, G. de With, C. E. Koning, *ChemPhysChem*, **2006**, *7*, 1912–1916.
- [16] K. L. Johnson, K. Kendall, A. D. Roberts, *Proc. Roy. Soc. A*, **1971**, *324*, 301–313.
- [17] H. Hertz, *Miscellaneous papers*, Macmillan, London **1896**, p. 146.
- [18] R. W. Carpic, D. F. Ogletree, M. Salmeron, *J. Colloid Interface Sci.* **1999**, *211*, 395–400.
- [19] B. V. Derjaugin, V. M. Muller, Y. P. Toporov, *J. Colloid Interface Sci.* **1975**, *53*, 314–326.
- [20] D. Maugis, *J. Colloid Interface Sci.* **1992**, *150*, 243–269.
- [21] O. Piétrement M. Tronoy, *J. Colloid Interface Sci.* **2000**, *226*, 166–171.
- [22] V. Muller, V. S. Yuschenko, B. V. Derjaugin, *J. Colloid Interface Sci.* **1980**, *77*, 91–101.
- [23] D. E. Packham, *Handbook of Adhesion*, Longman, Harlow, **1992**, p. 378.
- [24] B. Rånby, *Int. J. Adhes. Adhes.* **1999**, *19*, 337–343.
- [25] J. Y. Song, J. Yu J. *Acta Mater.* **2002**, *50*, 3985–3994.
- [26] S. S. Pesetskii, B. Jurkowski, A. I. Kuzakov, *Int. J. Adhes. Adhes.* **1998**, *18*, 351–358.
- [27] M. Kalnins, J. Malers, *J. Adhes.* **1995**, *50*, 83–102.
- [28] S. Siau, A. Vervaet, E. Schacht, S. Degrande, K. Callewaert, A. van Calster, *J. Electrochem. Soc.* **2005**, *152*, D136–D150.
- [29] J. L. Jordan, P. N. Sandra, J. F. Morar, C. A. Kovac, F. J. Himpsel, R. A. Pollak, *J. Vac. Sci. Technol. A*, **1986**, *4*, 1046–1048.

- [30] C. Seidel, H. Kopf, B. Gotsmann, T. Vieth, H. Fuchs, K. Reihs, *Appl. Surf. Sci.* **1999**, *150*, 19–33.
- [31] M. Mantel, J. P. Whightman, *Surf. Interface Anal.* **1994**, *21*, 595–605.
- [32] J. Ghädhe, *J. Adhes. Sci. Technol.* **1992**, *6*, 569–586.
- [33] J. Božović Vukić, *Block copolymers for adhesion improvement synthesized via RAFT-mediated polymerization*, PhD Thesis, Technische Universiteit Eindhoven, Eindhoven, **2006**.
- [34] F. S. Bates, *Science* **1991**, *251*, 898–905.
- [35] A. Noro, M. Iinuma, J. Suzuki, A. Takano, Y. Matsushita, *Macromolecules* **2004**, *37*, 3804–3808.
- [36] G. J. Fleer, M. A. Cohen Stuart, J. M. H. M. Scheutjens, T. Cosgrove, B. Vincent, *Polymers at Interfaces*, Chapman&Hall, London, **1993**, p. 30.
- [37] D. M. Kulich J. E. Pace, L. W. Fritch Jr. A. Brisimitzakis, *ABS Resins*, in R. E. Kirk, D. F. Othmer (Eds.) *Encyclopedia of Chemical Technology*, vol. 1, John Wiley & Sons, New York, **1993**, 391–411.
- [38] L. W. Flott, *Met. Finish.* **1996**, *94*, 55–58.
- [39] M. Schlesinger, M. Paunovic, *Modern electroplating*, Wiley-Interscience, New York, **2000**.
- [40] R. Sard, in M. V. Bever (Ed.) *Encyclopedia of Materials Science and Engineering*, vol. 2, Wiley, New York, **1986**, p. 1423.
- [41] W. H. Safranek, *The properties of electrodeposited metals and alloys: a handbook*, American Elsevier, Orlando, **1974**, p. 91.



## **CHAPTER 2**

### **QUANTIFYING ADHESION**

**Summary:** In this chapter the tools to quantify the adhesive energy will be addressed. The 90° peel test as the main tool for adhesion quantification will be described and main assumptions, experimental requirements and the theory behind the energy balance of the peel test used for data processing and the adhesive energy calculations will be discussed. A short look at the pull-off test design and possibilities will be given. Finally, at the end of the chapter, the basic ideas for the use of molecular dynamics (MD) calculations to calculate the thermodynamic work of adhesion will be given.

## 2.1 Peel test

Among more than 350 listed adhesion tests<sup>[1]</sup>, the 90° peel test was chosen as the main mechanical test tool to measure the adhesion experimentally because it has a number of advantages in comparison with the other adhesion quantification techniques. Since the basic idea is peeling of the film from the substrate over a large surface area, insight into the width averaged adhesive energy over the complete peeled length is achieved in contrast to more localized techniques such as scanning force microscopy measurements<sup>[2]</sup> where measurements are made on a spot or the pull-off test where an average adhesion value is measured over a relatively small surface area. In addition, no special preparation of the sample before testing and after the metallization is needed. This will allow us to monitor the changes of the adhesion in time, i.e. from freshly made samples to significantly aged ones. The peel test can also provide data about the influence of the environmental parameters (relative humidity, temperature, etc) on the adhesion.

### 2.1.1 Peel test: Hardware details

A custom made 90° peel testing device was used for all the measurements presented. The instrument has a motor–driven load–measuring device mounted and moving on a rail forming a 45° angle with respect to the substrate, ensuring that the macroscopic 90° peeling angle is maintained during the measurement (Figure 2.1a). Between motor and the load cell is a gear section. Depending on the expected force necessary for delamination, three different load cells are available: 0–0.5 N, 0–5 N and 0–50 N. Each force point output is an average of 100 subsequent measurements which are taken every millisecond. Force accuracy is better than 0.1 mN, while the motor cross-head speed ranges from 0.01 to 60 mm/min and it is related to the movement of the load cell along the 45° rail. The actual speed with which the crack is propagating, the delamination speed, is thus a factor of  $\frac{1}{2} \sqrt{2}$  lower than that of the motor. Play of the gear section is less than 0.1 μm.

The device is equipped with a camera which is moving in a synchronized way with the movement of the motor peeling the film off from the substrate (Figure 2.1b, part 4). Using this option, snapshots of the delaminating metallic foil can be taken at different moments in time, or a movie of a complete delamination process can be made.

In order to initiate an interfacial crack and to be able to start the peeling, a “V” shaped notch (Figure 2.1c) is made in the back side of the substrate prior to the copper coating deposition. After the coating has been deposited the sample is fixed in the frame of the device, the notch is cooled down with liquid nitrogen and broken (Figure 2.1d). Upon breaking, one end of the film (and the part of the substrate visible in the clamp in Figure 2.1d) is attached to the load cell and peeling is started.

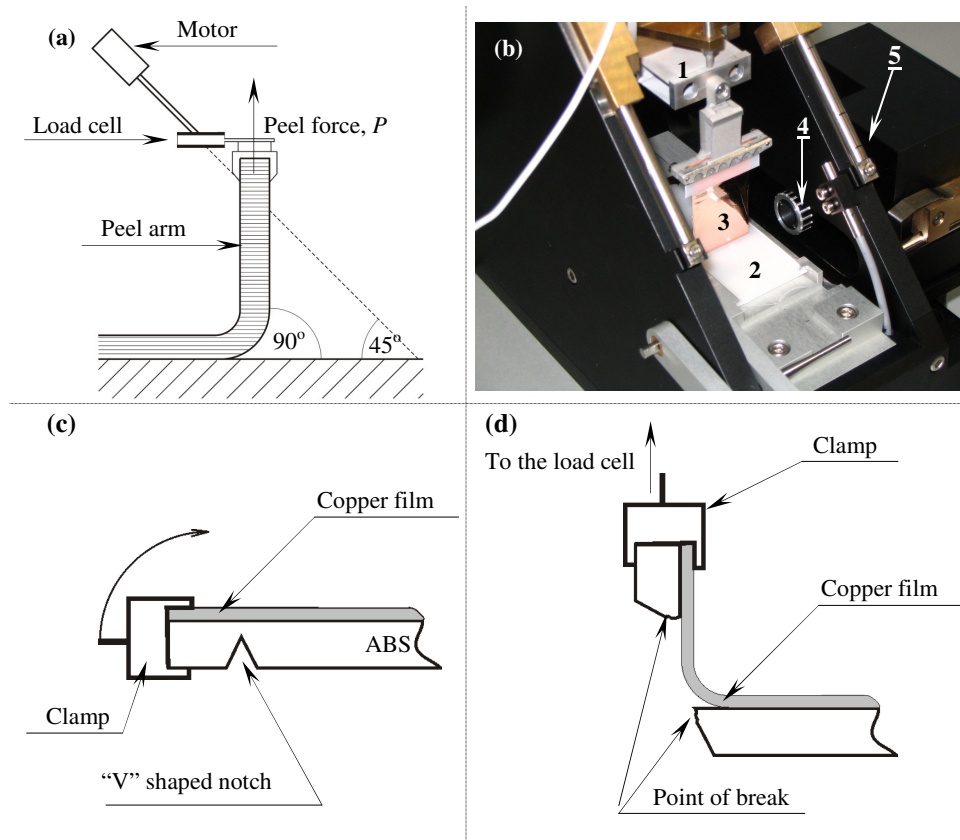


**Figure 2.1.** a) Scheme of the peel–testing device. The dashed line indicates the path traversed by the load cell assembly. b) Photo of a delaminating copper foil in the peel testing device (1-load cell; 2-substrate; 3-copper film; 4-camera; 5-45° rail). c) and d) Scheme of the peel test specimen before and after the breaking of the notch.

### 2.1.2 Peel test: Theory and the energy balance

The value of the peel force necessary for delaminating the coating from the substrate depends on the adhesion strength, the mechanical properties and the thickness of the film, the macroscopic peeling angle  $\theta$  (Figure 2.2), etc. A crack is assumed to have propagated over a sufficient period of time so that steady-state conditions prevail in the vicinity of the advancing crack tip<sup>[3-6]</sup>. For a steady-state to prevail the peel bend and the peel force should remain constant and, more importantly, the microscopic peeling angle  $\theta_0$  (Figure 2.2) should not change during the experiment. The reason is that the peel bend and the microscopic peeling angle have been identified as the two parameters that strongly influence the numerical accuracy of any analytical simulation of the peel test<sup>[6,7]</sup>.

Let us now consider an infinitesimal crack advance,  $dl$ , during the peeling of a sample at angle  $\theta$  under the steady-state delamination caused by the force  $P$  applied at the top of the film (Figure 2.2). Due to the crack advance, the point of the force application will move over an infinitesimal distance  $dx$  in the direction of the applied force. If the elongation of the peel arm is neglected,  $dx$  and  $dl$  are related by:

$$dx = (1 - \cos \theta)dl \quad (2.1)$$

Accordingly, the work supplied to the system is:

$$P dx = (1 - \cos \theta)P dl \quad (2.2)$$

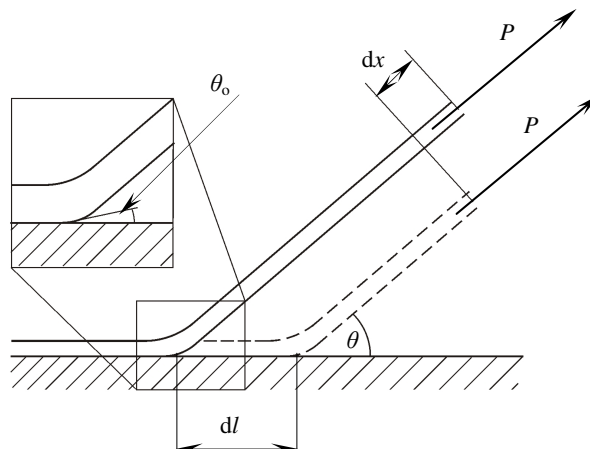


**Figure 2.2.** Schematic representation of crack advance, macroscopic peeling angle  $\theta$  and microscopic angle  $\theta_0$  in the generalized peel test experiment.

During crack advance, an infinitesimal surface area has been created and the total energy supply per unit area of crack advance for this process  $G_{\text{tot}}$  can be expressed as the supplied work divided by the width of the delaminating film:

$$G_{\text{tot}} = (1 - \cos \theta) \frac{P}{b} \quad (2.3)$$

where  $b$  is the width of the peel arm. For the case of 90° peeling the Equation 2.3 simplifies to:

$$G_{\text{tot}} = \frac{P}{b} \quad (2.4)$$

The value of  $G_{\text{tot}}$  as defined by Equation 2.4 includes several energetic contributions and can mathematically be formulated as:

$$G_{\text{tot}} = G_c + G_{\text{se}} + G_{\text{db}} + G_{\text{ps}} + G_{\text{ve}} + \dots \quad (2.5)$$

where  $G_c$  is the energy contribution associated with the fracture energy of the bilayer system, henceforth referred to as the adhesive energy,  $G_{\text{se}}$  the elastically stored energy in the peel arm,  $G_{\text{db}}$  the energy dissipated for plastic deformation of the peel arm due to bending,  $G_{\text{ps}}$  the energy (possibly) plastically dissipated within the substrate,  $G_{\text{ve}}$  the energy visco-elastically dissipated within the substrate (if the substrate is a polymeric material), etc.

The value of the adhesive energy  $G_c$  is the characteristic property of each interface and can be used to compare different material systems with respect to their adhesion and as such a final aim of any theory used to process the experimentally measured data. The elastically stored energy  $G_{\text{se}}$  is usually small for a film with a relatively high modulus such as metal film or, for an inextensible film, zero<sup>[8]</sup> and is neglected in most of the energy balances of the peel test. The peel arm is usually subjected to intense bending near the crack tip which can lead to significant plastic dissipation  $G_{\text{db}}$  that cannot be neglected. Plastically dissipated energy within the substrate  $G_{\text{ps}}$ , if present, could be a non-negligible part of the energy balance and has to be taken into account. Visco-elastic deformation of the substrate is, in our case, small as compared to the total energy input and plastically dissipated energy in the bending of the peel arm and thus can be neglected (this will be proven in Chapter 7). Apart from the described global energy dissipations, small scale energy dissipation at the crack tip, i.e. plastic dissipation within

the peel arm at the crack tip, should also be taken into account in the peel test energy balance. The adhesive energy  $G_c$  is expected to be equal to the sum of the work of adhesion  $W_A$  and plastically dissipated energy at the crack tip  $G_{lp}$ :

$$G_c = W_A + G_{lp} \quad (2.6)$$

In a number of cases local plastic dissipation is supposed to be directly proportional to the adhesive energy:

$$G_{lp} = C G_c \quad (2.7)$$

where  $C$  is a proportionality constant. Combination of Equations 2.6 and 2.7 gives:

$$G_c = W_A \frac{1}{1-C} \quad (2.8)$$

In essence, this shows a linear dependence of the crack tip plasticity on the work of adhesion, which has some support<sup>[9]</sup>, but approaches describing a non-linear dependence of the adhesive energy on the work of adhesion can also be found in the literature<sup>[10-12]</sup>.

In these cases the dependence should be written as:

$$G_c = C W_A^q \quad (2.9)$$

where  $q$  is the exponent of dependence and it is usually dependent on the mechanical properties of the delaminating film such as the work hardening exponent<sup>[10-12]</sup>. A non-linear dependence will be used in Chapter 7 to calculate the adhesive energy by correcting the work of adhesion for local plastic dissipation within the metallic film at the crack tip.

From this analysis it is clear that, only if all dissipation within the material system is absent or negligible, the total energy input into the peel test can be taken as the first order estimate of the actual work of adhesion. In the case of 90° peel test this leads to:

$$W_A = \frac{P}{b} \quad (2.10)$$

In most practical situations dissipation is always present and a suitable theory is needed to deduce the value of the adhesive energy from experimentally measured data.

### 2.1.3 Peel test: Calculating the adhesive energy

To calculate the adhesive energy from the total energy input into the peel test, as defined by Equations 2.4 and 2.5, a model adopted from Georgiou et al.<sup>[5,13]</sup> was used. This model calculates  $G_{db}$  the plastically dissipated energy in the bending of the peel arm while neglecting elastic deformation of the peel arm, any dissipations within the substrate and the plastic dissipation at the crack tip.

The non-delaminated part of the metallic coating is modeled as an elastoplastic beam attached to the substrate. The interface between the two materials at the vicinity of the crack tip (point ‘O’ to ‘B’ in Figure 2.3) is modeled using a cohesive zone. The linear elastic stiffness cohesive zone was chosen for our calculations, meaning that all stresses within the cohesive zone are assumed to be linearly proportional to the displacement undergone by the beam while the effect of shear forces is neglected.

In order to calculate the plastically dissipated energy during steady-state peeling the history of a slice of infinitesimal thickness of the film material, henceforth referred to as the material element, is considered. At first the material element is sufficiently far away from the crack tip within the non-delaminated part of the coating and it is stress free (point ‘O’ in Figure 2.3). As the material element approaches the crack tip it is gradually loaded to a certain bending moment and the corresponding curvature (point ‘A’ in Figure 2.3), the bending moment and the curvature of the material element reach the maximum value at the crack tip (point ‘B’ in Figure 2.3). As the material element moves away from the crack tip, into the delaminated part of the coating, the bending moment is gradually decreased reaching a zero value at a certain distance from the crack tip (point ‘C’ in Figure 2.3). However, if the plastic deformation has taken place during bending at the crack tip, the curvature of the peel arm will not go to zero and a negative bending moment (unbending) has to act on the material to reduce the curvature to zero (point ‘D’ in Figure 2.3). Finally, more unbending occurs as the material element moves beyond point ‘D’ towards point ‘E’ in Figure 2.3.

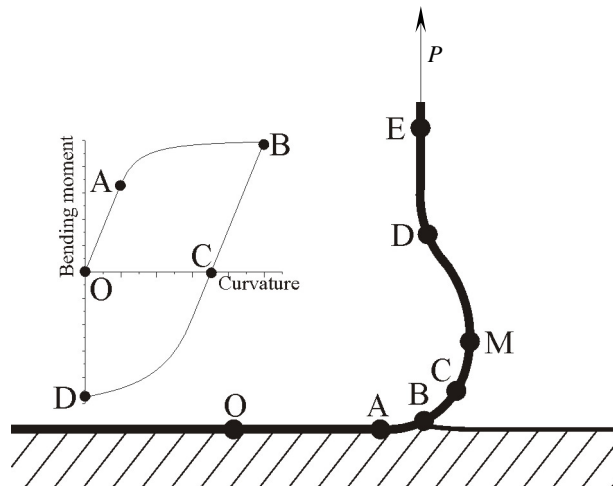


**Figure 2.3.** Schematic representation of the film delaminating under the steady-state conditions. The insert represents the corresponding moment-curvature diagram.

The model suggested by Georgiou et al.<sup>[5,13]</sup> estimates the plastically dissipated energy within the peel arm using a curvature-bending moment characteristics of a cross sectional slice of the coating material, based on power-law hardening and this model was used for adhesive energy calculations throughout the study (Figure 2.3 left). With reference to Figure 2.3 (right) during steady state peeling an arbitrary slice of the material located at ‘O’ moves in the course of time through ‘A’, ‘B’, ‘C’, ‘M’ and the inflection point ‘D’ to the point ‘E’ on the straightened part. The total energy used for plastic deformation (bending and unbending) is approximated by the OBD area in the moment-curvature diagram in Figure 2.3 (left). Energy thus estimated neglects the dissipation in the material element as it moves from ‘D’ to ‘E’ and beyond but this contribution is considered to be small as compared to the plastic energy. The moment-curvature diagram in Figure 2.3 also suggests that the maximal negative bending moment occurs as the material element goes through point ‘D’ however, based on the foil shape this has to occur at the point ‘M’ which might also result in an error in the estimated dissipation.

The moment-curvature characteristics have to be constant during the peeling, meaning that the curvature of the material element at the point B in Figure 2.3 and the

microscopic peeling angle  $\theta_o^*$  have to remain constant throughout the delamination<sup>[4]</sup>, emphasizing the importance of experimentally meeting the steady-state peeling conditions.

In contrast with the work of Georgiou et al.<sup>[5,13]</sup>, in our systems (see Sections 3.1 and 3.2) there were no adhesive layers between the metallic films and the substrates and the model was adapted accordingly. The complete set of equations and the algorithm of the protocol are available through reference 5.

## 2.2 Pull-off test

A schematic of the pull-off test is shown in Figure 2.4. For the test, a pull-off stud is glued to a coated substrate (Figure 2.4a). In such a test specimen, stud, glue, coating and the substrate are connected in series and a constant area for load transfer is important. To control the area, a precut around the stud is made, the sample is then clamped in the tensile machine and the force is applied at a 90° angle (Figure 2.4b). Maintaining the exact angle throughout the measurement is very important since any deviations will lead to the “peeling” of the coating rather than the direct pulling off. After the sample has been clamped, the load is increased until fracture occurs and force vs time records are taken during the test.

The outcome of the test is the average fracture stress. The main disadvantage of the test is that the (tensile) stress distribution along the coating-substrate interface is not uniform and to relate the highest stress to the average one, a finite element analysis could be used if sufficient details about the local geometry are known. However, if most of the system components are kept the same the test can be used for strength ranking purposes. To check whether the test is successful, post-mortem inspection of the samples is necessary. If it is found that the fracture occurred along the coating-substrate interface the test is taken as successful. If the fracture did not occur along the specific interface it is

---

\* The microscopic peeling angle is a consequence of the stretching of the substrate, actually the cohesive zone model, by the delaminating metallic coating just before it debonds completely from the substrate.

concluded that other system components, i.e. substrate material, coating material, glue or the stud, are weaker than the interface.

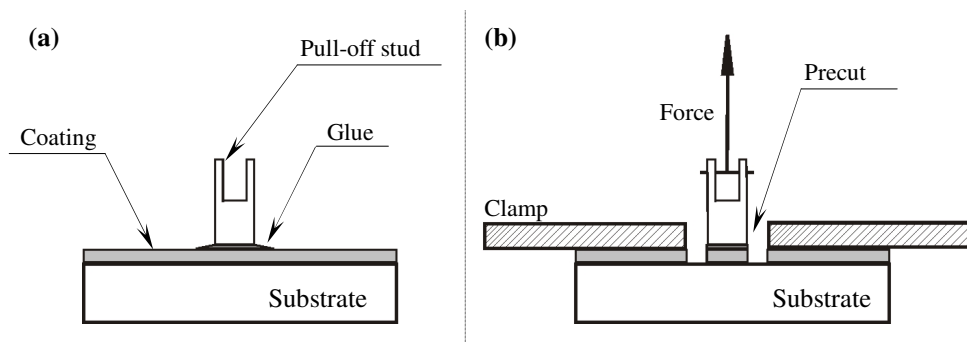


**Figure 2.4.** a) Schematic drawing of the pull-off test specimen and b) drawing of the pull-off test specimen, with a precut, in the clamping system.

For the measurements, pull-off studs (stainless steel,  $d = 8$  mm) were glued to the metallized substrates by 3M DP 460 epoxy glue (cured for 24 h at room temperature). After solidification of the glue, the precut around the stud is made. The samples thus prepared are then clamped in the tensile machine (TesT 810) and connected to the load cell via a long cable to make sure the force application angle is  $90^\circ$  at any moment. Subsequently, the clamped sample is moved downwards at a constant speed until the fracture occurs. The tests were performed in an air atmosphere at room temperature using a tensile machine cross-head velocity of 1 mm/min.

### 2.3 Adhesion on a molecular level: Molecular dynamics simulations

To deduce the thermodynamic work of adhesion, adhesion can be simulated using molecular dynamics (MD) calculations<sup>[14]</sup>. Influence of contact time on the adhesion hysteresis for JKR measurements<sup>[15]</sup> has already been successfully modeled using coarse grained bead-spring model for polymer molecules (lumped chemical nature, i.e. no individual atoms but (functional) groups of atoms). Tip-substrate interactions during the AFM measurements have also been simulated<sup>[16]</sup> but only for the interacting parts with the lumped chemical nature. Adhesion behavior of NaCl nanocrystals has been

numerically simulated<sup>[17]</sup> as well, but dealt with the study of the distance below which the crystals jump into contact.

MD will be used here to simulate the interactions of a single polymer molecule (with a defined chemical structure) and a metallic (oxide) surface(s). Throughout the work, the Materials Studio software package commercially available from Accelrys was used for all calculations. Force field calculations were performed through the Discover module of the package, using the condensed-phase optimized molecular potentials for atomistic simulation studies (COMPASS) force field. Simulations were carried out at a temperature of 298 K controlled by the Andersen algorithm<sup>[14, p. 143,144]</sup> and the equilibration of the structures was performed using the isothermal-isochoric (NTV) canonical ensemble with 3D periodic boundary conditions applied. The NTV ensemble was used because the basic simulation box remains orthorhombic, facilitating the determination of the contact area between the molecule and the copper (oxide) surface(s). Duration of the simulations was confined to 50 ps using a time step of 1 fs. The simulation time was confined to 50 ps because within this time period the temperature of the system reached its preset value and no changes of the non-bond (electrostatic and van der Waals) and the potential energy of the systems were observed, expecting that the system is in equilibrium.

### 2.3.1 Energetic analysis of contact between a single polymer molecule and a copper surface

Based on the interaction energy and the projected area of a single polymer molecule's van der Waals volume on the metallic surface (van der Waals contact area) the work of adhesion between the molecule and the metal can be calculated<sup>[18]</sup>. It will be shown that the work of adhesion calculated by the "single molecule" approach can be taken as an estimate of the work of adhesion between bulk polymer material and a bulk metal. The "single molecule" approach was adopted due to the difficulties of constructing a representative bulk structure of the polymer material of realistic density and the difficulties of constructing a (bulk metal)-(bulk polymer) interface. The choice of using van der Waals contact area to calculate the work of adhesion comes from the fact that

within the fully dense polymer material each molecule will occupy exactly the van der Waals volume, thus effectively leaving the van der Waals contact area as the area, per molecule, over which the adhesive interactions with the metal surface are achieved.

The first two components of the analyzed systems are a block of copper including a surface and a single polymer molecule (modeled as a cylinder) separated in equilibrium in vacuum, as shown in Figure 2.5.

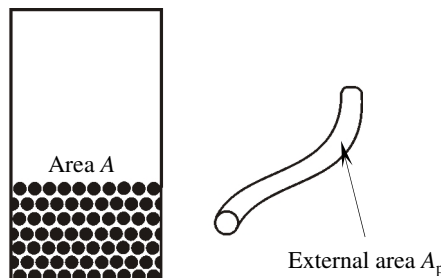


**Figure 2.5.** Copper surface in a simulation box and isolated polymer molecule.

The total internal energy of copper in the simulation box in equilibrium  $E_c$  is a sum of bulk internal energy  $E_{bc}$  and surface associated internal energy  $E_{sc}$ :

$$E_c = E_{bc} + E_{sc} \quad (2.11)$$

The surface associated internal energy can be expressed as:

$$E_{sc} = \gamma_c^{(i)} A \quad (2.12)$$

where  $\gamma_c^{(i)}$  is the copper surface internal energy and  $A$  the surface area in contact with vacuum. The total internal energy  $E_p$  of a free isolated polymer molecule in equilibrium in vacuum is:

$$E_p = E_{bp} + E_{sp} \quad (2.13)$$

where  $E_{bp}$  is the polymer bulk internal energy and  $E_{sp}$  is the surface associated internal energy for the polymer and equals to:

$$E_{sp} = \gamma_p^{(i)} A_p \quad (2.14)$$

where  $A_p$  is the external surface area of the polymer molecule and  $\gamma_p^{(i)}$  the surface internal energy of polymer. If, now, the polymer molecule is positioned on top of the

copper surface and the system is equilibrated (Figure 2.6), the total internal energy of copper in equilibrium  $U_c$  becomes:

$$U_c = U_{bc} + U_{sc} \quad (2.15)$$

where  $U_{bc}$  is the bulk internal energy and can be taken to be equal to the bulk internal energy of copper in vacuum  $E_{bc}$  and  $U_{sc}$  is the internal energy associated with the copper surface exposed to vacuum:

$$U_{sc} = \gamma_c^{(i)} (A - A_c) \quad (2.16)$$

Here  $A_c$  is the van der Waals contact area between the polymer molecule and a copper surface (Figure 2.6).

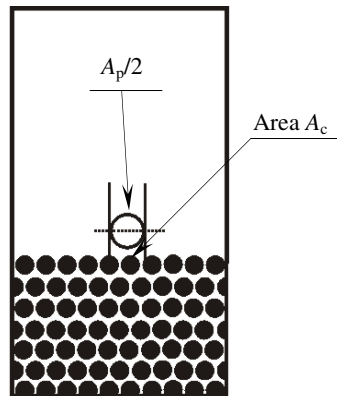


**Figure 2.6.** Copper surface and a single polymer molecule in contact in equilibrium.

The total internal energy of the polymer molecule in contact with the copper surface  $U_p$  is:

$$U_p = U_{bp} + U_{sp} \quad (2.17)$$

where  $U_{bp}$  is the bulk internal energy of the polymer molecule and  $U_{sp}$  is the surface associated internal energy:

$$U_{sp} = \gamma_p^{(i)} \frac{A_p}{2} \quad (2.18)$$

The bulk internal energy of the polymer molecule in contact with the copper surface is not equal to the bulk internal energy of the isolated molecule. When isolated, the molecule's internal energy is minimal and it was found to increase upon contact with the copper. The internal energy associated with the interface  $U_i$  can be defined as:

$$U_i = \gamma_i^{(i)} A_c \quad (2.19)$$

where  $\gamma_i^{(i)}$  is the interface internal energy. Now, the internal work of adhesion  $W_A^{(i)}$  is defined by:

$$W_A^{(i)} = \frac{1}{A_c} ((E_p + E_c) - (U_p + U_c + U_i)) \quad (2.20)$$

If now the polymer molecule is considered as a flexible but inextensible chain of radius  $r$  and length  $l$  ( $r \ll l$ ) the external surface area of the molecule  $A_p$  can be approximated as:

$$A_p = 2\pi r^2 + 2\pi r l \approx 2\pi r l \quad (2.21)$$

and

$$A_c = 2rl \quad (2.22)$$

After analyzing Equation 2.20, the internal work adhesion can be expressed as:

$$W_A^{(i)} = \gamma_p^{(i)} + \gamma_c^{(i)} - \gamma_i^{(i)} + \frac{E_{bp} - U_{bp}}{A_c} + \left(\frac{\pi}{2} - 1\right) \gamma_p^{(i)} \quad (2.23)$$

The third term in the Equation 2.23 is negative ( $U_{bp} > E_{bp}$ ) and the fourth term is positive and it is assumed that, for the “single molecule” approach, the third and the fourth term in Equation 2.23 add, effectively, to zero leading to:

$$W_A^{(i)} = \gamma_p^{(i)} + \gamma_c^{(i)} - \gamma_i^{(i)} \quad (2.24)$$

Using conventional MD simulations at constant temperature and volume (NTV ensemble) only the internal energy of the systems can be calculated. However, the surface energy and thus the work of adhesion are connected with the change of the Helmholtz energy at constant volume (see Section 1.3, Equations 1.1 and 1.2) or to the change of internal energy at constant entropy. So, if the internal work of adhesion, calculated by the “single molecule” approach would prove to be constant over a certain temperature range it would mean that it is a reliable estimate of the work of adhesion  $W_A$ , or:

$$W_A \approx W_A^{(i)} = \gamma_p^{(i)} + \gamma_c^{(i)} - \gamma_i^{(i)} \quad (2.25)$$

On the other hand, the surface energy  $\gamma$  and the internal surface energy  $\gamma^{(i)}$  can be connected through:

$$\gamma^{(i)} = \gamma - T \frac{\partial \gamma}{\partial T} \quad (2.26)$$

where  $T$  is the temperature. Now, if a linear dependence of the internal surface energy in temperature is assumed:

$$\gamma^{(i)} = \gamma_0^{(i)} \left( 1 - \frac{T}{T_c} \right) \quad (2.27)$$

where  $\gamma_0^{(i)}$  is the intercept and  $T_c$  the critical temperature at which the internal surface energy goes to zero. Combining Equations 2.26 and 2.27 and solving the differential equation using the boundary condition that at the critical temperature the surface energy is also zero, i.e.  $\gamma(T_c) = 0$ , the following relation between the surface energy and the internal surface energy is obtained:

$$\gamma = \gamma_0^{(i)} \left( 1 - \frac{T}{T_c} \right) + \gamma_0^{(i)} \frac{T}{T_c} \ln \frac{T}{T_c} \quad (2.28)$$

The second term in Equation 2.28 is the correction that needs to be applied to the calculated internal surface energy in order to make it equal to the surface energy<sup>†</sup>. This correction also has to be taken into account when estimating the work of adhesion. If the correction is small, or the corrections for each internal surface energy contribution in Equation 2.25 effectively add to zero, the internal work of adhesion can be taken as equal to the real work of adhesion.

---

<sup>†</sup> The internal surface energy for the copper (0 0 1) surface was estimated at 2.30 J/m<sup>2</sup> compared to 2.35 J/m<sup>2</sup> for the polycrystalline surface energy of copper<sup>[19]</sup> indicating that the discrepancy between the internal surface energy and the surface energy is small.

## References

- [1] K. L. Mittal, *Adhesion measurement of films and coatings*, VSP, Utrecht, **1995**, p. 5.
- [2] J. Božović Vukić, S. Hoeppener, D. A. Kozodaev, S. Kisín, B. Klumperman, U. S. Schubert, G. de With, C. E. Koning, *ChemPhysChem*, **2006**, 7, 1912–1916.
- [3] A. J. Kinloch, C. C. Lau, J. G. Williams, *Int. J. Fracture*, **1994**, 66, 45–70.
- [4] K. S. Kim, N. Aravas, *Int. J. Solids Structures*, **1988**, 24, 417–435.
- [5] I. Georgiou, H. Hadavinia, A. Ivankovic, A. J. Kinloch, V. Tropsa, J. G. Williams, *J. Adhes.* **2003**, 79, 239–265.
- [6] N. Aravas, K. S. Kim, M. J. Loukis, *Mater. Sci. Eng. A*, **1989**, 107, 159–168.
- [7] E. Breslauer, T. Troczynski, *Mater. Sci. Eng. A*, **2001**, 302, 168–180.
- [8] D. E. Packham, *Handbook of Adhesion*, Longman Scientific & Technical, Harlow, **1992**, p. 303.
- [9] J. Weertman, *Acta Metall.* **1978**, 26, 1731–1738.
- [10] D. M. Lipkin, G. E. Beltz, *Acta Mater.* **1996**, 44, 1287–1291.
- [11] Z. Suo, C. F. Shin, G. Varias, *Acta Metall. Mater.* **1993**, 41, 1551–1557
- [12] R. Thomson, *J. Mater. Sci.* **1978**, 13, 128–142.
- [13] Adhesion, Adhesives and Composites Group, Imperial College, London, website: <http://www.me.imperial.ac.uk/AACgroup/index.html> last accessed 23/01/2006.
- [14] D. Frenkel, B. Smit, *Understanding molecular simulation: From algorithms to application*, Academic Press, London, **2002**.
- [15] I. Yu. Sokolov, G. S. Henderson, F. J. Wicks, *Surf. Sci.* **2000**, 457, 267–272.
- [16] R. C. Baljon, J. Vorselaars, T. J. Dapuy, *Macromolecules*, **2004**, 37, 5800–5806.
- [17] O. Misbauer, M. Götzinger, W. Peukert, *Nanotechnology* **2003**, 14, 371–376.
- [18] P. G. Th. van der Varst, *Internal communication note*, October 31, **2006**.
- [19] G. de With, *Structure, deformation, and integrity of materials*, vol. 1, Wiley–VCH, Weinheim, **2006**.

## **CHAPTER 3**

### **SAMPLES AND SAMPLE PREPARATION**

**Summary:** In this chapter, the polymer substrate and the metallic coating chosen for the study will be presented. The procedures used to produce the samples will be elaborated and the samples micro-structure will be looked into. The initial results of measurements to check the reproducibility of the sample preparation procedure will be shown. Finally, the influence of the delamination speed and coating thickness on the adhesive energy will be discussed. Based on this part a choice for the values of coating thickness and the delamination speed, with which the rest of the peel test experiments are to be performed, will be made.

### 3.1 Samples: The polymer substrate

For the substrate material, bulk polymerized ABS was used. The molecular weight of the continuous *poly(styrene-co-acrylonitrile)* phase was 140 kg/mole and this phase constituted 86.5 wt. % of the material. The average size of the dispersed *poly(butadiene)* phase was 550 nm. The substrate material exhibits two glass transition temperatures, –40 °C and 107 °C for the pBd and SAN phase, respectively. The substrate plates were injection molded into plates with  $70 \times 70 \times 1$  mm<sup>3</sup> dimensions. The molding was done with an Engel ES 80/25 machine using a mold temperature of 60 °C and a cylinder temperature of 225 °C. The applied clamping force was 250 kN and a 1500 bar injection pressure was used.

A SEM image of the surface of the ABS substrate is shown in Figure 3.1 (left). The only visible feature on the substrate surface is the orientation of the polymer as a result of the molding process used to produce the substrate plates. This is expected to results in a highly anisotropic substrate. In Figure 3.1 (right) the expected orientation of the polymer molecules based on the SEM micrograph and on the characteristics of the injection moulding procedure is schematically shown. The substrate surface is very smooth with an R<sub>a</sub> value of 0.01 µm measured by the white light confocal microscopy (NanoFocus µSurf® 100x objective).

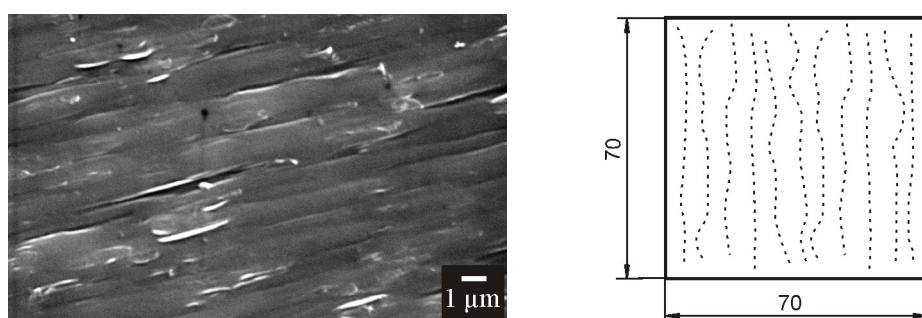


**Figure 3.1.** SEM micrograph of the ABS plate as used for copper deposition (accelerating voltage 15 kV) and the schematic representation of the polymer molecules orientation within the substrate as a result of the injection moulding processing.

To investigate the substrate anisotropy, uniaxial tensile tests on the substrate material were performed. The load was applied parallel to the chain orientation and perpendicular to the chains (Figure 3.1). The samples were prepared according to the ISO 527 type 1BA standard and the tests performed using a tensile machine crosshead speed of 1 mm/min up to 1 % strain and thereafter 10 mm/min until failure. All measurements were done at room temperature and atmospheric pressure. The properties obtained are summarized in Table 3.1.

Loading direction (with respect to chain orientation)	Young's modulus $E$ [GPa]	Yield stress $\sigma_Y$ [MPa]	Strain at failure $\varepsilon_f$ [%]
Parallel	$2.08 \pm 0.35$	$56 \pm 3$	$6.9 \pm 1.3$
Perpendicular	$1.91 \pm 0.10$	—	$2.6 \pm 0.1$

**Table 3.1.** Dependence of the ABS plate mechanical properties on the loading direction during the tensile test. The loading direction defined with respect to the polymer chain orientation as shown in Figure 3.1 (5 samples tested for each loading direction).

When loaded parallel to the chain orientation, the ABS material exhibits plastic flow and necking. When loaded perpendicular to the chains, the material shows only elastic deformation prior to brittle failure at  $46 \pm 2$  MPa. These observations are expected since in the first case strong intramolecular bonds are loaded and the sliding of the oriented molecules with respect to each other allows the plastic flow whereas in the second case only relatively weak intermolecular forces are loaded.

For the peel test samples, ABS pieces of  $25 \times 70$  mm<sup>2</sup> were cut out from the original plates. The cutting direction is shown in Figure 3.2 and the loading direction during the peeling is indicated by the arrow. So, for later discussions about the influence of the substrate mechanical properties on adhesive energy measured by the peel test, the fact that the substrate was loaded perpendicular to the chain orientation (direction exhibiting only elastic deformation in the tensile test) has to be taken into account.

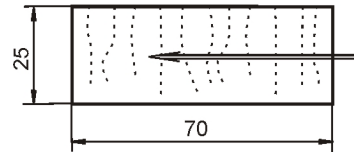


**Figure 3.2.** Schematic representation of the ABS plates cut out from the original  $70 \times 70 \text{ mm}^2$  plates. The arrow shows the loading direction during the peel testing.

In addition a stress relaxation test was performed on the substrate material with the loading direction corresponding to the loading direction during the peel testing. The experiment was performed using TA Instruments DMA Q800 instrument at atmospheric pressure and at  $25^\circ\text{C}$  with an applied step strain of  $\varepsilon_0 = 0.001$ . The mechanical behavior of the substrate was approximated by a standard linear element shown in Figure 3.3.

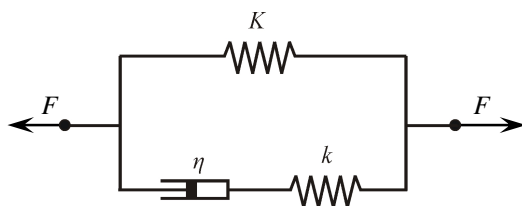


**Figure 3.3.** Standard linear element used to approximate the mechanical behavior of the ABS substrate plates during the stress relaxation experiment.

The stress relaxation behavior of the element were fitted using an exponential function  $E(t)$  described by:

$$E(t) = K + ke^{-\frac{k}{\eta}t} \quad (3.1)$$

with  $K = 1.6 \text{ GPa}$ ,  $k = 0.7 \text{ GPa}$  and  $\eta = 3.97 \times 10^{11} \text{ Pas}$ . The data and the fitted function are shown in Figure 3.4 (no literature data were available for comparison). These data will be used in Chapter 7 to estimate the visco-elastically dissipated energy within the substrate during peeling.

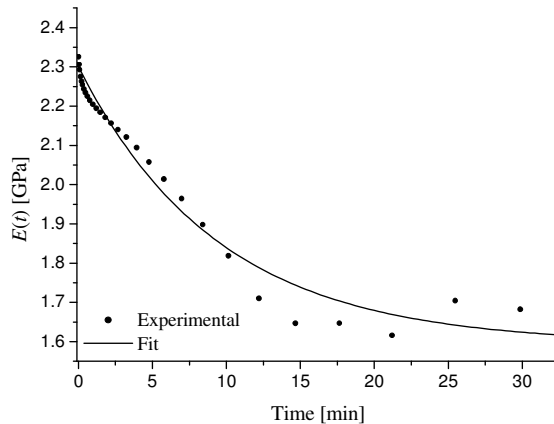


**Figure 3.4.** Stress relaxation experiment. Experimental data indicated with the point, while the continuous solid line represents the fit.

### 3.2 Samples: The metallic film

To investigate the adhesion between the pure materials, copper and ABS, it was decided to coat the substrates in two steps. Namely, the Cu layers were galvanically electroplated after the initial deposition of a seed layer by magnetron sputtering. The final sample structure was ABS/Cu(sputtered)/Cu(electroplated). Galvanic strengthening was needed as the sputtered films were too weak to withstand the applied force during the peel testing. The two-step deposition procedure also gives the possibility to influence the initially formed interface by galvanic deposition and no aggressive oxidative treatment of the substrate material is needed as compared to electroless or electrodeposition of copper on plastic substrates<sup>[1]</sup>. Prior to the copper deposition all the substrates were wipe-cleaned with isopropanol. The initial deposition of the 0.5 µm thick copper layers was done by magnetron sputtering from a 99.9% pure copper target under 0.03 mbar Ar<sup>+</sup> plasma and RF power of 500 W. The estimated deposition rate  $v_{\text{dep}}$  is 3.3 nm/min. For all depositions, an Alcatel<sup>TM</sup> SCM 850 device with  $2 \times 10^{-7}$  mbar background pressure was employed.

During the initial stages of the PVD process, copper nucleation centers are formed, while in the later stages the film exhibits a columnar growth in the direction normal to

the substrate surface<sup>[2,3]</sup> resulting in the open structure<sup>[4]</sup> shown schematically in Figure 3.5a. A top view of the deposited copper films is shown in Figure 3.5b. Due to the low magnification the columnar structure is not visible but one can observe large elongated cracks in the copper film. These cracks are most probably the result of different thermal expansion coefficients for copper and ABS and they will play an important role in the later chapters.

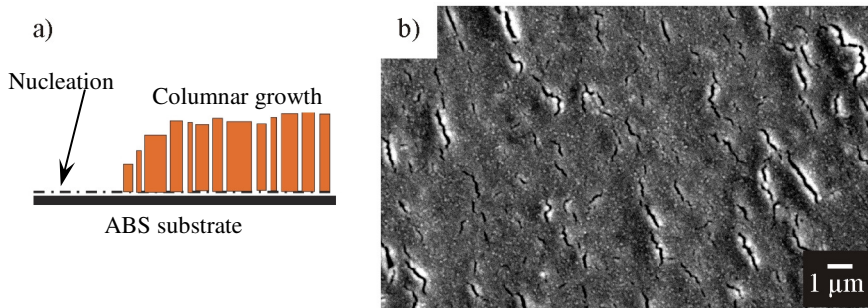


**Figure 3.5.** Nucleation and growth of the copper films during PVD deposition (a) and SEM micrograph of the copper PVD deposited on top of the ABS substrate (accelerating voltage 20 kV) (b).

During the deposition, a certain amount of water molecules and other contaminants (argon, oxygen, etc.) is present in the deposition chamber resulting in non-pure copper deposits. The amount of contamination (the amount of residual gas molecules adsorbed during the deposition divided by the total amount of copper atoms and residual gas molecules adsorbed during the deposition) can be estimated knowing the deposition conditions according to a simple equation<sup>[5]</sup>:

$$C = \frac{1}{1 + t_{rg} v_{dep} n_{at}^{1/3}} \cdot 100\% \quad (3.2)$$

In the Equation 3.2  $C$  is the percentage of the contamination,  $n_{at}$  the atomic density of the pure, fully dense copper film and  $t_{rg}$  the monolayer adsorption time of the contaminants (for our settings it is reasonable to estimate it at 3 s<sup>[5,6]</sup>). The atomic density of the pure, fully dense copper films can be calculated from:

$$n_{at} = \frac{N_{at}}{V_{cell}} \quad (3.3)$$

where  $N_{\text{at}}$  is the number of atoms in the copper unit cell and  $V_{\text{cell}}$  is the volume of the unit cell. Knowing that copper has a face centered cubic cell, Equation 3.6 can be rewritten to:

$$n_{\text{at}} = \frac{4}{8^{3/2} R_{\text{Cu}}^3} \quad (3.4)$$

where  $R_{\text{Cu}}$  is the radius of a single copper atom. The estimated atomic density based on Equation 3.4 ( $R_{\text{Cu}}$  taken as 1.28 Å) is 0.0843 atoms/Å<sup>3</sup>. Now, from Equation 3.2, the contamination of the sputtered films is estimated at around 58 %. Approximately 60 % of these contaminants is water<sup>[6]</sup>, which can easily react with copper and form oxides. Having in mind the above numbers, around 35 % of copper oxide is estimated to be present in the sputtered films. The amount of contaminants is, however, highly dependent on the metal deposition rate and can be manipulated by adjusting the deposition rate without changing the other deposition parameters.

Sputtering was followed by additional galvanic deposition to increase the film thickness up to the desired level. The deposition was performed at room temperature from an acidic copper bath (275 g/L CuSO<sub>4</sub> + 55 g/L H<sub>2</sub>SO<sub>4</sub>) using a current density of 26.7 A/m<sup>2</sup>. The bath volume was kept constant at 100 mL and it was renewed after 3 depositions at most. This procedure was used as it is supposed to result in internally stress free films<sup>[7, p.65]</sup>.

The deposition time for producing the films of desired thickness was estimated using Faraday's law of electrolysis and the resulting thickness of the films was subsequently measured from SEM micrographs of the film cross-sections. Five measurements on two randomly selected samples were done, after which data were averaged.

The deposited metallic films measured 35 mm in length and were 20 mm wide (Figure 3.6). Between the experiments, all samples were stored in a dry atmosphere (desiccator, relative humidity around 15 %) at room temperature and under atmospheric pressure.

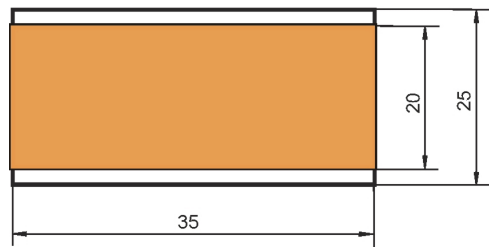


**Figure 3.6.** Schematic representation of the top view of sputtered and galvanically strengthened copper film on the ABS substrate.

The galvanically deposited copper films showed a typical coarsening of the columnar structure and concomitant grain growth<sup>[2,7 p.79,8]</sup>. These characteristic features can be seen in Figure 3.7 where a SEM image of the copper film cross-section and a tapping mode scanning force microscopy (TM-SFM) phase image of the top of the film is shown. To reveal the micro-structure of the copper film, etching of the film cross-section was done using a grain boundary etching solution for copper<sup>[9]</sup> (50 cm<sup>3</sup> water, 50 cm<sup>3</sup> ammonium hydroxide and 20 cm<sup>3</sup> 30 vol. % hydrogen peroxide). In Figure 3.7a, a thin, initially PVD sputtered, layer is visible and the columnar growth of the galvanically deposited film starts from its surface. The thickness of the PVD seed layer was  $0.48 \pm 0.05 \mu\text{m}$  (average of 10 measurements,  $\pm$  denotes the sample standard deviation) and this thickness was retained throughout the study.

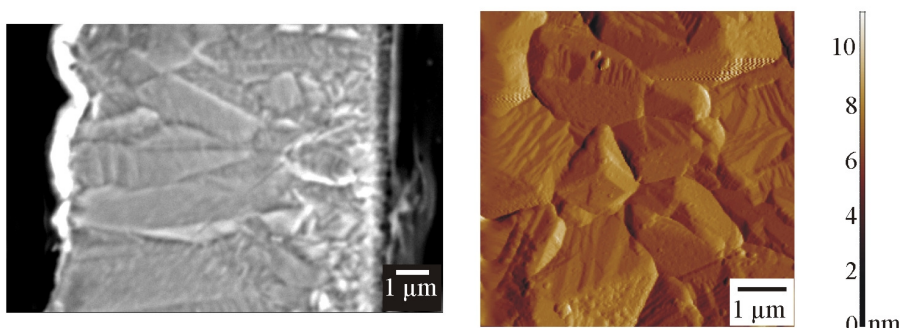


**Figure 3.7.** SEM micrograph of the copper film cross-section (accelerating voltage 10 kV) (a) and TM-SFM phase image of the galvanically deposited copper film top surface (b).

### 3.3 Samples: Reproducibility of the preparation procedure

To check whether the adhesion is homogeneous over the whole sample surface area and that the chosen deposition procedure produces reproducible samples, several peel tests on one sample were performed and the results compared with each other and with those found by testing different samples. All tests were done 24 hours after the additional galvanic deposition using a delamination speed of 0.707 mm/min in air atmosphere and room temperature. For the tests  $18.6 \pm 0.6 \mu\text{m}$  thick copper films were used. In the tests performed on the same sample, the force was reduced to zero after each delamination period and the starting time was also set to zero.

Obviously the peel force is constant for one and the same sample (Figure 3.8). In Figure 3.8, every time a measurement was done approximately 5 mm of the sample was peeled, making a total of 15 mm peeled length. Over this area there are no major deviations in the peel force, suggesting that the adhesion is uniform over the whole sample.

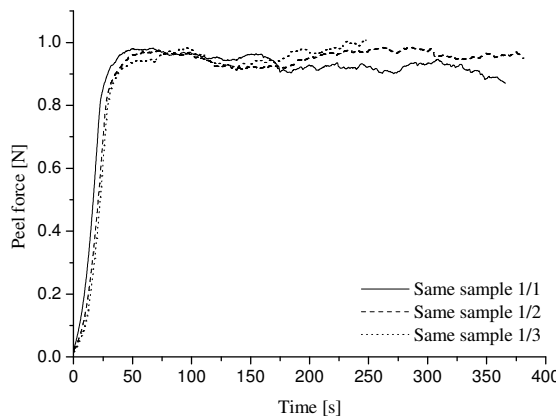


**Figure 3.8.** Comparison between the peel force levels on one sample (ABS/18.6  $\mu\text{m}$  Cu, 24 hours after galvanic deposition, delamination speed 0.707 mm/min).

The comparison between the different samples is plotted in Figure 3.9. Although not such a perfect match was obtained as in the case of the same sample (Figure 3.8), the adhesion is considered to be reproducible for the different samples within the experimental error margins. Also here, there are no major deviations of the peel force

during a single measurement. The results for the average peel force for one measurement and the sample standard deviation, representing the homogeneity of the adhesion along the substrate surface are summarized in Table 3.2. The average peel force for three different samples presented is 0.97 N with a mean standard deviation of 0.08 N.

Sample	Average peel force [N]	Standard deviation [N]
Sample 1	0.93	0.02
Sample 2	0.92	0.04
Sample 3	1.07	0.02
Overall	0.97	0.08

**Table 3.2.** Average peel force levels for 3 different samples (Figure 3.9).

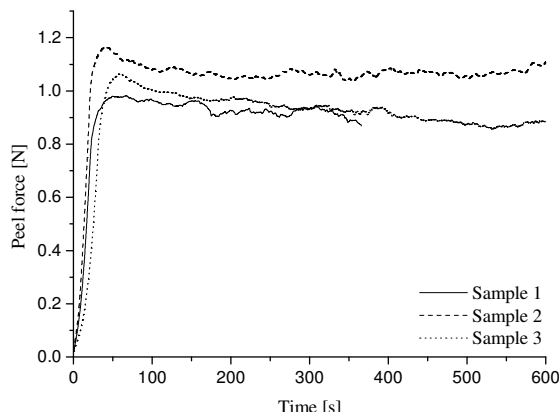


**Figure 3.9.** Comparison between the peel force levels on 3 different samples (ABS/18.6  $\mu\text{m}$  Cu, 24 hours after galvanic deposition, delamination speed 0.707 mm/min).

The samples tested here show that, by use of the chosen sample preparation procedure, the adhesion behavior between copper and ABS polymer can be measured reproducibly.

### 3.4 Delamination speed and coating thickness dependence of the adhesive energy

An experimental condition that can be changed in performing the peel test with the constructed peel testing device (see Section 2.1.1) is the speed of the delamination. To make the optimal choice of the delamination speed to be used in further experiments, the delamination speed dependence of the adhesive energy for three different coating thicknesses on ABS substrate was tested.

All peel tests were performed at room temperature and atmospheric pressure changing the delamination speed in a sequence:  $7.07 \times 10^{-3}$ ,  $35.35 \times 10^{-3}$ ,  $70.7 \times 10^{-3}$ , 0.3535, 0.707, 1.414, 2.121 and 3.535 mm/min. Three different coating thicknesses were used:  $11.5 \pm 0.4$ ,  $15.2 \pm 0.4$  and  $18.6 \pm 0.6$   $\mu\text{m}$  (average of 10 thickness measurements;  $\pm$  denotes the sample standard deviation). The delamination speed dependence of the adhesive energy for the coatings of mentioned thicknesses is shown in Figure 3.10.

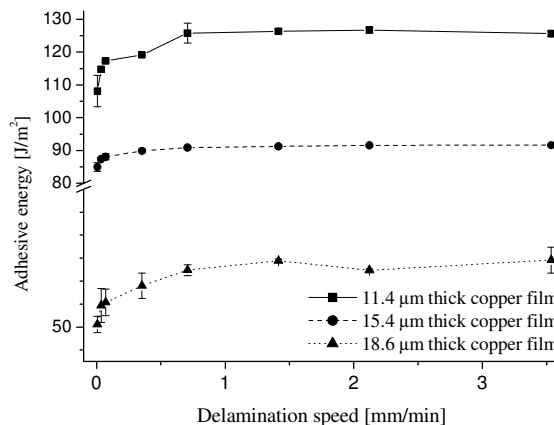


**Figure 3.10.** Delamination speed dependence of the adhesive energy for the copper coatings of different thicknesses on the ABS substrate (1008 h after the galvanic deposition; each point represents an average of 5 measurements). Note that for some points error bars are not visible as they are smaller than the symbol size used.

The delamination speed dependence of the adhesive energy is very similar for all three thicknesses used. In the delamination speed range from  $7.07 \times 10^{-3}$  mm/min to 0.707

mm/min an increase of the adhesive energy with the increasing delamination speed is observed. In the delamination speed range between 0.707 mm/min and 3.535 mm/min a region of a constant adhesive energy value is observed for all three thicknesses ( $126.11 \pm 0.51 \text{ J/m}^2$  for 11.4  $\mu\text{m}$  thick films,  $91.32 \pm 0.35 \text{ J/m}^2$  for 15.4  $\mu\text{m}$  films thickness and  $54.48 \pm 0.41 \text{ J/m}^2$  for 18.6  $\mu\text{m}$  thick copper films,  $\pm$  denotes the sample standard deviation). Since the adhesive energy is independent of the delamination speed for speeds between 0.707 mm/min and 3.535 mm/min, for all the following experiments the delamination speed of 0.707 mm/min will be used.

As far as the thickness dependent behavior is concerned it can be seen in Figure 3.10 that the adhesive energy increases with decreasing film thickness<sup>‡</sup>. Although for the thinner films a stronger interface is obtained and the deposition time can be reduced, the choice to proceed with peel experiments using 18.6  $\mu\text{m}$  thick copper films has been made only because these films proved to be the easiest to handle while preparing the samples for the peel test (thinner films often broke together with the substrate, see Section 2.1.1, Figure 2.1c and d).

---

<sup>‡</sup> Valid only for the thickness range mentioned. It has been suggested in the literature<sup>[10-12]</sup> that, in a wider thickness range, the adhesive energy shows increase with the increasing film thickness and subsequently decreases if the film thickness is increased further.

## References

- [1] J. E. Graves, M. T. Goosey, D. Hirst, M. A. Poole, *T. I. Met. Finish*, **2001**, *79*, 90–94.
- [2] R. F. Bunshah, J. M. Blocher Jr, T. D. Bonifield, J. G. Fish, P. B. Ghate, B. E. Jacobson, D. M. Mattox, G. E. McGuire, M. Schwartz, J. A. Thorton, R. C. Tucker Jr. *Deposition Technologies for Films and Coatings: Developments and Applications*, Noyes Publications, Park Ridge, **1982**, p. 213.
- [3] R. Tacken, V. J. A. R. Frenken, C. Schrauwen, *12. NDVaK Beschichtung und Modifizierung von Kunststoffoberflächen*, Dresden, October 14–15, **2004**.
- [4] P. Benjamin, C. Weaver, *P. Roy. Soc. A*, **1961**, *261*, 516–531.
- [5] J. E. Maham, *Physical vapor deposition of thin films*, Wiley–Interscience, Chichester, **2000**, p. 272.
- [6] C. Schrauwen, R. Tacken, V. Frencken, T. van Oudheusden, R. Renders, K. Spee, *Society of Vacuum Coaters: 49<sup>th</sup> Annual Technical Conference Proceedings*, **2006**, 17–22.
- [7] M. Schlesinger, M. Paunovic, *Modern electroplating*, Wiley-Interscience, New York, **2000**.
- [8] I. S. Park, J. Yu, *Acta Mater.* **1998**, *46*, 2947–2953.
- [9] C. J. Smithells, E. A. Brandes, *Metals reference book*, Butterworths, London, **1976**, p. 326.
- [10] J. Y. Song, Jin Yu, *Acta Mater.* **2002**, *50*, 3985-3994.
- [11] Y. B. Park, I. S. Park, Jin Yu, *Mater. Sci. Eng.* **1999**, *A266*, 261-266.
- [12] T. Ikeda, A. Yamashita, D. Lee, N. Miyazaki, *Trans. ASME*, **2000**, *122*, 80-85.



## CHAPTER 4

### INFLUENCE OF WET CHEMICAL PROCESSING ON THE ADHESIVE ENERGY AND THE INTERFACE STRUCTURE<sup>§</sup>

**Summary:** Throughout this chapter the adhesion of the model system (sputtered and galvanically strengthened copper coatings on ABS substrate) will be considered as a function of the time the sample was stored after the galvanic deposition of the coating. It will be shown that the magnitude of the adhesion changes in time, on two different time scales and with two different rates. During the galvanic strengthening water and electrolytes are introduced to the interface and the initial fast increase of adhesion will be correlated with the removal of water caused by the sample storage in a dry atmosphere. The subsequent slower increase will be correlated to the structural rearrangements of the substrate taking place near the interface. At the end of the chapter an idea about the copper-ABS interface evolution in time will be given.

---

<sup>§</sup> The main part of this chapter has been submitted for publication:

S. Kisin, P. G. Th. van der Varst, G. de With, Adhesion and adhesion changes at the copper metal-(acrylonitrile-butadiene-styrene) polymer interface, *Thin Solid Films*, 2006

## 4.1 Introduction

It is known that the adhesion strength between dissimilar materials, such as polymers and metals, is often inherently poor, and residual stresses arising from thermal mismatches or pressures exerted by vaporized moisture often lead to delaminations of interfaces<sup>[1]</sup>. Furthermore, most synthetic polymers used for metallization purposes have a surface of low surface energy and low adhesion to high surface energy metallic coatings<sup>[2]</sup>. All these aspects make the realization and reproducibility of good adhesion of metallic coatings on polymer substrates an important industrial and scientific problem since they are used for a variety of applications<sup>[1]</sup>.

There are views that any interface can exist in a number of metastable states separated by a number of energy barriers and that the interface structure can evolve from one state to another as a function of time, temperature and/or applied force<sup>[3,4]</sup>. It is obvious that chemical changes of each of the surfaces can induce a change in the interface structure<sup>[5]</sup>. Although it is thermodynamically possible to reach an equilibrium interface state, due to kinetic limitations it may never be achieved<sup>[3]</sup>.

An increase of the adhesion strength between PDMS and thiol-functionalized Au surfaces as a function of contact time of two materials during the JKR measurements has been demonstrated<sup>[6]</sup>. This result has been confirmed in a computational study and the increase was ascribed to a reorganization of the interfacial polymer molecules and increase in the number of hydrogen bonds rather than to chemical changes and formation of stronger bonds<sup>[7]</sup>. In these studies<sup>[6,7]</sup>, the interface was exposed to a continuous mechanical load which might act as a trigger for structural changes in itself. These changes were further facilitated by the increased polymer mobility as all the materials studied were above their glass transition temperature.

The opposite situation is possible too. Copper–polymer interfaces have been shown to be susceptible to water attack and an interface exposed to an electrolyte solution can show a decrease in adhesive energy and, eventually, a complete loss of adhesion<sup>[8]</sup>.

A significant amount of work has been done on sputtered and electroplated Cr and Cu layers on polyimide substrates<sup>[1,9,10]</sup>, a structure comparable to the samples used here

(see Section 3.2). However, no data have been reported about the influence of water, introduced to the samples by the galvanic processing, on the adhesive energy.

## 4.2 Experimental

### 4.2.1 Peel test, adhesive energy calculations and film mechanical properties

The experiments were done on sputtered and galvanically strengthened copper coatings on ABS substrate (for the preparation procedure see Section 3.2). The thickness of the copper films used was  $18.6 \pm 0.6 \mu\text{m}$ . Peel test measurements were performed on freshly deposited samples (right after the galvanic deposition) and on samples stored for 2, 5, 24, 48, 120, 240, 384 and 1008 hours in a desiccator. Peeling was done at room temperature, ambient humidity and atmospheric pressure using delamination speed of 0.707 mm/min. Tests were repeated twice on the same sample, averaging over at least 3 samples meaning that every value for the adhesive energy is an average of at least 6 measurements. After peeling, the fracture surfaces of both materials were examined by means of optical confocal and electron microscopy. The adhesive energy was calculated from 90° peel test data (see Section 2.1.3).

Electrochemically deposited metal films have a significantly different yield stress and hardening behavior as compared to the bulk metals owing to the large number of defects introduced during the deposition procedure<sup>[1]</sup>. So, the mechanical properties of the copper films have to be determined. To do so, ABS substrates of copper coated samples were dissolved in chloroform and tensile tests were done on the remaining free copper films. The density of the free films was calculated from weight and dimensional data and yielded  $7.0 \pm 0.2 \text{ g/cm}^3$ , corresponding to a relative density of  $78.4 \pm 2.5 \%$ . The experimental stress-strain data were fitted in two different ways. First, from the Ramberg–Osgood model<sup>[11, p. 27]</sup> the  $E$  modulus and the yield stress  $\sigma_Y$  were determined, a fit shown in Figure 4.1a. The post-yield behavior was described assuming a power-law using the previously determined  $E$  and  $\sigma_Y$  values while the hardening exponent was used as free parameter, a fit shown in Figure 4.1b. Second, direct fitting of the power-

law hardening model was done with  $E$ ,  $\sigma_Y$  and  $m$  as free parameters, fit Shown in Figure 4.1c. The mechanical properties found are summarized in Table 4.1.

Fitting procedure	Ramberg-Osgood	Ramberg-Osgood and power-law for post yield behavior	Direct power-law
$E$ [GPa]	55.6	55.6	49.6
$\sigma_Y$ [MPa]	99.3	99.3	164
$m$ [-]	-	0.526	0.372
Ramberg-Osgood parameter $\beta$ [-]	0.02	0.02	-
Ramberg-Osgood exponent $m_{RO}$ [-]	5.5	5.5	-

**Table 4.1.** Mechanical properties of the copper films determined by different fitting procedures.

The large difference in values for the film's yield stress values most likely is a consequence of different fitting procedures used. The Ramberg–Osgood model predicts more accurately the values for the Young's modulus and the yield stress, while the power law is less reliable in this region (compare Figure 4.1 a and c). The energy consumed for the plastic deformation of the films was calculated using these values. If the obtained properties are compared with the mechanical properties of the bulk annealed copper (Young's modulus  $E_b = 119$  GPa<sup>[12]</sup> and the yield stress  $\sigma_Y = 60$  MPa<sup>[11]</sup>) it is concluded that the Young's modulus is much lower than the bulk value while the yield stress exceeds the bulk value by a factor 1.5 or 2.5.

The low value of the Young's modulus could be a consequence of the high porosity of the films. The influence of the porosity can be estimated according to<sup>[11, p. 386]</sup>:

$$\frac{E}{E_b} = 1 - aP + bP^2 \quad (4.1)$$

where  $P$  is the film porosity and  $a$  and  $b$  can be taken as<sup>[11, p.386]</sup>  $a = 1.9$  and  $b = 0.9$ . Based on Equation 4.1 the expected Young's modulus is 75 GPa, which is 35 % higher than the experimental value. The texture of the films and the columnar structure<sup>[9,13,14]</sup> (see Section 3.2, Figure 3.7) could also affect the values of the Young' modulus but were not considered. The high yield stress can be explained by a large number of defects introduced during the deposition procedure<sup>[9]</sup>.

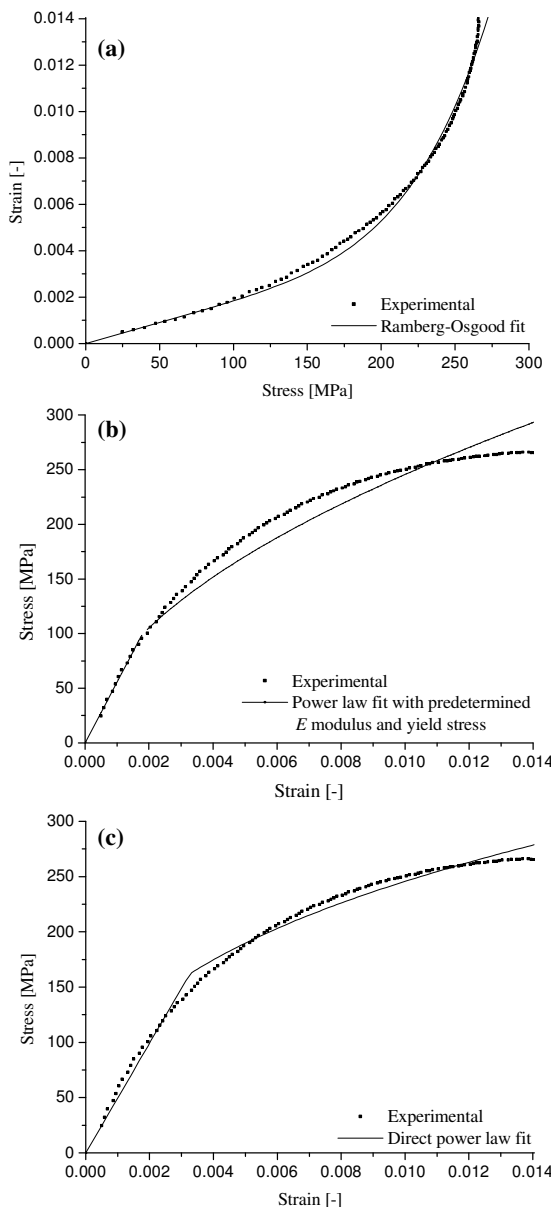


**Figure 4.1.** Stress-strain curves of the galvanically deposited copper films. Determining the  $E$  modulus and the yield stress by fitting to the Ramberg–Osgood model (a) subsequent power–law fit of the yield region keeping the Young’s modulus and the yield stress fixed (b) and a direct power–law fit (c).

## 4.2.2 Water content in the sample: Consequence of the galvanic deposition

The water content in the sample after the galvanic deposition was measured by weighing the sample. After the galvanic deposition was finished, the sample surfaces were briefly rinsed with distilled water, dried with ethanol and the sample was weighed on a laboratory analytical balance to accuracy of about 10 µg. Weight measurements were repeated after 2, 5, 24, 48, 120, 240 and 384 hours. Finally, the sample was baked in the vacuum oven at 100 °C for 2 hours and the resulting weight measured was assumed to be the weight of the completely dry specimen. The water content was calculated from:

$$\omega_{\text{water}} = \frac{w_{\text{wet}} - w_{\text{dry}}}{w_{\text{wet}}} \cdot 100\% \quad (4.2)$$

where  $\omega_{\text{water}}$  is the water content in wt. %,  $w_{\text{wet}}$  is the weight of a specimen and  $w_{\text{dry}}$  is the weight of a baked (dry) sample. Measurements were done on one sample only.

## 4.2.3 Microscopy and contact angle measurements

To monitor the changes of the interface, SEM and contact angle measurements were done. The structure of copper films in contact with substrates for two samples, one right after the galvanic deposition and one kept in a desiccator for about 2880 hours is examined. The substrates were dissolved using chloroform and the copper surfaces were observed under the SEM.

Structural changes, after 1008 hours of storage time, on the polymer side of the interface were monitored using water contact angle measurement after the copper coating had been etched off at the end of the storage period. Etching was done using 40% sulfuric acid. The procedure is schematically shown in Figure 4.2 and all the measurements were done with demineralized water using a Dataphysics OCA30 contact angle system. After the copper coating was etched off, changes of the water contact angle on the interface side of the substrate were tracked in time. Similar contact angle measurements on the (non-coated) backside of the plate were done as reference measurements. The non-

coated, reference side of the plate was treated with the sulfuric acid in the same way as during the copper etching procedure to exclude any influence of the etching procedure on the contact angle measurements.

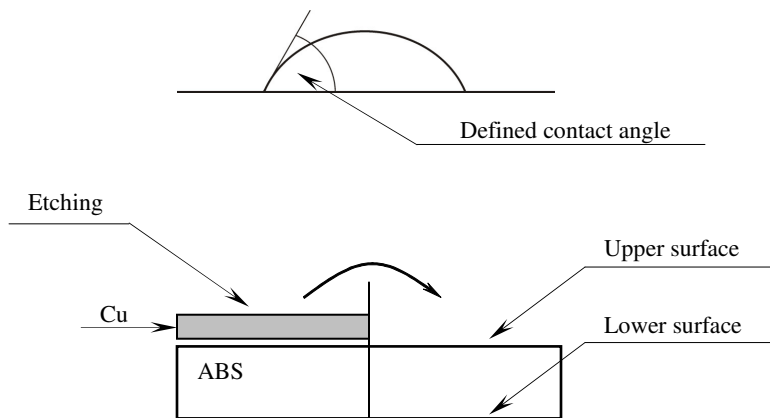


**Figure 4.2.** Definition of the contact angle and scheme of the contact angle measurements.

### 4.3 Results and discussion

The adhesive energy estimated on the basis of the energy balance of the peel test shows a strong increase in time. As shown in Figure 4.3 the adhesive energy increases from the initial  $6.3 \text{ J/m}^2$  to  $53.7 \text{ J/m}^2$  after  $1008 \text{ h}$  storage. At the same time, the energy dissipated by the plastic deformation of copper films increases, accounting for 59% of the complete energy input for the test at storage time zero and for 72% at the end of the studied storage interval (Figure 4.3). The standard deviation of the adhesive energy is between 0.3 and  $1.2 \text{ J/m}^2$ , 2.2% of the highest value measured, indicating a good reproducibility of the interface. For the calculation of data in Figure 4.3 the film properties determined by the first fitting procedure (see Section 4.2.1) were used ( $E = 55.6 \text{ GPa}$ ,  $\sigma_Y = 99.3 \text{ MPa}$  and  $m = 0.526$ ). Using the mechanical properties of the copper films as determined by the second fitting procedure of Section 4.2.1 ( $E = 49.6 \text{ GPa}$ ,  $\sigma_Y = 184 \text{ MPa}$  and  $m = 0.372$ ) to calculate the adhesive energies, the same trends of the curves are retained and the values of the adhesive energies change within only 15% margin (dotted line in Figure 4.3).

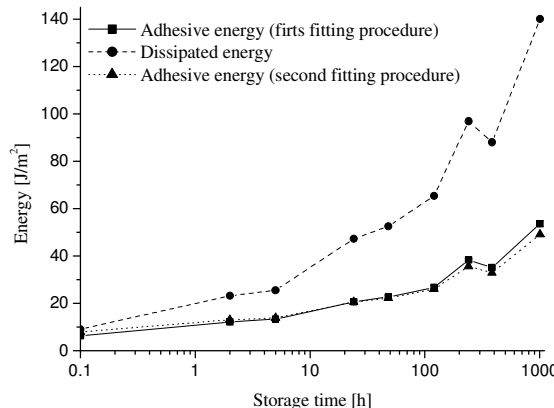


**Figure 4.3.** Storage time dependence of the adhesive energies and the energy dissipated for the plastic deformation of the copper coating. The largest standard deviation of the adhesive energy is about  $1.2 \text{ J/m}^2$ .

A fast increase of the adhesive energy, by a factor of 3.5, is observed during the initial 48 hours of sample storage after the galvanic deposition. The increase continues even after this period but at a much lower rate. The adhesive energy increases another 2.5 times over the next 960 hours. The water content in the sample changes as a function of the storage time (Figure 4.4) as well. It decreases strongly and reaches a constant value after 48 hours of the storage time.

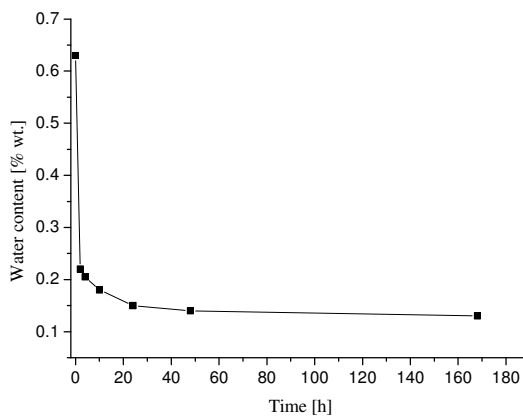


**Figure 4.4.** Change of the water content in the sample following galvanic deposition (sample stored in a desiccator between the measurements).

Water at the interface significantly influences the adhesive energy measured by the peel test. In Figure 4.5 a drop of the peel force is visible if water is added to the crack tip during the crack propagation. The peel force plateau changes from 2.46 N in the ambient conditions to 2.22 N once the water is present at the crack tip. The corresponding adhesive energies are 35.3 J/m<sup>2</sup> and 32.2 J/m<sup>2</sup>.

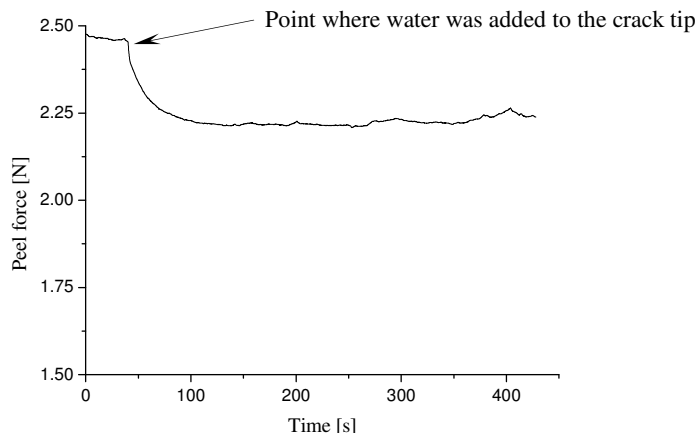


**Figure 4.5.** Peel force plateau for the crack propagation under the ambient conditions and with water at the crack tip (ABS/18.6 µm Cu, 400 hours after galvanic deposition, delamination speed 0.707 mm/min).

A close look at the fracture surfaces reveals completely adhesive failure of the interface directly after galvanic deposition (micrographs not shown), which changes during the period of 1008 h of storage time to cohesive failure, mostly within the substrate and, for the small remainder, in the film. The roughness of the substrate peeled within the first 48 h remains close to the roughness of the blank substrate, roughness  $R_a = 0.02 \mu\text{m}$  compared to  $0.01 \mu\text{m}$  (see Section 3.1), while after 1008 hours of storage, due to the cohesive break, the roughness of the peeled substrate increases to  $R_a = 0.11 \mu\text{m}$ . In Figure 4.6 residues of the polymer on the peeled copper film and the damaged substrate fracture surface are shown. These micrographs indicate the cohesive failure within the substrate, an occurrence characteristic for contact between oxidized polymers and metals<sup>[4]</sup>.

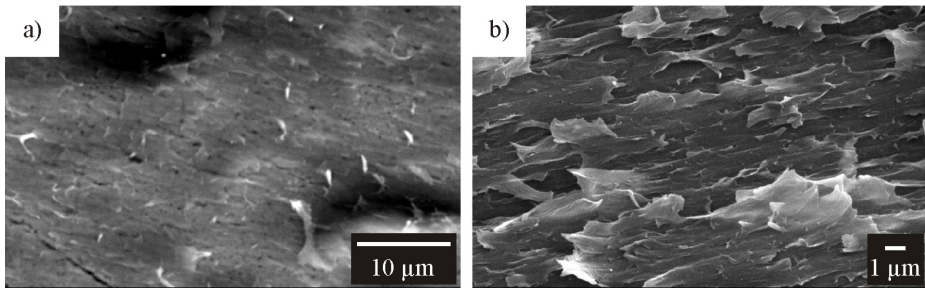


**Figure 4.6.** SEM images of fracture surfaces (a) copper side (b) substrate side. (Accelerating voltage 15 kV). Storage time 1008 hours.

The cohesive failure within the coating is strongly localized and becomes visible through copper islands on the peeled substrate (Figure 4.7). The size of the islands is  $30.0 \pm 9.5 \mu\text{m}$  and the number density is  $6.94 \text{ mm}^{-2}$  estimated on the basis of 44 measurements. So, the cohesive break in the film constitutes 2 % of the total fracture surface. Because the height of the copper islands on the peeled substrate ( $0.55 \pm 0.04 \mu\text{m}$ , 10 measurements) matches the thickness of the sputtered films ( $0.48 \pm 0.05 \mu\text{m}$ ), it is concluded that the crack, at these points, runs along the copper(sputtered)/copper(electroplated) interface.

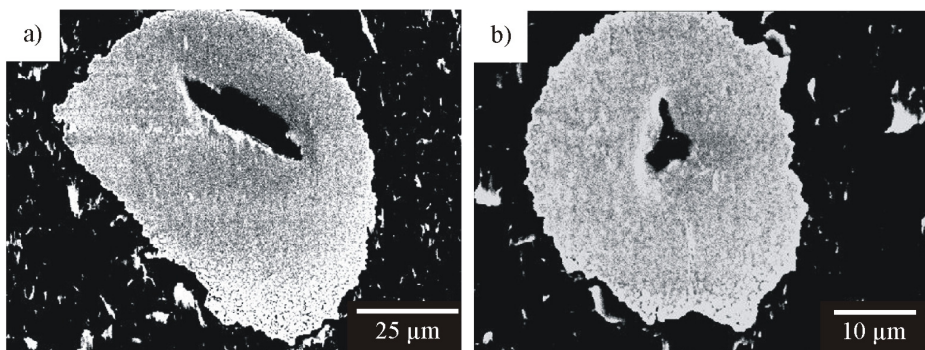


**Figure 4.7.** Copper remains on the substrate after the peeling (a and b). (Accelerating voltage 15 kV). Storage time 1008 hours.

In Figure 4.8 SEM micrographs of non-peeled copper surfaces in contact with the substrate are shown. Freshly deposited copper films have a fine structure, with visible circular pores uniformly distributed along the surface, while the aged copper film has

much rougher structure with larger elongated voids on the surface. The differences in the images indicate that time dependent structural changes take place within the copper films. The reason for these changes remains a puzzle so far.

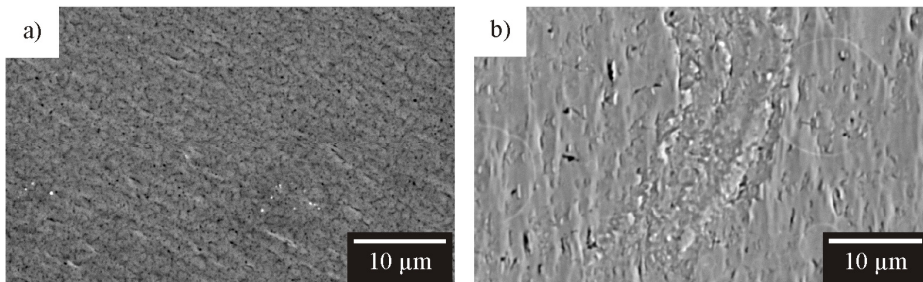


**Figure 4.8.** SEM images of a) freshly deposited (Accelerating voltage 20 kV) and b) copper films stored for 2880 h (Accelerating voltage 15 kV). Side originally in the contact with the substrate is shown. Note the much rougher features on the image b).

Contact angle measurements (Figure 4.9) show a large difference between the two ABS surfaces that were investigated. The initial difference of approximately  $18^\circ$  indicates a large difference between the substrate surface that has been in contact with the copper coating for 1008 h (upper surface in Figure 4.2) and the opposite, non-coated side (lower surface in Figure 4.2). The latter acts as a reference and is expected to represent the starting surface structure of the ABS substrate. Apparently, the upper surface structure is unstable in contact with air as the contact angle changes in time towards the value measured on the lower, reference surface. However, because the contact angle reaches a more or less constant value after 48 hours, a complete matching of the two values is not expected to occur afterwards (see Section 5.4 for explanation). Gradual changes of the surface energy (or the contact angle) for *poly(vinylchloride)* and *poly(ethyelene)* surfaces after the contact with gold have already been reported<sup>[15]</sup>.

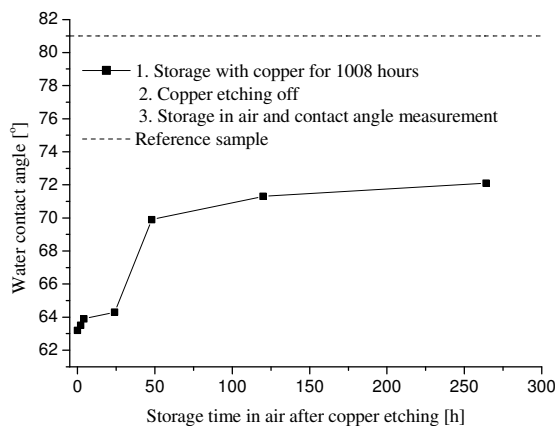


**Figure 4.9.** Water contact angle change on ABS surface in contact with air. After 1008 h of storage time the copper coating was etched off. The reference value is  $81.0 \pm 0.6^\circ$  (average of 7 measurements).

The increase of the adhesion strength with time is most likely related to the nature of the galvanic deposition process. One of the main consequences of the combination of sputtering and galvanic deposition for the sample preparation is introduction of water into the sample during the galvanic deposition. Because the initially sputtered copper layers are very porous<sup>[16]</sup> and have large cracks (see Section 3.2 Figure 3.5b), water easily diffuses and accumulates at the interface. If small amounts of copper oxide are initially present in the sputtered films, they will be dissolved by acid present in the galvanic deposition bath, resulting in voids where water can accumulate. In a preliminary phase it was even observed that heavily oxidized initial layers cause a complete delamination of the films from the substrate before the electrochemical deposition started.

Once the galvanic deposition is completed, a sample has a water-saturated interface. Accordingly, the copper and ABS surfaces cannot make an intimate contact to form strong van der Waals interactions but are separated by a layer of molecular ‘contamination’<sup>[3,5,17]</sup>. During the initial 48 hour period, water diffuses out of the sample lowering both the interface and the bulk water content. The two materials come into closer contact establishing stronger bonds thereby causing a steep adhesive energy

increase within this period. A similar effect was reported for spontaneous recovery of the adhesion strength for polymer–aluminum system exposed to aqueous salt solution<sup>[18,19]</sup>. Diffusion of water to the interface lowers the adhesion compared to the original value<sup>[20,21]</sup> when the water was added to the propagating crack tip, and its removal causes spontaneous recovery of the adhesion strength<sup>[18]</sup>.

If the samples are stored for longer than 48 hours, the magnitude of the adhesion still increases in time, but this can no longer be ascribed to the removal of the water present at the original interface. One explanation for the additional increase of the adhesive energy is that structural changes occur on both materials near the interface. Indication that the interface changes its structure and therefore the adhesive energy can be found in Figure 4.5. Although water was added to the crack tip (water saturated interface similar to the starting sample directly after the galvanic deposition), the measured adhesive energy is much higher than the one measured at zero storage time. The only reason these two values show mismatch is that two interfaces are actually structurally (and possibly chemically) different. Roughening of the interface, identified by a change of the morphology of the copper surface in contact with the substrate, increases the contact area of the two materials, leading to the increase of the adhesive energy. On the other hand, once intimate contact is achieved a rearrangement within the polymer surface takes place. Molecules reorient themselves into an energetically most favorable position thereby increasing van der Waals interactions and possibly establishing Coulomb interactions. At certain points these van der Waals and Coulomb interactions become stronger than on the rest of the ABS/copper interface as manifested by the presence of the copper islands on the peeled polymer surface. For the samples stored for a long time and regions where the copper islands are seen, the intermaterial interactions are stronger than the strength of either the polymer itself or the copper–copper interface. A strong influence of the contacting surface on the polymer structure near the interface for *poly(ethylene)*-steel system has already been reported<sup>[22]</sup>.

An interesting fact to notice is that the adhesion increase ascribed to the water removal from the interface is ten times faster than the increase associated with the structural changes of the interface,  $0.3 \text{ J/m}^2\text{h}$  as compared to  $0.03 \text{ J/m}^2\text{h}$ .

Having all of the above in mind, a suggestion for the interface development can be made here. Due to prolonged contact time between the copper and ABS, a third interface in the system is developing. In addition to the originally PVD formed copper/ABS interface and copper(sputtered)/copper(electroplated) interface a (bulk ABS)/(ABS with changed structure) interface is formed. Schematically, the formation of this interface in time and its consequences on the measured adhesive energy can be represented as in Figure 4.10. The only assumption that needs to be made is that the copper(sputtered)/copper(electroplated) interface has a constant adhesive energy in time. Due to the rearrangements of polymer molecules near the interface (see Chapters 5 and 6), bonding between copper and ABS becomes stronger in time, increasing the ABS/copper adhesive energy (Figure 4.10 solid line). At the same time, triggered by the same changes, the ABS/ABS interface is formed and its adhesive energy decreases starting from the bulk strength of the polymer (Figure 4.10 dotted line). As long as the adhesive energy is measured in the time region where the three curves do not cross each other, the ABS/copper adhesive energy is measured and the interface exhibits a completely adhesive break. The moment the interception point is crossed, failure during the peel test will change to cohesive and one will measure the adhesive energy of the ABS/ABS interface. It is concluded from these measurements that after a certain time the copper/ABS interface becomes stronger than the ABS/ABS interface.

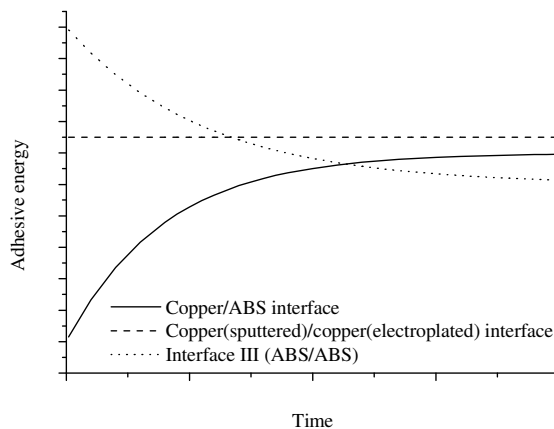


**Figure 4.10.** Schematic representation of the adhesive energy dependence on the storage time.

The presented idea of the additional interface development can explain the time dependence of the failure characteristics qualitatively. However, the nature of the changes within the polymer is still puzzling and the phenomena will be investigated in more detail in the following chapter.

#### 4.4 Conclusions

The adhesive energy increases with time as a result of two different processes. An initial steep increase on a relatively short time scale (48 h storage) is a result of the water removal from the water saturated interface formed during the galvanic deposition. A slower increase is observed on a longer time scale (next 960 h storage) and this is attributed to the structural rearrangement of the materials in contact. Roughening of the copper surface increases the contact area between the two materials, while the polymer surface changes, as detected by the contact angle measurements, probably causing formation of stronger bonds along the interface. The mode of failure also changes with time from purely adhesive to partially cohesive within the substrate and the film.

## References

- [1] J. Y. Song, J. Yu *J. Acta Mater.* **2002**, *50*, 3985–3994.
- [2] B Rånby, *Int. J. Adhes. Adhes.* **1999**, *19*, 337–343.
- [3] K. Kendall, *Science*, **1994**, *263*, 1720–1726.
- [4] S. S. Pesetskii, B. Jurkowski, A. I. Kuzakov, *Int. J. Adhes. Adhes.* **1998**, *18*, 351–358.
- [5] N. A. de Bruyne, *Nature*, **1957**, *180*, 262–265.
- [6] S. Kim, G. Y. Choi, A. Ulman, C. Fleischer, *Langmuir*, **1997**, *13*, 6850–6856.
- [7] A. R. C. Baljon, J. Vorselaars, T. J. Dapuy, *Macromolecules*, **2004**, *37*, 5800–5806.
- [8] K. M. Yin, H. Z. Wu, *Surf. Coat. Technol.* **1998**, *106*, 167–173.
- [9] I. S. Park, J. Yu, *Acta Mater.* **1998**, *46*, 2947–2953.
- [10] Y. B. Park, I.S. Park, Jin Yu, *Mater. Sci. Eng. A* **1999**, *266*, 261–266.
- [11] G. de With, *Structure, deformation, and integrity of materials*, vol. 1, Wiley–VCH, Weinheim, **2006**.
- [12] J. E. Shigley, C. R. Mische, *Mechanical engineering design*, McGraw–Hill Higher Education, London, **2001**, p. 1173.
- [13] M. Schlesinger, M. Paunovic, *Modern electroplating*, Wiley-Interscience, New York, **2000**, p. 79.
- [14] R. F. Bunshah, J. M. Blocher Jr, T. D. Bonifield, J. G. Fish, P. B. Ghate, B. E. Jacobson, D. M. Mattox, G. E. McGuire, M. Schwartz, J. A. Thorton, R. C. Tucker Jr. *Deposition Technologies for Films and Coatings: Developments and Applications*, Noyes Publications, Park Ridge, **1982**, p. 213.
- [15] J. F. M. Pennings, B. Bosman, *Colloid Polym. Sci.* **1979**, *257*, 720–724.
- [16] P. Benjamin, C. Weaver, *Proc. Roy. Soc. A*, **1961**, *261*, 516–531.
- [17] R. G. Horn, J. N. Israelachvili, *J. Chem. Phys.* **1981**, *75*, 1400–1411.
- [18] I. V. Kalashnikova, V. V. Matveev, V. V. Arslanov, *Colloid J.* **1996**, *58*, 722–729.
- [19] V. V. Arslanov, I. V. Kalashnikova, *Colloid J.* **1996**, *58*, 697–706.
- [20] S. Devasahayam, *J. Appl. Polym. Sci.* **2006**, *99*, 2052–2061.
- [21] A. Jain, V. Gupta, S. N. Basu, *Acta Mater.* **2005**, *53*, 3147–3153.
- [22] W. Kalnins, J. Ozolins, *Int. J. Adhes. Adhes.* **2002**, *22*, 179–185.

## CHAPTER 5

### CHEMICAL CHANGES OF THE ABS NEAR THE INTERFACE WITH COPPER<sup>\*\*</sup>

**Summary:** In this chapter the structural changes of the polymer near the interface, observed and described in Chapter 4, will be probed in more detail. Possible chemical changes of the ABS near the interface will be analyzed as well. It will be shown that developed carbonyl functionalities on the ABS surface are most likely responsible for the large increase in the adhesion strength. The chemical changes of the polymer are probably a consequence of the galvanic deposition and a close contact of the ABS with copper which is known to facilitate the oxidation of ABS. The ABS changes will be monitored using attenuated total reflectance Fourier transform infrared spectroscopy (ATR–FTIR) and contact angle measurements. Using scanning force microscopy measurements, the FTIR and contact angle results will be further supported. Finally a more or less complete picture of the ABS/Cu(sputtered)/Cu(electroplated) system lifeline will be presented.

---

<sup>\*\*</sup> The main part of this chapter has been accepted for publication: S. Kisin, F. Scaltro, P. Malanowski, P. G. Th. van der Varst, G. de With, Chemical and structural changes at the ABS polymer–copper metal interface, *Polym. Degrad. Stabil.* **2006**.

## 5.1 Introduction

Due to a large mismatch between the surface energies of metals and polymers, the adhesion between these two types of materials is usually low<sup>[1]</sup>. Oxidation of polymer substrate surfaces is one of the techniques most commonly used to promote the adhesion of polymers to metals. The oxidation can be done prior to the interface formation or during the interface formation<sup>[2-7]</sup>. Polymer substrates can also be selectively oxidized to provide local high adhesion to metallic coatings, a procedure used in “plasma” printing<sup>[8]</sup>. Not only does the adhesion strength depend on the oxygen containing groups present at the polymer surface, but also on the nature of the metallic surface in contact with it<sup>[9,10]</sup>.

In the specific case of ABS, chemical modification of the ABS surface with polar groups such as carbonyl, carboxyl, or sulphate enhances the chemical interaction with the metallic coatings<sup>[11,12]</sup>. However, for copper coated ABS an increase of adhesion strength with sample storage time was observed even though no intentional pre and/or post-treatment of materials in contact was done. An energy of  $6.3 \pm 0.3 \text{ J/m}^2$  is needed to separate the interface directly after the galvanic deposition and this value rises to  $53.7 \pm 1.2 \text{ J/m}^2$  if the samples are stored for 1008 hours (see Section 4.3). During this time interval the mode of failure changes from completely adhesive to partially cohesive within the polymer and, very localized, within the copper film (see Section 4.3).

To investigate possible chemical and structural changes of the polymer near the interface, samples were prepared in the same way as those used for the peel test in Section 4.3 and analyzed using contact angle measurements and attenuated total reflectance Fourier transform infrared spectroscopy (ATR-FTIR).

For independent conformation of the changes of the polymer chemistry and/or morphology, scanning force microscopy (SFM) examinations were performed on the freshly deposited ABS substrate and on the substrate in contact with copper for 1008 hours.

## 5.2 Experimental

All experiments were done on the samples prepared according to the procedure described in Section 3.2. No changes to the film deposition procedure have been made as compared to the conditions used to prepare the samples analyzed in Chapter 4, so the thickness of the copper films is assumed to remain around 18.6 because the PVD and galvanic deposition process parameters were the same as for the samples in Chapter 4.

### 5.2.1 Contact angle, infrared and SFM measurements

Two different sets of water contact angle measurements were done. Directly after galvanic deposition the copper coating was peeled<sup>††</sup> from the substrate and the measurement was done. The substrate thus prepared was then stored in air and the measurement repeated after 2 and 4 hours. Secondly, the ABS–copper samples were stored for 2, 4, 24, 48, 120, 240, 384 and 1008 hours in a dry atmosphere. After each storage period the copper coating was etched off using 40% sulfuric acid and the water contact angle was measured. The water contact angle measurements on the original ABS polymer plates, treated with sulfuric acid, were done as reference measurements to make sure that any changes observed are not a consequence of the etching procedure. For the exact procedure followed for the contact angle measurements, see Section 4.2.3 and Figure 4.2.

ATR-FTIR spectroscopy was done using a BioRad spectrometer equipped with a diamond crystal. Spectra were recorded with  $4\text{ cm}^{-1}$  resolution co-adding 30 scans in a range  $4000\text{--}650\text{ cm}^{-1}$ . The original substrate used for copper deposition, the substrate after the PVD deposition (copper etched off), the substrate treated in the same way as during the etching procedure and the substrate of the samples stored for 100, 384 and 1008 hours in a desiccator (copper etched off) were analyzed. Changes were monitored

---

<sup>††</sup> For the freshly deposited sample, the interfacial water layer is expected to be present between copper and ABS. The coating was thus peeled off because the interfacial layer would have been removed if a wet etching procedure was used to remove the copper coating.

in the carbonyl region ( $1730\text{ cm}^{-1}$ ) and in the butadiene region ( $960\text{ cm}^{-1}$  and  $910\text{ cm}^{-1}$ )<sup>[13]</sup>.

Force distance curves for a freshly deposited sample and on ABS substrate stored with copper for 1008 h were recorded using Solver P47H SFM (NT-MDT, Russia) under a controlled relative humidity (17 %) conditions (within a home build atmosphere chamber). Measurements were done with the standard silicon tip (NSG01, NT-MDT, Russia). The presented curves consist of the average of 50 force curves recorded on the same surface spot. After each measurement it was carefully checked, that the recording of the force curves did not modify or destroy the sample surface.

### 5.3 Results

If water contact angle values measured on the substrate, from which the copper coating was removed directly after the galvanic deposition, are compared to the reference samples a large difference is visible. The contact angle for the deposited plate, around  $65.4^\circ$ , is approximately  $15^\circ$  lower than for the reference sample (Figure 5.1). However, after 4 hours of exposure to air this value increases up to  $79.9^\circ$ , close to  $81.0^\circ$  the value measured on the reference sample (Figure 5.1).

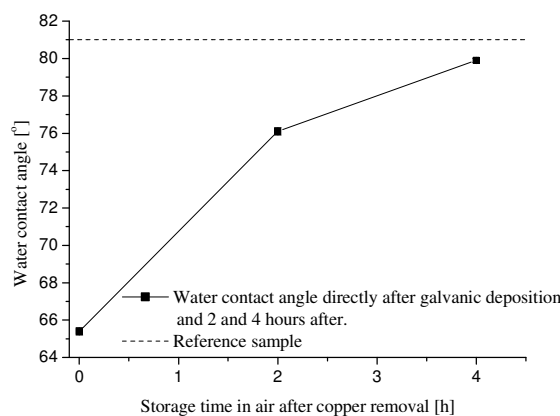


**Figure 5.1.** Water contact angle change on the ABS surface stored in air. At time zero (directly after the galvanic deposition) the copper coating has been peeled off and the measurement was done. This substrate sample was subsequently stored in air and the measurements repeated after 2 and 4 hours. The reference value is  $81.0 \pm 0.6^\circ$  (average of 7 measurements).

In the case of samples stored with a copper coating, a different trend is observed. The initial value, corresponding to zero storage time, is, of course, the same as in Figure 5.1, it reaches a value similar to the reference sample within 2 hours<sup>‡‡</sup> and subsequently decreases with storage time to 61.5° (Figure 5.2).

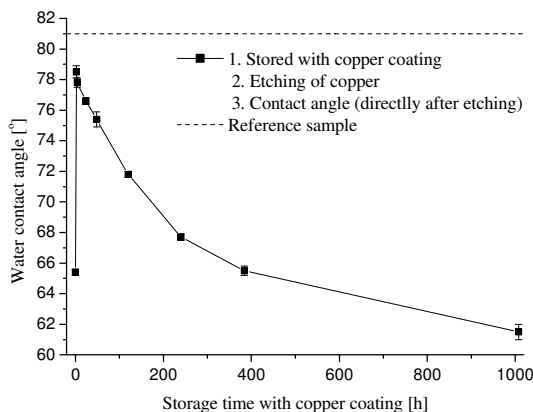


**Figure 5.2.** Change of the water contact angle on the ABS surface stored with the copper coating. The reference value is  $81.0 \pm 0.6^\circ$  (average of 7 measurements). Point for 0 storage time taken from Figure 5.1.

An observation made in Section 4.3 and plotted in Figure 4.8 will be repeated here for the sake of clarity and completeness of the results. If the substrate stored for 1008 hours in contact with the copper coating is exposed to air after etching off the copper, a gradual increase of the water contact angle is observed (Figure 4.8). The value does not reach the reference value within the storage time interval studied but it reaches a more or less constant value after 48 hours and a complete matching of the two values is not expected to occur afterwards.

In Figure 5.3 the ATR–FTIR spectra of the blank substrate, the substrate treated with 40% sulfuric acid (the same treatment as during the copper etching procedure) and the substrate from which the copper coating has been etched off after the PVD deposition only are compared. No differences can be observed.

<sup>‡‡</sup> The contact angle values for the samples stored for 2, 4, 24 and 48 hours might have been more representative if the copper coating for these samples was peeled off the substrate rather than etched as the interfacial water layer is expected to be present.

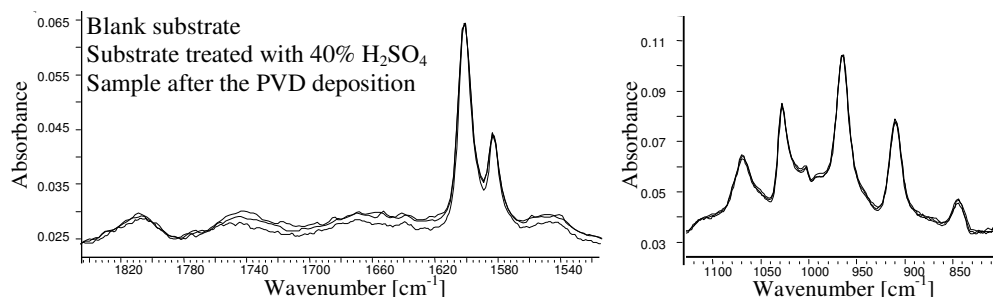


**Figure 5.3.** ATR-FTIR spectra of the blank substrate, substrate treated with 40% sulfuric acid (same as during the copper etching procedure) and the substrate from which the copper was etched off after the PVD deposition only.

If the FTIR spectra of the blank substrate and those which were in contact with the copper coating for 100, 384 and 1008 hours are compared, differences are visible (Figure 5.4). The main discrepancies in the spectra appear in the 1730 cm<sup>-1</sup> range, and more subtle differences are observable at 960 cm<sup>-1</sup> and 910 cm<sup>-1</sup>. If these four samples are compared and the area under the curve in the region between 1784 and 1616 cm<sup>-1</sup> of the blank sample is used as a unit of measurement, the samples can be ranked in the sequence shown in Table 5.1. As a baseline for these calculations, the intensity of the spectra in the inert region, 2200–2000 cm<sup>-1</sup>, was used. Comparing only the blank substrate and the substrate stored with the copper coating for 1008 hours, it can be said that the surface area under the 960 cm<sup>-1</sup> peak decreases by approximately 15% and the area under the 910 cm<sup>-1</sup> peak goes down by 5%. The surface areas under the same peaks for the remaining two samples are in between the two extremes.

Storage time with copper [h]	Rank
0 (Blank substrate)	1
100	1.4
384	1.5
1008	2.1

**Table 5.1.** Ranking of the samples stored for different times with the copper coating according to the surface area under the FTIR spectra in Figure 6 (Region 1784–1616 cm<sup>-1</sup>).

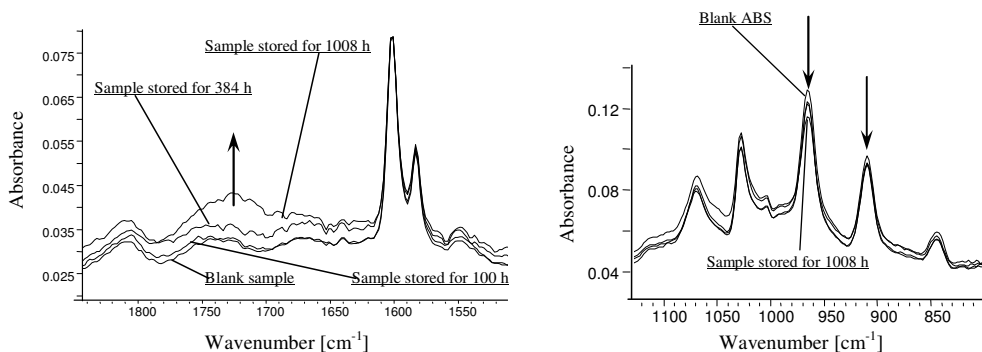


**Figure 5.4.** ATR-FTIR spectra of the blank ABS substrate and the substrates that were stored with the copper coating for 100, 384 and 1008 hours. Arrows indicate increasing and decreasing peaks. Note that in the right spectra lines for the samples stored for 100 and 384 hours with copper almost coincide and are in between the blank and 1008 hour stored sample.

In Figure 5.5 FTIR spectra of the fracture surfaces are shown and compared to the blank sample. Both fracture surfaces differ from the starting ABS surface. The ABS residues on the copper film show the highest intensity peak at 1730 cm<sup>-1</sup> region. Peaks at 965 cm<sup>-1</sup> are identical for the blank substrate and the ABS fracture surface while the copper fracture surface shows a significantly lower intensity peak. At 910 cm<sup>-1</sup> all three surfaces are different and the peak intensity decreases from the blank substrate via the ABS fracture surface to the ABS residues on copper.

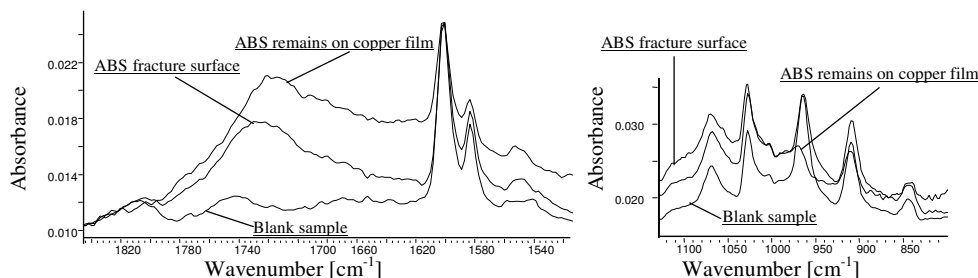


**Figure 5.5.** Comparison of the fracture surfaces and the blank ABS substrate. The sample used for the peel test was stored for 1008 hours.

The surfaces of the freshly deposited substrate and the substrate stored for 1008 hours with copper coating were independently checked by SFM measurements and the resulting force-distance curves are shown in Figure 5.6. Differences can be seen by

comparing the two sets of the curves. For the sample from which the copper coating was removed directly after the galvanic deposition, the cantilever approaches the ABS surface without showing a snap-in effect (Figure 5.6a) and starts indenting the sample once it approached the surface completely. The retracting curve shows a significant retardation as compared to the approach curve suggesting that the tip penetrated the surface significantly and is “trapped” within the surface. For the 1008 hours old sample, only a small snap-in effect can be seen and the retraction curve follows the approach curve very well (Figure 5.6b).

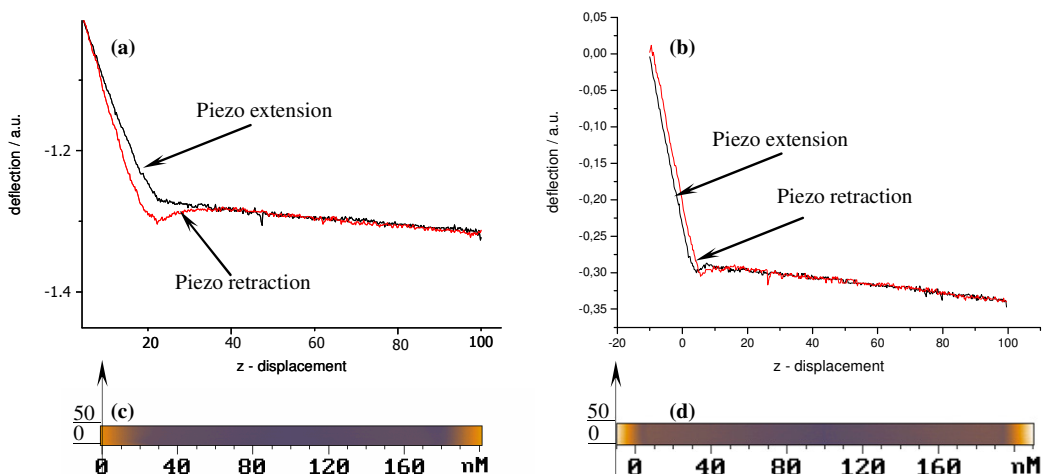


**Figure 5.6.** Force–distance curves (deflection expressed in arbitrary units) recorded with silicon tips on ABS substrate from which the copper coating was removed directly after the galvanic deposition (a) and on the substrate stored with copper for 1008 hours (b) (copper coating etched off). Figures (c) and (d) are a collection of 50 subsequently recorded force curve cycles and are the indication for the reproducibility of the measurements.

## 5.4 Discussion

Due to the high porosity<sup>[14]</sup> and cracks present in the initially PVD sputtered films (see Section 3.2, Figure 3.5b), water and ions present in the galvanic bath will diffuse to the interface during the galvanic deposition. If the copper coating is removed directly after the deposition and the water contact angle  $\theta$  is measured on the substrate, the value of  $\theta$

is low due to water and ions present on the surface. After 4 hours of exposure to air, this layer dries out and the contact angle returns to the original, reference level. If the copper is not removed, the contamination layer remains trapped and induces changes at the interface.

The main constituent of the chemically non-modified ABS is the SAN phase. In the case of this copolymer it can be expected that the nitrile group, the functional group of the acrylonitrile residue, shows only a relatively weak interaction with a metal center via coordination through the lone pair of the N atom and through the  $\pi$ -system of the CN triple bond<sup>[15]</sup>. The styrene residue can show a somewhat higher interaction via the aromatic ring<sup>[16]</sup> and attribute more significantly to the adhesion strength. However, chemical changes of the polymer were confirmed by FTIR measurements and identified them as the initial stages of ABS oxidation<sup>[17,18]</sup>. During this process, saturated and  $\alpha$ - and  $\beta$ - unsaturated carbonyl bands developed at 1725, 1665, 1685 and 1699  $\text{cm}^{-1}$  resulting in a wide band (area twice the size as compared to the blank ABS) as can be seen in Figure 5.4 between 1784 and 1616  $\text{cm}^{-1}$ . Peaks originating from pBd double bonds decrease at 965 and 910  $\text{cm}^{-1}$ . The newly formed oxidized surface is more hydrophilic as compared to the original ABS surface and the water contact angle, accordingly, decreases (Figure 5.2). Once the copper is etched off the substrate in a sample stored for 1008 hours and the surface is exposed to air, the water contact angle starts to increase, but never reaches the reference level (see Section 4.3, Figure 4.9). In the view of the fact that the sample stored for 1008 hours is chemically different from the reference sample, the mismatch of the contact angle values is understandable. The increase of the water contact angle value with time, when the oxidized surface is exposed to air, indicates that structural rearrangement of the polymer at the surface takes place too.

Although no changes were observed when FTIR spectra of the ABS plates sputtered with copper were compared to the blank substrate (Figure 5.3), it is plausible that during the PVD procedure oxidation of the polymer substrate starts. In the PVD chamber is ABS exposed to severe copper atom bombardment and water is readily present during the sputtering process. If only a few atomic layers are oxidized during this procedure it is impossible to spot these changes from the ATR-FTIR spectra. Subsequently, water

and ions from the galvanic bath can accelerate the oxidation process. The influence of the PVD preparation process on the properties of metal-polymer hybrid systems has been reported<sup>[19,20]</sup>. Copper is also known to accelerate the oxidation of ABS<sup>[21]</sup> as well as some other polymers<sup>[3]</sup>. One must not forget here that during the sputtering process not only pure copper is deposited, but copper-oxides as well and the catalytic activity of metal oxides for polymer oxidation<sup>[22]</sup> could very well be the reason for starting the ABS oxidation. The influence of copper-oxides at the copper surface on the adhesion will be evaluated later using the molecular dynamics simulations.

The oxygen containing groups so formed, bond strongly to copper causing a ten-fold increase of adhesion energy with time. During the same period the mode of failure changes from adhesive to cohesive, an occurrence characteristic for contact between oxidized polymers and metals<sup>[2]</sup>. Copper does exhibit a strong adhesion to polymers with high oxygen content<sup>[19]</sup> and an adhesion increase due to copper-oxygen-polymer bonding in *poly(styrene)*-copper systems has already been observed<sup>[23,24]</sup>. Since styrene constitutes a significant part of the ABS, a similar mechanism can be expected for our system.

In Figure 5.5 the highest intensity of the carbonyl groups is seen on the copper fracture surface. This can be explained in two different ways. Either the majority of the groups is left on the copper film after the peeling, or the polymer residues on copper are more oxidized as compared to the ABS fracture surface. On the other hand, the pBd carbon-carbon double bonds are either mainly left over on the substrate after the peeling or are strongly degraded in the residues on the copper. If the pBd carbon-carbon double bonds are mainly left over on the substrate, it can be said that the bonding between ABS and copper is achieved mainly via the SAN-copper interactions and pBd-copper interactions contribute to the adhesion to a lower extent. If pBd carbon-carbon double bonds are strongly degraded within the polymer residues on copper nothing can be said about the contribution of the individual phases to adhesion, but it can be said that it seems likely that the oxidation of the pBd phase is confined to a much thinner surface layer as compare to the SAN phase.

The change of failure mode during the peel test (0 hours stored sample compared to 1008 hours stored one) and the identified chemical changes strongly suggest that, in

time, a layer of ‘changed’ polymer is formed near the interface. This layer is bonded more strongly to copper than to the underlying polymer and the crack propagation during the peel test follows this additionally formed interface rather than the original copper–ABS interface.

### 5.5 Proposition for the ABS–copper interface “life line”

Finally, the idea of the interface evolution presented in brief in Figure 4.10 can be elaborated, the interface “life line” is schematically shown in Figure 5.7. In time a layer of chemically and morphologically altered layer of ABS is formed near the interface with copper. This layer has different properties as compared to the bulk ABS properties, thus creating an ABS/ABS interface. During the time period where the adhesion of this interface is higher than the adhesive energy of the ABS/Cu interface, the peel failure is completely adhesive and the adhesive energy of the interface of interest is measured. The moment the ABS/ABS adhesive energy becomes similar or lower than that of the ABS/Cu interface, failure becomes partially adhesive and partially cohesive within the substrate. At localized points of stronger interactions, the ABS/ABS and ABS/Cu adhesive energy is very high and the Cu/Cu interface becomes the weakest link of the system making the crack propagate along Cu/Cu interface, leaving a copper island on the ABS upon peeling (see Section 4.3, Figure 4.7). Finally, what can be experimentally measured by the peel test is the width averaged adhesive energy for all three interfaces.

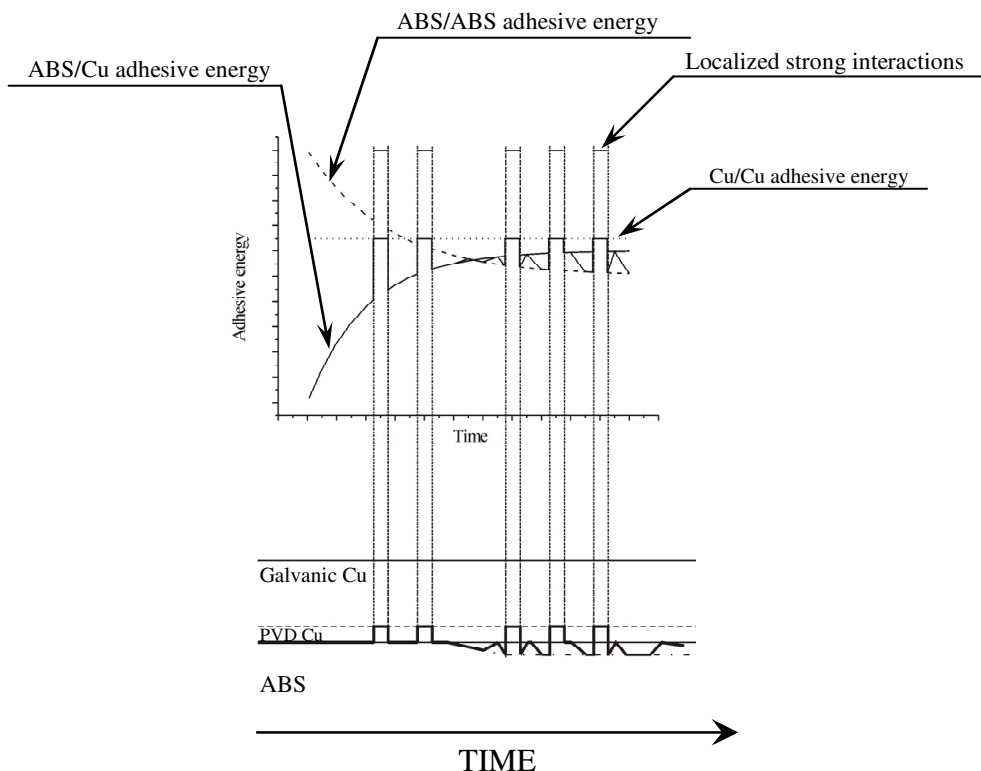


**Figure 5.7.** Schematical representation of copper–ABS interface “life line”.

## 5.6 Conclusions

In this chapter, the chemical and structural changes of ABS polymer near the interface in the ABS–copper system were reported. Using water contact angle and SFM measurements, structural changes of the polymer were identified, while chemical changes were observed using ATR–FTIR measurements. In time, carbonyl moieties develop at the substrate side of the interface causing the change of the contact angle and most probably causing the increase of the copper adhesion to ABS. Oxidation of the substrate might be started during the copper PVD deposition and subsequently accelerated by the water and ions from the galvanic bath, or could be just triggered by the galvanic deposition. In giving a conclusive answer to this question, ATR–FTIR was not useful due to its detection limit. Possible catalytic influence of copper–oxides should not be overlooked. There are also some indications that in the system investigated,

adhesion is achieved predominantly through SAN-copper interactions and not via pBd-copper interactions (discussed in more detail in Chapter 6). To compare the behavior of the two ABS constituent polymers (SAN and pBd) on copper and copper–oxides surfaces, MD simulations will be used to estimate their thermodynamic work of adhesion and gain more insight into the adhesion mechanism of ABS to copper.

All data discussed were used to present a proposal for the development of the copper–ABS interface in time. Most notable, the interface strength of the original interface increases causing a large increase in the measured adhesive energy. A third interface is believed to develop at the end of the studied time interval.

## References

- [1] B Rånby, *Int. J. Adhes. Adhes.*, **1999**, *19*, 337–343.
- [2] S. S. Pesetskii, B. Jurkowski, A. I. Kuzakov, *Int. J. Adhes. Adhes.*, **1998**, *18*, 351–358.
- [3] M. Kalnins, J. Malers, *J. Adhes.*, **1995**, *50*, 83–102.
- [4] S. Siau, A. Vervaet, E. Schacht, S. Degrande, K. Callewaert, A. van Calster, *J. Electrochem. Soc.*, **2005**, *152*, D136–D150.
- [5] J. L. Jordan, P. N. Sandra, J. F. Morar, C. A. Kovac, F. J. Himp sel, R. A. Pollak, *J. Vac. Sci. Technol. A*, **1986**, *4*, 1046–1048.
- [6] J. Cognard, *C. R. Chimie*, **2006**, *9*, 13–24.
- [7] J. Y. Song, J. Yu, *J. Acta Mater.*, **2002**, *50*, 3985–3994.
- [8] S. Kreitz, C. Penache, M. Thomas, C. P. Klages, *Surf. Coat. Tech.*, **2005**, *200*, 676–679.
- [9] K. Bright, B. W. Malpass, D. E. Packham, *Nature*, **1969**, *223*, 1360–1361.
- [10] C. Seidel, H. Kopf, B. Gotsmann, T. Vieth, H. Fuchs, K. Reih s, *Appl. Surf. Sci.*, **1999**, *150*, 19–33.
- [11] P. Yen, *Polymer*, **1995**, *36*, 3399–3400.
- [12] C. A. Villamizar, J. Rojas, P. Frias, *Met. Finish.*, **1981**, *79*, 27–33.
- [13] M. V. Motyakin, S. Schlick, *Polym. Degrad. Stabil.*, **2006**, *91*, 1462–1470.
- [14] P. Benjamin, C. Weaver, *P. Roy. Soc. A*, **1961**, *261*, 516–531.
- [15] B. H. L. T. Kato, *Surf. Sci.*, **1993**, *284*, 167–174.
- [16] W. Possart, S. Dieckhoff, *Int. J. Adhes. Adhes.*, **1999**, *19*, 425–434.
- [17] X. Jouan, J. L. Gardette, *J. Polym. Sci. A*, **1991**, *29*, 685–696.
- [18] J. F. Rabek, *Polymer Photodegradation: Mechanisms and Experimental Methods*, Chapman & Hall, London, **1995**, p. 243.
- [19] J. Božović Vukić, S. Hoeppener, D. A. Kozodaev, S. Kis in, B. Klumperman, U. S. Schubert, G. de With, C. E. Koning, *ChemPhysChem*, **2006**, *7*, 1912–1916.
- [20] J. Božović Vukić, *Block copolymers for adhesion improvement synthesized via RAFT-mediated polymerization*, PhD Thesis, Technische Universiteit Eindhoven, Eindhoven, **2006**.
- [21] M. Day, J. D. Cooney, M. MacKinnon, *Polym. Degrad. Stabil.*, **1995**, *48*, 341–349.
- [22] W. Brockman, *J. Adhes.*, **1989**, *29*, 53–61.
- [23] J. M. Burkstrand, *Appl. Phys. Lett.*, **1978**, *33*, 387–389.
- [24] J. M. Burkstrand, *J. Appl. Phys.*, **1981**, *52*, 4795–4800.

## CHAPTER 6

### ADHESION ON A MOLECULAR LEVEL: MOLECULAR DYNAMICS CALCULATIONS<sup>§§</sup>

**Summary:** In this chapter the option to use force field molecular dynamics calculations to deduce the work of adhesion for copper–ABS interface will be investigated. The work of adhesion will be calculated from the “single molecule” approach using interactions between single molecules constituting the ABS polymer (SAN and pBd) and copper (oxide) surface using their van der Waals contact area as interaction surface. It will be shown that the calculated work of adhesion is independent of the number of polymer molecules present on the copper surface, of the monomer residue sequence within the polymer molecule and independent of the type of the copper surface. The influence of introducing oxygen atoms to the metallic surface and the polymer molecules on the work of adhesion will be evaluated. Finally, interactions between copper (oxide) surfaces and a high oxygen content copolymer will be investigated. Based on the results, comments about the block copolymer structure with an experimentally proven potential<sup>[1]</sup> as an adhesion promoting linker between ABS and copper will be given.

---

<sup>§§</sup> Part of this chapter has been accepted for publication: S. Kisin, J. Božović Vukić, P. G. Th. van der Varst, G. de With, C. E. Koning, Estimating the polymer–metal work of adhesion from molecular dynamics simulations, *Chem. Mater.* **2006**.

## 6.1 Introduction

Most of the mechanical adhesion tests provide a largely overestimated work of adhesion due to the large energy dissipation originating in the test samples during the measurements<sup>[2]</sup>. A mechanically measured adhesive strength usually also strongly depends on time and/or temperature<sup>[3-5]</sup>, and only for a mechanically simple system<sup>[6]</sup> is it possible to correlate the mechanically measured adhesive energy to the work of adhesion. Additional influences of the preparation process in the case of metal–polymer hybrid systems (e.g. metal sputtering procedure) have been found on the macroscopic level. Recently it was successfully demonstrated<sup>[1,7]</sup> that macroscopic mechanical pull-off forces can be qualitatively correlated to substrate–tip interaction forces using nanoscale scanning force microscopy (SFM) measurements. However, even SFM measurements showed a strong dependence of the adhesion properties on the mechanical properties of the polymers<sup>[7]</sup>, which prohibits the quantitative analysis of the work of adhesion. A possible way to overcome this problem is to numerically simulate SFM measurements using molecular dynamics<sup>[8]</sup> (MD). This has also been done for JKR measurements<sup>[9]</sup> but the mechanical properties of the polymers also played an important role here.

To exclude all these influences and calculate the work of adhesion caused only by the pure physico–chemical interactions between the materials, adhesion of *poly(styrene–co–acrylonitrile)* and *poly(butadiene)* molecules (constituents of the ABS) on copper (oxide) surfaces was simulated. The work of adhesion was estimated as the interaction energy divided by the projected area of the van der Waals volume of the molecules on the copper surface. This surface is denoted as the van der Waals contact area.

As shown before (see Sections 4.3 and 5.3), the ABS–copper interfaces are susceptible to morphological and chemical changes (oxidation of the SAN phase) which strongly influence the adhesion strength (see Chapters 4 and 5). To theoretically verify these results, the work of adhesion for oxidized SAN molecule to pure and oxidized copper surfaces was calculated.

One of the most common ways for adhesion promotion is chemical modification<sup>[10]</sup> of the polymer surfaces with polar groups such as carbonyl, hydroxyl and carboxylic acid

groups<sup>[11]</sup> and it can be applied to ABS as well<sup>[12,13]</sup>. In an accompanying project<sup>[11]</sup> oxygen containing moieties were incorporated into a single well defined block copolymer which was used as an ABS surface modifying agent and showed to lead to stronger interfaces with copper (see Chapter 8). One suitable molecule for this purpose was shown to be *poly(styrene-alt-maleic anhydride)*<sup>[11]</sup> (SMAh) copolymer and its adhesion properties on copper and oxidized copper surfaces were simulated and contrasted with those of the SAN and pBd molecules.

## 6.2 Molecular dynamics calculations

For the general settings and software details used for all simulations see Section 2.3. In addition to the information given earlier, it has to be mentioned here that the duration of the simulations was confined to 50 ps using a time step of 1 fs. Within this time period the temperature of the system reached its preset value and no changes of the non-bond and the potential energy of the systems were observed.

### 6.2.1 Description of the metal–polymer simulations

Metallic copper was simulated as a face centered cubic crystal having a unit cell with lattice parameters of  $a = b = c = 3.6147 \text{ \AA}^3$ . This unit cell was used to create a super cell of  $51.1196 \times 51.1196 \times 20.0000 \text{ \AA}^3$  in dimensions. On top of the copper (0 0 1) surface a 50.00 Å thick vacuum layer was added, to obtain a simulation box of size  $51.1196 \times 51.1196 \times 70.0000 \text{ \AA}^3$ . The vacuum layer simply means that no periodic boundary conditions were used orthogonal to the copper surface plane, while keeping the periodicity lateral to the plane. Only the 6 top most atomic layers of copper were allowed to move during the calculations while the coordinates of the remaining copper atoms were fixed. In a similar way a simulation box of size  $51.1196 \times 51.1196 \times 70.0000 \text{ \AA}$  having a copper (1 1 1) surface as interface to the vacuum layer was constructed. These structures were equilibrated using the general settings described under Sections 2.3 and 6.2. The temperature of the systems reached its preset value within the first 10 ps of the simulation time and afterwards fluctuated within  $\pm 3 \text{ K}$ .

margins. The potential and non-bond energies reached a constant level within the first 10 ps of the simulation time and fluctuated within  $\pm 0.1\%$  boundaries around the average level afterwards.

Density and mechanical properties of copper were calculated to assess whether the COMPASS force field is suitable for the calculations. The density was estimated at 8.85 g/cm<sup>3</sup>, the elastic constants at  $C_{11} = 173.8$  GPa,  $C_{12} = 99.7$  GPa and  $C_{44} = 102.2$  GPa. Using the Voigt–Reuss–Hill<sup>[14]</sup> rule the calculated polycrystalline Young's modulus was 172.7 GPa and Poisson's ratio was 0.365. Experimental values are 8.90 g/cm<sup>3</sup> for the density<sup>[15]</sup>, the elastic constants<sup>[16]</sup> are  $C_{11} = 168$  GPa,  $C_{12} = 121$  GPa and  $C_{44} = 75.4$  GPa. Following the Voigt–Reuss–Hill rule the polycrystalline Young's modulus is 127.3 GPa and Poisson's ratio<sup>[15]</sup> 0.326.

For simulations of polymer interactions with oxidized copper surfaces, 2 different copper–oxygen layers on top of the original copper (0 0 1) and (1 1 1) surface were added; in the case of copper (0 0 1) surface layers contained 0.075 and 0.143 oxygen atoms/Å<sup>2</sup> whereas in the case of copper (1 1 1) surface the layers contained 0.077 and 0.142 oxygen atoms/Å<sup>2</sup>. The initial configuration of the low density layer was taken as a (1 0 1) Cu<sub>2</sub>O plane while for the initial configuration of the high density layer a (1 1 1) CuO plane was chosen. These oxygen enriched layers on top of the copper surfaces were equilibrated in the same fashion as the pure copper surface leading to an amorphous structure of about 3 Å thickness on top of the non-perturbed copper surface\*\*\* (6 surface layers allowed to move).

The SAN molecule was constructed as a random copolymer having 20 repeat units, 15 styrene and 5 acrylonitrile units, a ratio similar to the real material; the pBd was polymerized from 10 1,4-butadiene monomer units; the SMAh was an alternating copolymer containing 20 repeat units. Structures of all the repeat units are shown in Figure 6.1. The oxidized SAN was constructed by changing 5 aromatic styrene rings of the original SAN molecule into a quinone structure (Figure 6.2).

---

\*\*\* Although the equilibration time was kept at 50 ps like in all other cases, the energy equilibrium was reached after approximately 5 ps of simulation time retaining the reached average level with fluctuations less than 0.1 %; the preset temperature level was reached within 5 ps of simulation time (fluctuation  $\pm 3$  K).

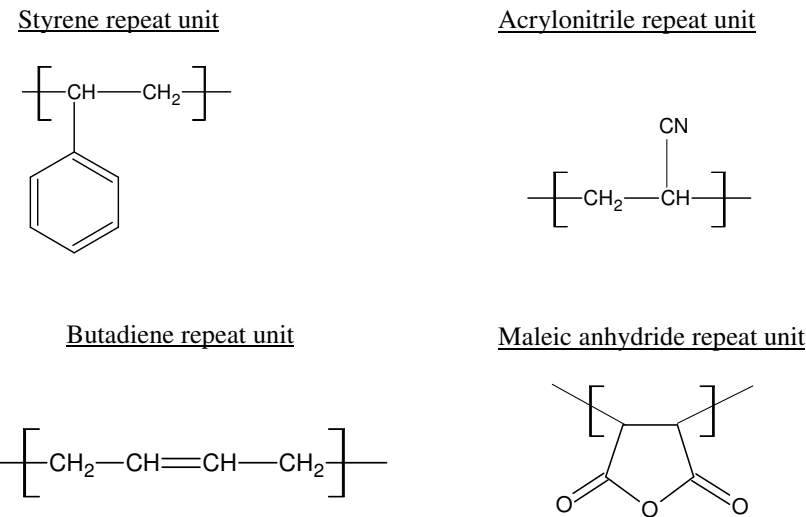


**Figure 6.1.** Structures of the monomer residues used to construct SAN, pBd and SMAh molecules.

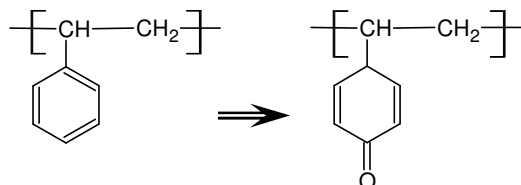


**Figure 6.2.** To construct an oxidized SAN molecule, 5 styrene rings of the entire SAN molecule were changed to a quinone structure.

All the polymer molecules used were equilibrated in vacuum prior to positioning them on the copper (oxidized) surface(s).

Interactions of the four polymer molecules with all pure and oxygen modified copper (0 0 1) surface were simulated (Table 6.1). In addition to this, the interactions of 1, 2 and 3 SAN molecules with the surfaces were simulated.

1, 2 and 3 SAN molecules on (0 0 1) copper and oxygen modified copper surfaces (0.075 and 0.143 oxygen atoms/Å <sup>2</sup> ).
1, 2 and 3 SAN molecules on (1 1 1) copper and oxygen modified copper surfaces (0.077 and 0.142 oxygen atoms/Å <sup>2</sup> ).
1 SAN molecule on (0 0 1) copper surface under NTP ensemble.
1 SAN molecule on (0 0 1) copper surface, molecule rotated for 45, 90 and 180°
1 SAN/pBd molecule on (0 0 1) copper surface (0, 2, 4 and 6 copper atomic layers allowed to move).
1 pBd molecule on (0 0 1) copper and oxygen modified copper surfaces (0.075 and 0.143 oxygen atoms/Å <sup>2</sup> ).
1 oxidized SAN molecule on (0 0 1) and oxygen modified copper surfaces (0.075 and 0.143 oxygen atoms/Å <sup>2</sup> ).
1 SMAh molecule on (0 0 1) and oxygen modified copper surfaces (0.075 and 0.143 oxygen atoms/Å <sup>2</sup> ).

**Table 6.1.** Overview of the simulated systems.

To further exclude even the influence of the starting orientation of the polymer molecule on top of the copper surface on the work of adhesion, a SAN molecule was placed on top of the copper (0 0 1) surface in different orientations and the work of adhesion calculated for every orientation. The influence of the number of the non-confined copper atomic layers on the work of adhesion between SAN molecule and the pure copper (0 0 1) surface was checked by confining the complete copper atoms block and allowing 2, 4 and 6 atomic layers to move. Finally, one simulation of SAN molecule on a pure copper (0 0 1) surface for the isothermal-isobaric NTP ensemble, using the Andersen barostat and keeping the cell orthorhombic, was done to determine the influence of the ensemble type on the work of adhesion. It was found to deviate 3.5% from the work of adhesion calculated under isothermal-isochoric NTV conditions.

### 6.2.2 Calculations of interaction energies and work of adhesion

The interaction energy between the polymer molecules and the three surfaces was calculated according to the following equation:

$$E_{\text{interaction}} = (E_c + E_p) - E_{\text{total}} \quad (6.1)$$

where  $E_{\text{interaction}}$  is the internal interaction energy,  $E_{\text{total}}$  is the total internal energy of the copper and the molecule in contact in equilibrium,  $E_c$  is the total internal energy of the copper in the simulation box (see Section 2.3.1, Equation 2.11) and  $E_p$  is the total internal energy of the free isolated polymer molecule in equilibrium in vacuum<sup>[1]</sup> (see Section 2.3.1, Equation 2.13).

The work of adhesion  $W_A$  was calculated as<sup>†††</sup>:

$$W_A = \frac{E_{\text{interaction}}}{A_c} \quad (6.2)$$

where  $A_c$  is the van der Waals contact area between the molecules and the surfaces. To calculate the van der Waals contact surface area  $A_c$  the top view of the molecule equilibrium configuration on the copper (modified) surface using van der Waals' radii of all the constituent atoms was plotted, this structure was exported as a bitmap image, the color mode of the image was changed to black and white (Figure 6.3) and the percentage of white pixels (molecule) was determined. Knowing the dimensions of the system used, it was possible to calculate  $A_c$ .

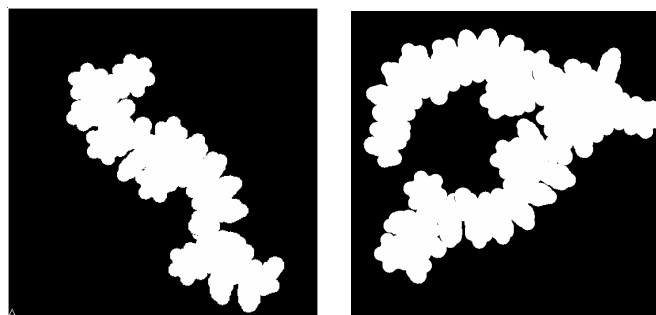


**Figure 6.3.** Top view of the molecules' equilibrium configuration on copper (0 0 1) surface used for calculation of the contact area and the work of adhesion between the two (one SAN molecule shown on the left and two on the right; total surface area for each image corresponds to  $2613.25 \text{ \AA}^2$ ).

---

<sup>†††</sup> Note that this definition is related to the internal work of adhesion (see Section 2.3.1, Equation 2.24) and it estimates the true work of adhesion only in the case it shows no temperature dependence. For the temperature range 248–348 K the work of adhesion of one SAN molecule on pure copper (0 0 1) surface shows weak temperature dependence (at 248 K  $W_A = 0.510 \text{ J/m}^2$ , at 298 K  $W_A = 0.505 \text{ J/m}^2$  and at 348 K  $W_A = 0.498 \text{ J/m}^2$ ). If the relation between the internal and the real work of adhesion is approximated by the Equation 2.28, the discrepancy between these two values is about 20%.

### 6.3. Results and discussion

In Figure 6.4 a and b, a free SAN molecule close to the copper surface and the equilibrium conformation of a SAN molecule interacting with the copper surface can be seen, showing that particularly the conformation of the polymer changes significantly.

After 50 ps of MD simulation the molecule has approached the copper surface to an equilibrium distance of  $3.62 \pm 1.20 \text{ \AA}$  (Table 6.2) and, as far as geometrical restrictions allow, the aromatic rings flatten out parallel to the surface. The positions of the aromatic rings are significantly below the average position of the molecule (Figure 6.5). Apparently, the presence of the copper surface induces the molecule to reorient it self as flat as possible on top of the surface attracting especially strongly the aromatic rings. Similar observations can be made when 2 and/or 3 SAN molecules are present on the copper surface; a similar behavior has been reported for other phenyl containing polymers on a copper surface<sup>[17]</sup>. The average distances between the copper surface and pBd and SMAh molecules are shown in Table 6.2.

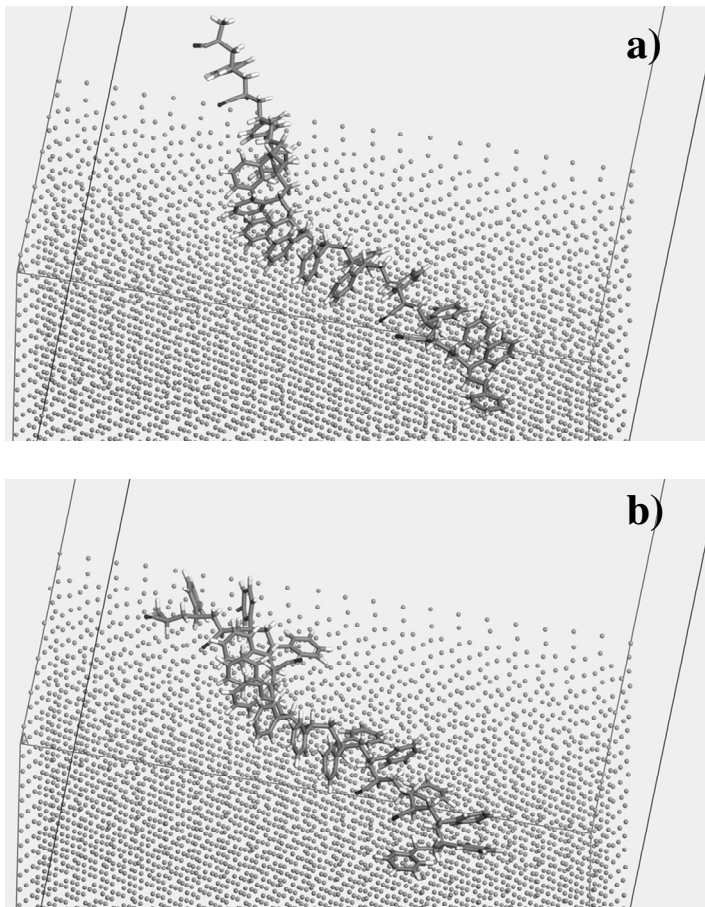


**Figure 6.4.** Free SAN molecule close to the copper surface (a) and the equilibrium conformation of the SAN molecule interacting with the copper surface (b). The copper surface used was (0 0 1).

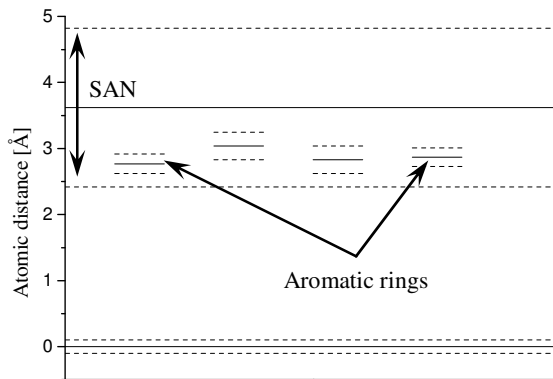


**Figure 6.5.** Distance between the top copper atomic layer of the (0 0 1) surface and the SAN molecule. Solid lines show the average atomic position and the dashed lines indicate the sample standard deviation of the atomic positions (horizontal axis not drawn to scale). Only the aromatic rings oriented parallel to the copper surface are shown; note that not all the aromatic rings present in the SAN molecule orient parallel to the copper surface due to geometric restrictions.

Molecule	Distance to copper (0 0 1) surface [Å]
SAN	$3.62 \pm 1.20$
pBd	$3.20 \pm 0.83$
SMAh	$4.72 \pm 1.78$

**Table 6.2.** Average distance between the top copper atomic layer and the SAN, pBd and SMAh molecules ( $\pm$  denotes the sample standard deviation).

Although the presence of copper influences the conformation of the SAN molecule strongly, the reverse seems not to be the case. As can be seen in Figure 6.6, the standard deviation of the atomic positions within the 6 top atomic layers of the copper surface does not differ significantly whether the surface is in contact with the polymer molecule or not. Even locally, the copper surface retains its vacuum equilibrium structure when in contact with the SAN molecule.

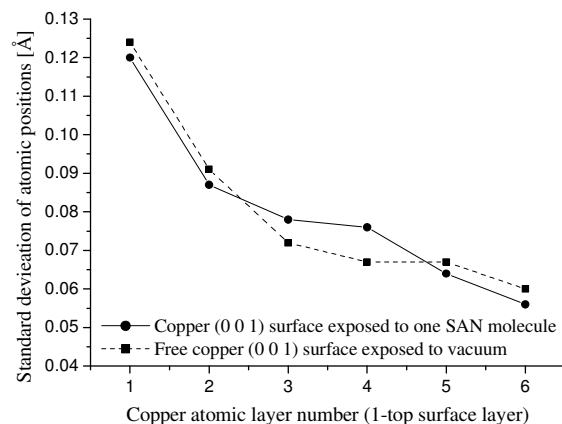


**Figure 6.6.** Standard deviations of copper atomic positions within the 6 top most atomic layers. Copper surface in contact with SAN molecule and exposed to vacuum.

The layer-to-layer distance within the copper block if the copper surface exposed to vacuum, to the SAN and to the pBd molecule, respectively, can be compared. The nature and the presence of the molecules on the surface do not, indeed, have any influence on the copper structure (Figure 6.7). The top most surface atomic layer retracts towards the bulk of the material (first point, Figure 6.7) as a result of the cleaving procedure only, while the second layer slightly shifts up (second point, Figure 6.7) compared to its bulk equilibrium position (approximated by the two last points, Figure 6.7). This retraction and the structure (Figure 6.6) of the surface are not perturbed by the polymer molecules in any significant way.

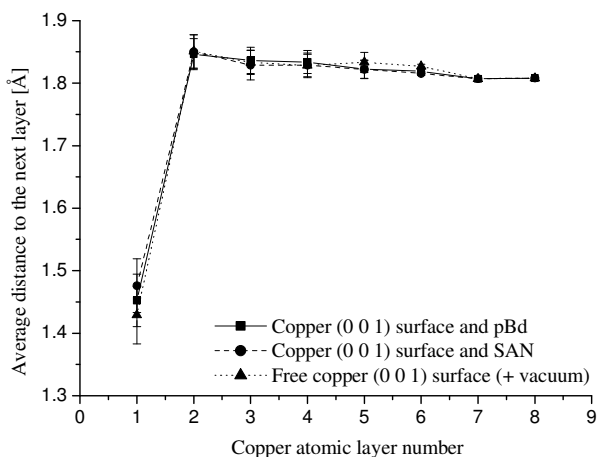


**Figure 6.7.** Layer-to-layer distance in the copper atomic block when the pure copper (0 0 1) surface is exposed to SAN, pBd molecule and vacuum.

If the work of adhesion between 1, 2 and 3 SAN molecules and the pure copper surface is calculated, no differences between the obtained values are observed (Figure 6.8). The same is true for the work of adhesion between SAN molecules and the oxygen modified copper surfaces (Figure 6.8). However, upon oxidation the work of adhesion changes from  $0.51 \pm 0.02 \text{ J/m}^2$  over  $1.47 \pm 0.03 \text{ J/m}^2$  to  $1.68 \pm 0.06 \text{ J/m}^2$  with increasing oxygen content on the copper surface (0, 0.075 and 0.143 oxygen atoms/ $\text{\AA}^2$ ). The same is visible in Figure 6.9 where the work of adhesion of 1, 2 and 3 SAN molecules on pure and oxidized copper (1 1 1) surfaces are shown. Here, the work of adhesion with the pure copper surface is  $0.51 \pm 0.02 \text{ J/m}^2$  (0 oxygen atoms/ $\text{\AA}^2$ ) and upon oxidization it increases over  $1.52 \pm 0.08 \text{ J/m}^2$  to  $1.66 \pm 0.05 \text{ J/m}^2$  with increasing oxygen content on the copper surface (0.077 and 0.142 oxygen atoms/ $\text{\AA}^2$ ). The fact that the work of adhesion of SAN molecules on all considered surfaces shows no significant dependence on the number of the polymer molecules and the type of the copper surface suggests that it can be taken as a reliable estimate of the thermodynamic work of adhesion for the bulk SAN polymer and the copper (oxidized) system. These were the main reasons that the work of adhesion for the other molecules, pBd, oxidized SAN and SMAh were calculated only for one molecule on top of the pure copper (0 0 1) and the oxygen modified copper surfaces.

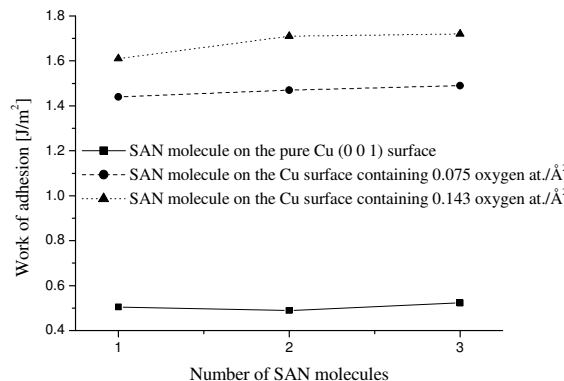


**Figure 6.8.** Work of adhesion between SAN molecules and the pure copper (0 0 1) surface and oxygen modified copper surfaces.

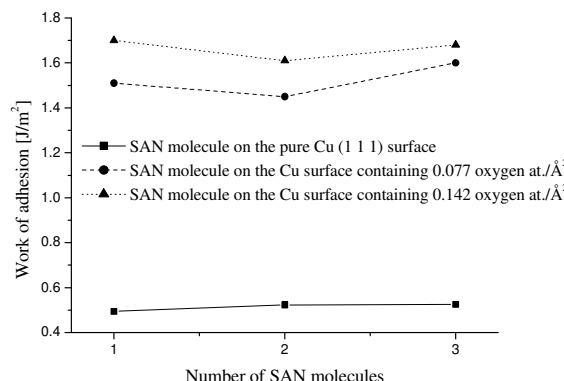


**Figure 6.9.** Work of adhesion between SAN molecules and the pure copper (1 1 1) surface.

Furthermore, as shown in Figure 6.10 the work of adhesion is also independent of the orientation<sup>\*\*\*</sup> of the SAN molecule on top of the copper surface. Since the orientation of the molecule plays no role in the work of adhesion, it is expected that different sequences of the repeat units within the polymer molecule will show the same result, provided the actual type and their sequence along the molecular backbone does not differ too much from their statistically expected values.

<sup>\*\*\*</sup> The 0° rotation is a randomly chosen position of a SAN molecule on the copper surface and the molecule was rotated for the fixed angle with respect to this position. The final, equilibrium, rotation angle does not have to correspond to the initial one, however, no large changes of the final angle have been observed.

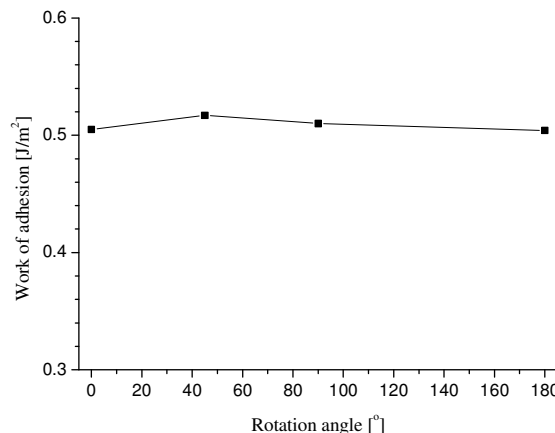


**Figure 6.10.** Dependence of the work of adhesion on the orientation of SAN molecule on a copper (0 0 1) surface. The  $0^\circ$  rotation angle is a randomly selected and the molecule was rotated for preset angles with respect to this position.

The situation is quite similar if the work of adhesion is analyzed as a function of the number of the moving copper surface atomic layers. Only if the complete copper surface is immobile, the work of adhesion shows a significant deviation from the rest of the values (Figure 6.11). The work of adhesion in this case,  $0.38 \text{ J/m}^2$  is approximately 18% lower as compared to the work of adhesion between the SAN molecule and the copper surface with 2 atomic layers allowed to move ( $0.46 \text{ J/m}^2$ ). The difference between the work of adhesion calculated with 2 and 4 layers moving is 2% and the discrepancy between 4 and 6 layers moving is 6%. So it can be safely said the interactions between SAN and the pure copper are confined to only a few top most atomic layers within the copper surface.

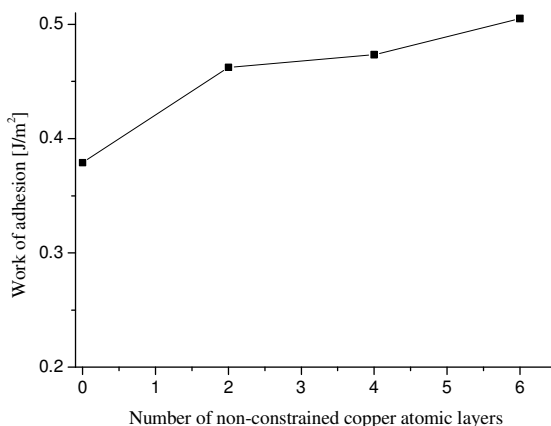


**Figure 6.11.** Dependence of the SAN–copper work of adhesion on the number of non-constrained copper atomic layers below the (0 0 1) surface.

With increasing oxygen content on the copper surface (0, 0.075 and 0.143 oxygen atoms/ $\text{\AA}^2$ ), the work of adhesion between the surfaces and the pBd, oxidized SAN and SMAh molecules increase as well (Figure 6.12). In the case of pBd on the three surfaces, the work of adhesion increases from 0.42 via 0.93 to 1.13 J/m<sup>2</sup>, in the case of the oxidized SAN molecule, the work of adhesion changes from 0.48 over 1.55 to 2.10 J/m<sup>2</sup> and for SMAh it goes up from 0.48 via 2.55 to 3.36 J/m<sup>2</sup>. Although all four molecules have more or less the same work of adhesion with the pure copper surface (around 0.5 J/m<sup>2</sup>, Figure 6.12 points for 0 oxygen at./  $\text{\AA}^2$ ), with increasing oxygen content in both interacting parts (copper surface and the molecules), the work of adhesion increases strongly (Figure 6.12). The highest work of adhesion is achieved for the combination of SMAh molecule–copper surface modified with a Cu–O layer containing 0.143 oxygen atoms/ $\text{\AA}^2$ .

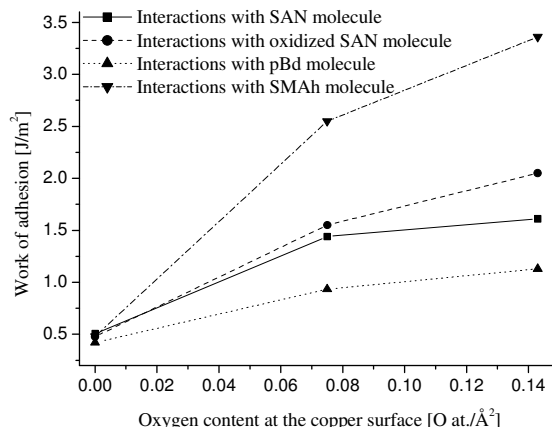


**Figure 6.12.** Work of adhesion between SAN, oxidized SAN and poly(butadiene) molecules with the pure copper (0 0 1) surface and oxygen modified copper (0 0 1) surfaces.

Since SAN is the main constituent of the ABS (more than 85 wt. %) and SMAh was identified as a possible adhesion promoting molecule<sup>[1]</sup>, adhesion properties of these two molecules will be contrasted in more detail. From the average equilibrium distance of the molecules to the copper surface it can be noted that the SAN molecule approaches the copper surface to a shorter average equilibrium distance as compared to the SMAh molecule,  $3.62 \pm 1.20$  Å and  $4.72 \pm 1.78$  Å (Table 6.2) for SAN and SMAh, respectively. It has to be mentioned here that the copolymers interact with copper (oxide) surface(s) via van der Waals and Coulomb forces only, both of which diminish strongly with increasing distance between the interacting parts. This suggests that if the SAN molecule would be on the same average distance as the SMAh molecule it would exhibit lower work of adhesion. On the other hand comparison of the average distances may be somewhat deceiving as the positions of the lowest atoms within both molecules differ by only 0.3 Å. So the difference in average distance may also be caused by the fact that SMAh is more voluminous molecule as compared to SAN.

Introducing oxygen atoms to the copper surface in the form of two distinct atomic monolayers with surface density of 0.075 and 0.143 oxygen atoms/Å<sup>2</sup>, the adhesion with both molecules increases. It is important to notice that in this specific case the SMAh copolymer shows higher adhesion as compared to the SAN molecule. As seen in Figure 6.12, modifying the copper surface with a low oxygen density layer leads to a 70%

increase of the SMAh work of adhesion compared to SAN ( $1.44 \text{ J/m}^2$  compared to  $2.55 \text{ J/m}^2$ ), while modification with the high oxygen density layer causes a two fold increase of the SMAh work of adhesion compared to SAN ( $1.61 \text{ J/m}^2$  compared to  $3.36 \text{ J/m}^2$ ).

These findings support the experimental results of macroscopic and nanoscopic adhesion measurements<sup>[1]</sup> where indications of a significantly higher binding affinity of SMAh were found. For both measurements it is realistic to assume the presence of copper oxide on the copper, originating either from the CVD/PVD<sup>\$\$\$[1,18]</sup> process or due to the fact that the experiments were performed in air.

Since the specific work of adhesion of SAN and the pBd molecules appeared to be independent of the number of molecules present on the copper surface, the work of adhesion between the ABS and copper can be estimated from the values of the work of adhesion of the constituent molecules (SAN and pBd) using a mixing rule. There is no difference in the work of adhesion between the SAN and pBd molecules and the pure copper surface, but if the copper surface should contain any oxygen, the SAN part of the ABS will play the dominant role in the adhesion between the two (Figure 6.12). This is due to the higher work of adhesion between the SAN and oxidized copper surfaces and to the larger number of SAN molecules present in the ABS itself. Using oxidized SAN instead of regular SAN will not contribute significantly to the adhesion increase to the pure copper surface but the presence of oxygen in both the SAN molecule and on the copper surface will increase the adhesion strength as compared to the adhesion between the pure components (Figure 6.12).

As far as the adhesion promotion between ABS and copper is concerned, SMAh does not show any potential for adhesion promotion as compared to SAN when the adhesion to pure, oxygen free copper is considered. However, a small amount of oxygen is always expected to be present in real PVD/CVD deposited copper layers and thus SMAh seems to be a very good candidate. One suggestion for promoting adhesion is to use a block SAN-*b*-SMAh copolymer combined with controlled addition of oxygen on the copper side of the interface. SAN-*b*-SMAh copolymer is a microphase separating block

---

<sup>\$\$\$</sup> For macroscopic measurements, copper films were applied on top of the SAN and SMAh copolymer films using physical vapor deposition (PVD), while for the nanoscopic measurements chemical vapor deposited (CVD) copper SFM tips were used to probe the adhesion to SAN and SMAh.

copolymer<sup>[19,20]</sup> which can provide interaction with the ABS substrate through SAN entanglement formation<sup>[1]</sup> while the polar block, SMAh, will provide enhanced interactions with the metal (oxide) coating<sup>[21,22]</sup>.

## 6.4. Conclusions

The work of adhesion of a single molecule on a metallic surface as calculated from the interactions and the van der Waals contact surface area between the two interacting parts, is equal to the work of adhesion calculated from interactions of 2 or 3 molecule containing clusters on a metallic surface and is not influenced by the molecular orientation on the surface, a choice of the surface and the repeat units sequence in the polymer molecule. The results suggest that the energy thus calculated can be taken as a reliable estimate of the thermodynamic work of adhesion between the polymer and the metal surfaces. In the specific case of interactions between the ABS and copper, separate simulation of the interactions of the constituent molecules with the copper can provide an insight into the adhesion mechanism. For the pure materials, both components will contribute to the bonding to the same extend, whereas the introduction of the oxygen to SAN molecules and on the copper surface will lead to an adhesion increase and bonding of the two materials predominantly via the (oxidized) SAN–(oxidized) copper interactions.

SMAh and SAN copolymers were found to have similar works of adhesion to pure metallic copper. However, with the introduction of oxygen to the copper surface, the interaction of SMAh copolymer becomes much stronger as compared to SAN. The highest work of adhesion of  $3.36 \text{ J/m}^2$  was found for a combination of SMAh copolymer and a copper surface with  $0.143 \text{ oxygen atoms}/\text{\AA}^2$ . Bearing this in mind, SMAh copolymer can be further incorporated into block copolymers and then used as an adhesion promoting agent in metal(oxide)–polymer systems.

## References

- [1] J. Božović Vukić, *Block copolymers for adhesion improvement synthesized via RAFT-mediated polymerization*, PhD Thesis, Technische Universiteit Eindhoven, Eindhoven, **2006**.
- [2] D. E. Packham, *Int. J. Adhes. Adhes.* **1996**, *16*, 121–128.
- [3] K. Kendall, *Science*, **1994**, *263*, 1720–1726.
- [4] S. S. Pesetskii, B. Jurkowski, A. I. Kuzakov, *Int. J. Adhes. Adhes.* **1998**, *18*, 351–358.
- [5] S. Kim, G. Y. Choi, A. Ulman, C. Fleischer, *Langmuir*, **1997**, *13*, 6850–6856.
- [6] E. H. Andrews, A. J. Kinloch, *Proc. Roy. Soc. A.* **1973**, *332*, 385–399.
- [7] J. Božović Vukić, S. Hoeppener, D. A. Kozodaev, S. Kisin, B. Klumperman, U. S. Schubert, G. de With, C. E. Koning, *ChemPhysChem*, **2006**, *7*, 1912–1916.
- [8] I. Yu. Sokolov, G. S. Henderson, F. J. Wicks, *Surf. Sci.* **2000**, *457*, 267–272.
- [9] R. C. Baljon, J. Vorselaars, T. J. Dapuy, *Macromolecules*, **2004**, *37*, 5800–5806.
- [10] K. L. Mital (Ed.), *Polymer Surface Modification: Relevance to Adhesion*, VSP, Utrecht, **1995**.
- [11] C. Seidel, H. Kopf, B. Gotsmann, T. Vieth, H. Fuchs, K. Reihs, *Appl. Surf. Sci.* **1999**, *150*, 19–33.
- [12] P. Yen, *Polymer*, **1995**, *36*, 3399–3400.
- [13] C. A. Villamizar, J. Rojas, P. Frias, *Met. Finish.* **1981**, *79*, 27–33.
- [14] G. de With, *Structure, deformation, and integrity of materials*, vol. 1, Wiley–VCH, Weinheim, **2006**, p. 381, 382.
- [15] J. E. Shigley, C. R. Mische, *Mechanical engineering design*, McGraw–Hill Higher Education, London, **2001**, p. 1173.
- [16] R. F. S. Hearmon, *Adv. Phys.* **1956**, *5*, 323–382.
- [17] W. Possart, S. Dieckhoff, *Int. J. Adhes. Adhes.* **1999**, *19*, 425–434.
- [18] N. Serin, T. Serin, S. Horzum, Y. Celik, *Semicond. Sci. Technol.* **2005**, *20*, 398–401
- [19] F. S. Bates, *Science*, **1991**, *251*, 898–905.
- [20] A. Noro, M. Iinuma, J. Suzuki, A. Takano, Y. Matsushita, *Macromolecules*, **2004**, *37*, 3804–3808.
- [21] G. Hadzioannou, S. Patel, S. Granick, M. Tirell, *J. Am. Chem. Soc.* **1986**, *108*, 2869–2876.
- [22] Y. Q. Zhu, E. T. Kang, K. G. Neoh, L. Chan, D. M. Y. Lai, A. C. H. Huan, *Appl. Surf. Sci.* **2004**, *225*, 144–155.



## **CHAPTER 7**

### **CORRELATING MD CALCULATIONS WITH PEEL TEST MEASUREMENTS**

**Summary:** In this Chapter an attempt, to bridge the gap present between the adhesive energy calculated from the energy balance of the peel test and the values for the work of adhesion calculated from the MD simulations, will be presented. The possible energy contributions to the total energy dissipation arising from the deformation of the substrate (plastic and visco-elastic) will be looked into. The influence of the substrate roughness on the adhesive energy will be briefly addressed. The sensitivity of the adhesive energy calculations from the peel test data on the errors in determination of the copper mechanical properties will be evaluated. Work of adhesion for the copper-ABS interface will be evaluated based on the results of MD simulations using a mixing rule. These values will be corrected for the crack tip plasticity during the peel test to get the estimate of the corresponding adhesive energies. Finally, a comparison between peel test measured adhesive energies and the adhesive energies calculated from MD simulations will be compared and an explanation for the observed behavior offered.

## 7.1 Introduction

If any energy dissipation within the material system is present during peel testing, the total energy supply to the system cannot be taken as a reliable estimate of the adhesive energy (see Section 2.1.2). If one is to estimate the adhesive energy from the experimental peel test results, an energy balance based model of the peeling is needed to deduce all the energy dissipations and estimate the real adhesive energy.

The peel test results in this study were processed using an energy balance based model, which corrects the total energy supply to the material system for the plastic dissipation caused by the bending of the delaminating metallic film<sup>[1]</sup>, but neglects (possible) plastic and visco-elastic dissipations within the substrate as well as the local plasticity of the film at the crack tip (see Section 2.1.3). Accordingly, the adhesive energy calculated by the model (results presented in Chapter 4) is expected to be larger than the real work of adhesion. Here, the neglected energy contributions will be estimated and the adhesive energy calculated from the peel test data will be corrected for the obtained values.

On the other side, it has been shown that the adhesive energy is strongly dependent on the values of the work of adhesion (see Section 2.1.2, Equations 2.8 and 2.9) and also encompasses the contribution of the small scale, local, plastic dissipation within the metallic film at the crack tip. Knowing the values of the work of adhesion and the mechanical properties of the delaminating metallic film, the effect of local plasticity at the crack tip can be evaluated and thus the real adhesive energy can be estimated. Using a mixing rule and the MD calculated work of adhesion (Chapter 6), a work of adhesion for copper-ABS interface will be estimated and corrected for the local plastic dissipation at the crack tip, resulting in the corresponding adhesive energy values.

The final goal is to compare the adhesive energy values calculated from the peel test data, corrected for all the neglected energy contributions, with the values of the adhesive energies estimated on the basis of the MD calculated work of adhesion.

## 7.2 Influence of the energy dissipation within the substrate and the substrate roughness on the adhesive energy calculated from the peel test

### 7.2.1 Plastic dissipation within the substrate

Plastic dissipation within the substrate has been neglected in the previous adhesive energy calculations, but if present, it could be a non-negligible part of the total energy input during the peel test. During the peel test the ABS substrate is loaded perpendicular to the polymer chains orientation (see Section 3.1, Figure 3.2). If loaded in this direction, the substrate material exhibits only the elastic deformation and shows a brittle failure before reaching the yield stress (see Section 3.1 Table 3.1). The elastically stored energy within the substrate during the peeling is expected to be small as compared to the total energy input into the test and not to significantly influence the adhesive energy calculated from the peel test data. It can be concluded that, as a consequence of the loading direction during the peeling the substrate will not plastically deform and contribute significantly to the total energy input.

### 7.2.2 Visco-elastic dissipation within the substrate

The contribution of the visco-elastic dissipation within the substrate material to the total energy input during the peel test has also been neglected in the energy balance based model used to process the peel test data, so here an approach to estimate this contribution will be presented.

To estimate the dissipation in the foundation, the internal variable theory<sup>[2]</sup> will be used. The internal variable theory can be easily applied<sup>[3]</sup> if the foundation material is modeled as combination of two springs (spring constants  $k$  and  $K$ ) and one damper (damping constant  $\eta$ ) connected as shown in Figure 7.1.

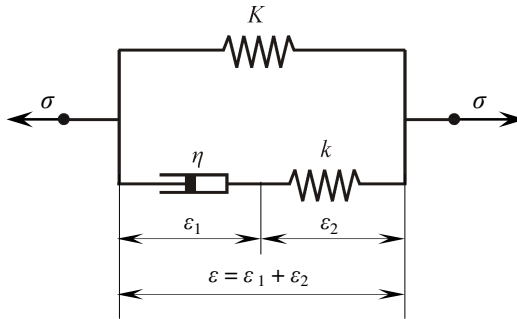


**Figure 7.1.** Standard linear element used to approximate the stress-strain behavior of the foundation material and to calculate the visco-elastically dissipated energy within the foundation material.

The state of the system shown in Figure 7.1 is defined by the two kinematical variables,  $\varepsilon$  and  $\varepsilon_1$ . The variable  $\varepsilon$  is a conventional, external variable and  $\varepsilon_1$  is an internal variable. As a result of the damper that is present in the system, the element will exhibit visco-elastic behavior\*\*\*\*. The power  $p$  dissipated per volume element is:

$$p = (\sigma - K\varepsilon)\dot{\varepsilon}_1 = \frac{1}{\eta}(\sigma - K\varepsilon)^2 \quad (7.1)$$

The creep response function  $\Gamma(t)$  of the foundation material in Figure 7.1 is:

$$\Gamma(t) = \frac{1}{K} - \frac{R}{K} e^{-\Omega t} \quad (7.2)$$

with

$$R = \frac{k}{K+k}, \quad \Omega = \frac{kK}{\eta(K+k)} \quad (7.3)$$

leading to

$$\varepsilon = \Gamma(0)\sigma(t) + \int_0^t \Gamma(t-\tau)\dot{\sigma}(\tau)d\tau = \sigma^* d\Gamma \quad (7.4)$$

where the Stieltjes convolution operator  $*d$  (see Ref. 4) is introduced to shorten the notation. Therefore, upon setting  $\Psi = R e^{-\Omega t}$  one finds

---

\*\*\*\* The applied load has to result in a stress value below the material's yield stress value, otherwise also the plastic dissipation of the substrate has to be accounted for.

$$p = \frac{1}{\eta} (\sigma - K\varepsilon)^2 = (\sigma * d\Psi)^2 \quad (7.5)$$

as the dissipated power per unit volume of the foundation.

The stress distribution in Equation 7.5 is considered to be the same as for a static beam (thickness  $h$ , width  $b$  and Young's modulus  $E$ ) on an elastic foundation of thickness  $h_s$ , width  $b$  and Young's modulus  $E_s = 1/\Gamma(0)$  loaded by a force  $P$  acting at distance  $l$  (Figure 7.2) except that this stress distribution is “moving bodily” with speed  $v$ .

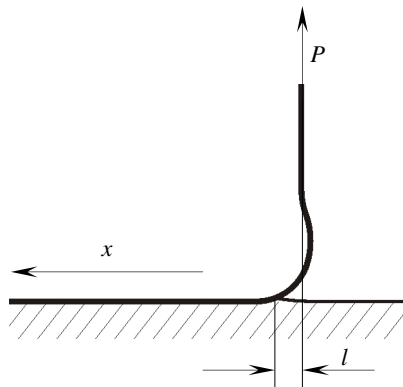


**Figure 7.2.** Schematic of a metallic foil delaminating under the force  $P$  applied at a distance  $l$  from the crack tip.

Using results from Maugis<sup>[5]</sup> one finds:

$$\sigma(x, t) = \sigma_m e^{-\lambda(x-vt)} \left( \cos(\lambda(x-vt)) - \frac{\lambda l}{1+\lambda l} \sin(\lambda(x-vt)) \right) \quad (7.6)$$

with

$$\sigma_m = \frac{2P\lambda(1+\lambda l)}{b}, \quad \lambda^4 = \frac{3E_f}{Ebh^3} \quad (7.7)$$

The parameter  $E_f$  is the foundation modulus given by<sup>[6]</sup>:

$$E_f = \frac{E_s b}{h_s} \quad (7.8)$$

The  $E_s$  can be estimated if the damper constant in the standard linear element, used to model the foundation material (see Section 3.1 Figure 3.3), is made arbitrarily large, this yields  $E_s = 2.3$  GPa.

The total power  $P(t)$  dissipated per unit width in the foundation is now given by:

$$P(t) = \frac{h_s}{\eta} \int_{x=0}^{\infty} (\sigma * d\Psi)^2 dx \quad (7.9)$$

and one finds that eventually, that is after all transients have died out, that

$$P = \frac{h_s \sigma_m^2 R^2}{\eta \lambda} Q\left(\lambda l, \frac{\Omega}{\lambda v}\right) \quad (7.10)$$

with  $Q$  a function of  $\lambda l$  and  $\Omega/\lambda v$ . Substituting the typical numerical values for the copper-ABS material system:

$$P = 3 \text{ N} \quad b = 20 \text{ mm} \quad h = 18 \text{ } \mu\text{m} \quad l = 100 \text{ } \mu\text{m}$$

$$v = 1 \text{ mm/min} \quad \eta = 396.7 \text{ GPa} \cdot \text{s} \quad K = 1.6 \text{ GPa}$$

it is found that the visco-elastically dissipated power equals to approximately  $2 \times 10^{-4} \%$  of the total power input into the peel test. This means that there is no significant dissipation within the substrate as a consequence of visco-elastic deformation.

### 7.2.3 Influence of the substrate roughness on the adhesive energy

The roughness of the substrate surface can also influence the measured adhesive energy. However, for aluminum-epoxy interfaces it was observed that the increase in roughness up to 10 times ( $R_a$  value increased 10 times) will lead to almost no changes of the adhesive energy<sup>[7]</sup>. For steel-poly(ethylene-terephthalate) interfaces it has been demonstrated that a roughness increase up to  $3 \mu\text{m}$  leads to only 6% change in the adhesive energy<sup>[8]</sup>. Since in the case of ABS substrate the  $R_a$  value is around  $0.01 \mu\text{m}$ , one does not expect the roughness to significantly influence the adhesive energy, or at least not up to the values corresponding to the gap between peel test measured values and calculated work of adhesion.

#### 7.2.4 Influence of the energy dissipation within the substrate and the substrate roughness on the adhesive energy calculated from the peel test: Conclusion

As a concluding remark for this section it can be said that the energy dissipation within the substrate is either not present (plastic dissipation) or negligible as compared to the total energy input or the other energy contributions (visco-elastic dissipation). As the substrates used were very smooth, it is also expected that the roughness of the substrate has no significant influence on the values of the calculated adhesive energy.

### 7.3 Sensitivity of the adhesive energy calculations to errors in determination of the mechanical properties of the copper film

The energy contributions neglected in the energy balance model of the peel test have now been looked into in more detail and proved to be negligible in comparison to the total energy input into the test or to the plastically dissipated energy in the bending of the delaminating film. It remains to analyze the influence of the input parameters (mechanical properties of the delaminating film) on the adhesive energy calculations. As seen in Section 4.2.1, Table 4.1 the numerical values for the mechanical properties of the copper films depend strongly on the fitting procedure used to deduce them from the stress-strain data. A  $\pm 20\%$  difference in the film's Young's modulus, yield stress or the hardening exponent is easily achievable. To assess the influence of such a change on the adhesive energy, the peel test data from the Figure 4.3 were used, the mechanical properties of the copper films were varied within these boundaries and the highest and the lowest estimate for the adhesive energy was determined.

The result of the analysis is shown in Figure 7.3. The solid line represents the adhesive energy calculated with the reference set of mechanical properties (deduced by the two-step fitting procedure, Ramberg–Osgood fit to get the Young's modulus and yield stress and the subsequent power law fit to deduce the hardening exponent). The dashed lines are the extreme changes of the adhesive energy. One can see that by changing the

mechanical properties, the calculated adhesive energy can easily change within  $\pm 30\%$  margins.

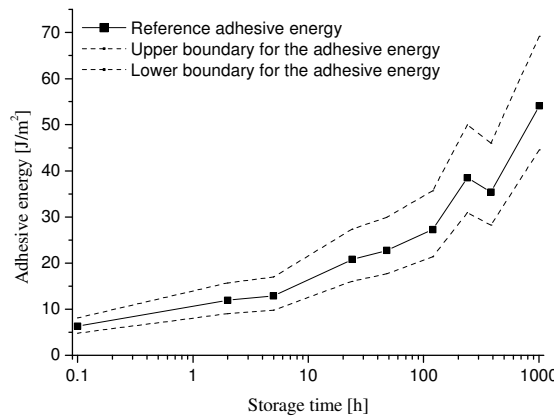


**Figure 7.3.** Influence of the change of the mechanical properties in the copper film on the adhesive energy calculated from the energy balance of the peel test.

The adhesive energy calculated from the energy balance based model of the peel test is thus quite sensitive to the values for the mechanical properties of the copper film and therefore to the fitting procedure used to determine them.

After taking into account all the (significant) energy contributions and analyzing the sensitivity of the calculations to the values of the mechanical properties of the metallic film, it can be said that the adhesive energy of the copper-ABS system is reliably represented by the data presented in Chapter 4 (Figure 4.3) which can change in a  $\pm 30\%$  margins depending on the fitting procedure and the accuracy with which the copper mechanical properties are determined. These adhesive energy values determined in this way thus include only the contribution of the work of adhesion of the copper-ABS interface and the plastically dissipated energy at the crack tip within the copper film.

## 7.4 Relation between work of adhesion and adhesive energy in the presence of plastic dissipation at the crack tip

The local plastic dissipation at the crack tip within the delaminating copper film, in the energy balance model used to analyze the peel test results, is considered as a part of the adhesive energy. This plastically dissipated energy at the crack tip has a strong dependence on the values of the actual work of adhesion<sup>[9]</sup>. The ratio between the work of adhesion and the measured adhesive energy can be calculated using a relatively simple consideration.

For the analysis, a monolithic body loaded by remote tractions containing a sharp crack, loaded in opening mode, is considered. The material within a zone, much smaller in comparison to other length scales in the problem, can plastically deform and strain harden (Figure 7.4). Within the plastic zone, a small elastic core of size  $R_c$ , free of dislocations, immediately ahead of the crack tip is embedded<sup>[10]</sup> (Figure 7.4).

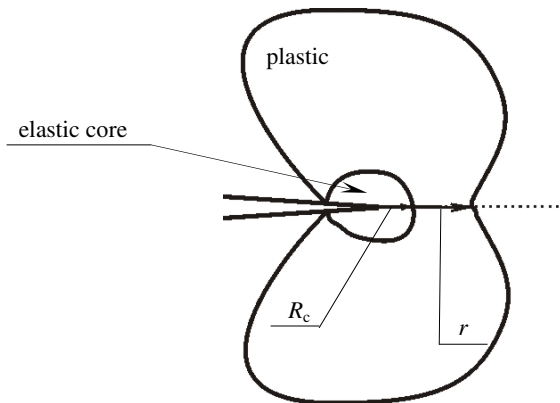


**Figure 7.4.** Schematic of the local plasticity at the crack tip concept.

The effective stress  $\bar{\sigma}$  that is acting directly ahead of the crack tip for  $r > R_c$  can be described as<sup>[9]</sup>:

$$\bar{\sigma} = f_n \sigma_Y \left( \frac{\xi}{\beta I_n} \frac{K_{I_\infty}^2}{r \sigma_Y^2} \right)^{n/(1+n)} \quad (7.11)$$

where  $n$  is the inverse of the Ramberg-Osgood exponent ( $n = 0.2$  see Section 4.2.1, Table 4.1),  $\beta$  is the Ramberg-Osgood factor ( $\beta = 0.02$  see Section 4.2.1, Table 4.1),  $I_n$  and  $f_n$  are functions of the exponent  $n$  ( $I_n = 5.0^{[9]}$ ;  $f_n = 0.46^{[9]}$ ),  $\sigma_Y$  is the uniaxial yield stress ( $\sigma_Y = 99.3$  MPa, see Section 4.2.1, Table 4.1),  $r$  is the distance ahead of the crack tip, parameter  $\xi$  is  $1-v^2$  ( $v$  is the Poisson's ratio;  $v = 0.326$ ) and  $K_{I\infty}$  is the applied stress intensity factor.

Alternatively, for  $r < R_c$  the effective stress in that zone can be described as:

$$\bar{\sigma} = \Lambda \frac{K_{I,\text{tip}}}{\sqrt{r}} \quad (7.12)$$

where the parameter  $\Lambda$  is  $\frac{1-2v}{\sqrt{2\pi}}$  and  $K_{I,\text{tip}}$  is the crack tip stress intensity factor:

$$K_{I,\text{tip}}^2 = E W_A \quad (7.13)$$

The stress field around the crack tip is completely described if the maximum effective flow stress  $\bar{\sigma}_{\text{flow}}^{\max}$  to which the material has hardened is expressed as:

$$\bar{\sigma}_{\text{flow}}^{\max} = \frac{\alpha Eb_v}{R_c} \quad (7.14)$$

where  $b_v$  is the magnitude of the Burgers vector,  $\alpha$  is a parameter describing the strength of interactions between moving dislocations in a plastically deforming body and  $E$  is the material Young's modulus. The magnitude of the Burgers vector  $b_v$  can be calculated from:

$$b_v = \frac{a}{2} \sqrt{2} \quad (7.15)$$

where  $a$  is the material lattice constant (for copper  $a = 0.36$  nm).

Finally, knowing that the crack will start to propagate once the stress intensity factor at the crack tip has reached its critical value and enforcing the stress continuity at the elastic core-plastic zone boundary  $r = R_c$  ( $R_c = (E/\Lambda^2)(E(\alpha b_v)/W_A)$ ) the ratio between the adhesive energy and the work of adhesion is:

$$\frac{G_c}{W_A} = \beta I_n \left( \frac{\Lambda^2}{\xi_n^{1+n}} \right)^{1/n} \left( \frac{W_A}{\alpha b_v \sigma_Y} \right)^{(1-n)/n} \quad (7.16)$$

To be able to utilize the Equation 7.16, the work of adhesion for the material system has to be known and the parameter  $\alpha$  has to be estimated. For the parameters  $\sigma_Y$ ,  $\xi$ ,  $f_n$ ,  $I_n$  and  $b_v$  the values for copper will be used. For the rest it is assumed that the relation 7.16 between  $G_c$  and  $W_A$  also applies to a two material system if one of the materials has negligible crack tip dissipation.

## 7.5 Work of adhesion: Calculations from the MD results using a mixing rule

The work of adhesion for the copper–ABS system will be calculated from MD calculated works of adhesion for SAN, pBd and oxidized SAN molecules (see Section 6.3) using a mixing rule. For the PVD sputtering conditions that were used in the experiments (see Section 3.2), it is expected to have around 30 % of copper–oxides present in the sputtered films<sup>[11]</sup>. Since in the case of the oxygen surface density of 0.143 atoms/Å<sup>2</sup> there is a complete coverage of the copper surface with oxygen atoms, the works of adhesion of the molecules calculated on copper surface modified with 0.075 oxygen atoms/ Å<sup>2</sup> (see Section 6.2.1) were used, as this is closer to reality where the surface is not completely covered by the copper oxides. The work of adhesion between the surface of choice and the oxidized SAN molecule was used in order to simulate the storage time dependence of the work of adhesion originating from the oxidation of ABS (see Section 5.3).

The mixing rule used was defined by the following equation:

$$W_A = \omega_{\text{SAN}} (\omega_{\text{pSAN}} W_{\text{ApSAN}} + \omega_{\text{oSAN}} W_{\text{AoSAN}}) + \omega_{\text{pBd}} W_{\text{ApBd}} \quad (7.17)$$

Here  $\omega_{\text{SAN}}$  and  $\omega_{\text{pBd}}$  are the weight factors describing the contribution of the continuous SAN phase and dispersed pBd phase, respectively,  $\omega_{\text{pSAN}}$  and  $\omega_{\text{oSAN}}$  are the weight factors for pure, non–oxidized and oxidized SAN, respectively. The corresponding works of adhesion values calculated from MD simulations are labeled as  $W_{\text{ApSAN}}$ ,  $W_{\text{AoSAN}}$  and  $W_{\text{ApBd}}$ . Remains is to determine the work of adhesion for oxidized SAN molecule and the weight factors.

Earlier the work of adhesion for oxidized SAN molecule was calculated for the molecule containing 30 % of oxidized phenyl rings, which does not have to correspond to the oxidation degree observed by the FTIR measurements (see Section 5.3 Table 5.1). So, an estimate of the oxidation degree at the copper-ABS interface will have to be determined and the corresponding work of adhesion estimated. To estimate the oxidation degree the following analysis is used. The oxidation of ABS normally starts within the pBd rubber particles and the generated radicals act as the initiators for the oxidation of SAN phase<sup>[12]</sup>. Every double bond of the pBd molecules is thus assumed to generate a radical which is responsible for oxidation of one phenyl ring within the SAN molecule (see Section 6.2.1 Figure 6.2).

Within the ABS material pBd phase constitutes 14 % wt. and SAN phase 86 % wt. Based on these values and the molecular weights of the repeat units within pBd (54 g/mole) and SAN (96.6 g/mole) molecules, the total number of double bonds and the phenyl rings can be estimated (for 1 g of ABS this is  $1.55 \times 10^{21}$  of double bonds and  $4.57 \times 10^{21}$  phenyl rings). The area below the FTIR peaks corresponding to the butadiene double bonds (see Section 5.3 Figure 5.4) decreases, on average, by 10 % for the longest stored samples. It will be taken that this decrease corresponds to 10 % of double bonds being transferred to radicals ( $1.55 \times 10^{20}$  double bonds per gram ABS), causing the oxidation of the same number of phenyl rings within the SAN molecules. Thus, only around 3 % of totally present phenyls is oxidized during 1008 hours. The work of adhesion for a SAN molecule containing 3 % of oxidized phenyl rings can be estimated in a following manner. The work of adhesion for a 0 % oxidation degree is 1.44 J/m<sup>2</sup> (value of the work of adhesion for the pure SAN molecule), for the oxidation degree of 30 % it is 1.55 J/m<sup>2</sup> and for the degree of oxidation of 50 % it equals<sup>††††</sup> 2.21 J/m<sup>2</sup>. These three values are linearly extrapolated (setting the intercept value at 1.44) and it is estimated that for a degree of oxidation of 3 % the work of adhesion  $W_{\text{AoSAN}}$  should be (approximately) 1.48 J/m<sup>2</sup>.

The weight factors  $\omega_{\text{SAN}}$  and  $\omega_{\text{pBd}}$  were taken to be approximately equal to the weight fractions of the SAN and pBd phases within the ABS, meaning 0.86 and 0.14,

---

<sup>††††</sup> The work of adhesion for 50 % oxidized SAN molecule on copper surface modified with 0.075 O atoms/Å<sup>2</sup> was calculated following the procedure described in Chapter 6.

respectively (the density of the two phases is around 1 g/cm<sup>3</sup> so the weight fractions will correspond to the volume fractions). The weight factors for the pure and oxidized SAN,  $\omega_{\text{pSAN}}$  and  $\omega_{\text{oSAN}}$  respectively, are time dependent variables since the amount of oxidized SAN is increasing in time at the expense of the non-oxidized molecules (see Chapter 5). During the storage time between 0 and 48 hours no oxidation of the ABS takes place and the weight factors for pure SAN molecule  $\omega_{\text{pSAN}}$  equals 1 during this period. At 1008 hours of the storage time 3 % of all phenyl rings has been oxidized, and accordingly  $\omega_{\text{oSAN}}$  is taken as 1 at this point. For the storage time in between 48 and 1008 hours the weight factors for the oxidized SAN are taken to diminish according to the ratios of the data shown in Table 5.1\*\*\*\*. The time dependence of the weight factors is summarized in Table 7.1.

Storage time [h]	Weight factors	
	SAN	Oxidized SAN
0	1	0
2	1	0
5	1	0
24	1	0
48	1	0
120	0.6	0.4
240	0.55	0.45
384	0.5	0.5
1008	0	1

**Table 7.1.** Storage time dependence of the weight factors of pure and oxidized SAN molecules.

The time dependence for the work of adhesion of copper-ABS interface can now be estimated using Equation 7.16 and Table 7.1. The dependence is shown in Figure 7.5.

---

\*\*\*\* For example at the storage time of 384 hours the ratio (1.5-1)/(2.1-1) is approximately 0.5, thus the ratio of weight factors at 1008 hours and 384 hours has also to be 0.5.

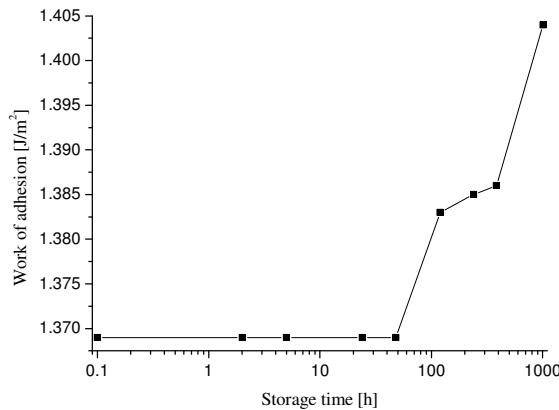


**Figure 7.5.** Storage time dependence of the work of adhesion calculated using the mixing rule (Equation 7.16).

## 7.6 Discussion

It has been shown that the substrate properties and the possible energy dissipation within this material component have no significant influence on the adhesive energy calculated using an energy balance based model described in Chapter 2. Thus, the estimates for the adhesive energy, based on the experimental data are reliable and can only depend on the material properties of the copper coating (Young's modulus, yield stress, hardening exponent etc) used to determine the adhesive energy which is, accordingly, taken to lay in a region shown in Figure 7.3.

On the other side this adhesive energy includes the local plasticity at the crack tip and the adhesive energy can be estimated based on the model presented in Section 7.4 and the work of adhesion calculated from MD calculations. The only missing parameter to be able to use the Equation 7.16 is the parameter  $\alpha$ . This parameter will be determined by matching the adhesive energy calculated from the peel test with the work of adhesion calculated from MD simulations at the storage time 48 hours. The matching will be done for this point as it is expected that here a pure copper-ABS interface adhesive energy is measured (no water presence and a purely adhesive break at this point make it suitable

for comparison with the MD results). The matching leads to the value of the parameter  $\alpha = 0.393$ . The value seems reasonable as it differs not too much from the value of 0.3 for a random dislocation distribution within the material<sup>[9]</sup>. If now the adhesive energy is calculated from Equation 7.16 and compared with the experimentally obtained values, the situation as shown in Figure 7.6 is obtained.

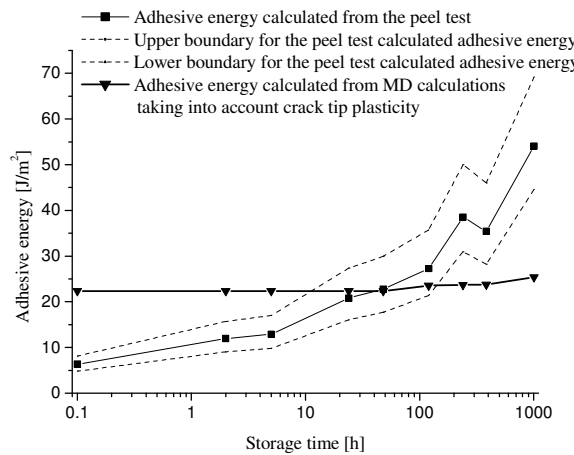


**Figure 7.6.** Comparison of the experimentally determined adhesive energy and the adhesive energy calculated based on the MD simulation taking into account the crack tip plasticity.

The difference during the first 48 hours of the storage time is expected since the water that is present at the interface immediately after the galvanic deposition has a detrimental influence on the adhesion. The discrepancy for the longer storage time may come from the fact that the mode of failure changes. Since in all of the calculations a completely adhesive break along the coating-substrate interface is assumed, it is possible that the gap is caused by the energy consumed for the break of the polymer during the cohesive break or that the values of the thermodynamic work of adhesion have to be estimated for the polymer-polymer interactions within the substrate material and not for the interactions between substrate and the coating.

## 7.7 Conclusions

The most significant energy dissipation contributions to the total energy input into the peel test for copper-ABS system come from the overall bending of the delaminating metallic film while all the substrate contributions are negligible. Using the mixing rule and the work of adhesion estimated from the MD simulations, the work of adhesion was estimated for the material system used (no literature data were available for comparison). The work of adhesion thus calculated can be corrected for the local plasticity at the crack tip within the film and the corresponding adhesive energy can be calculated. Matching of these values and the adhesive energies measured by the peel test was possible only for a small storage time interval (24-120 h of storage).

## References

- [1] I. Georgiou, H. Hadavinia, A. Ivankovic, A. J. Kinloch, V. Tropsa, J. G. Williams, *J. Adhes.* **2003**, *79*, 239–265.
- [2] G. A. Maugin, *The thermomechanics of plasticity and fracture*, Cambridge University Press, Cambridge, **1992**, p. 276-282.
- [3] P. G. Th. van der Varst, *Internal communication note*, September 21, **2006**.
- [4] R. M. Christensen, *Theory of viscoelasticity, an introduction*, Academic Press, New York, **1971**, p. 3-9.
- [5] D. Maugis, *Contact, adhesion and rupture of elastic solids*, Springer, Heidelberg, **2000**, p. 377.
- [6] M. Hetényi, *Beams on elastic foundation*, The University of Michigan Press, Ann Arbor, **1958**, p. 214.
- [7] Y. L. Zhang, G. M. Spinks, *J. Adhes. Sci. Technol.* **1997**, *11*, 207–223.
- [8] R. van Tijum, *Interface and surface roughness of polymer–metal laminates*, PhD Thesis, Rijksuniversiteit Groningen, **2006**.
- [9] D. M. Lipkin, G. E. Beltz, *Acta Mater.* **1996**, *44*, 1287-1291.
- [10] R. Thomson, *J. Mater. Sci.* **1978**, *13*, 128-142.
- [11] C. Schrauwen, R. Tacken, V. Frencken, T. van Oudheusden, R. Renders, K. Spee, *Soc. Vac. Coaters*, **2006**, 505/8560–7188, 17–22.
- [12] Rabek, J. F. *Polymer photodegradation: Mechanisms and Experimental Methods*, Chapman & Hall, London, **1995**, p. 203.



## CHAPTER 8

### MANIPULATING THE ADHESION: BLOCK COPOLYMERS AS ADHESION PROMOTING LINKERS\$\$\$\$

**Summary:** In this part the possibilities of intentionally manipulating the adhesion will be explored. In collaboration with an accompanying project<sup>[2, p. 163-201]</sup> it was found that the adhesion can be influenced by using different block copolymers as adhesion promoting linkers between the ABS on the one side and the copper coating on the other. These block copolymers consisted of a *poly(styrene-co-acrylonitrile)* (SAN) block and of a polar block, *i.e.* a *poly(styrene-alt-maleic anhydride)* (SMAh) or a *poly(4-vinylpyridine)* (P4VP) block. The adhesion promoting capacity, combined with the influence of the use of solvent, will be explained using pull-off test results.

---

\$\$\$\$ This chapter has been submitted for publication: S. Kisin, J. Božović Vukić, S. Hoeppener, B. Klumperman, C. E. Koning, G. de With, Block copolymers as adhesion promoting linkers between copper and acrylonitrile–butadiene–styrene (ABS) polymer, *Chem. Mater.* **2006**.

## 8.1 Introduction

In Chapter 5 it was seen that the adhesion, as measured by the peel test, shows a strong increase in time owing to development of oxygen containing moieties in the ABS near the interface. These results were confirmed by the MD calculations presented in Chapter 6. In the same chapter it was showed that a copolymer with a high oxygen content exhibits strong interactions with oxidized copper surfaces. To experimentally confirm results and gain better understanding of the adhesion mechanism the adhesion of (block) copolymer modified ABS substrates to copper will be evaluated.

To quantify the adhesion and to evaluate the influence of (block) copolymers on the adhesion the pull-off test was used. The test has proven to be very reliable as the results can be successfully related to scanning force microscopy adhesion measurements<sup>[1,2]</sup>.

The designed block copolymers are composed of two different blocks, whose compatibility with the respective layers of the laminate (the SAN phase of the ABS substrate and the copper coating) is controlled by their chemical composition and structure. For the SAN-compatible block, a copolymer similar to SAN was the obvious choice. If the acrylonitrile content of the SAN block is similar to the acrylonitrile content of the ABS SAN phase, molecular entanglement formation<sup>[3]</sup>, and accordingly adhesion enhancement, is possible. An alternating copolymer, *poly(styrene-*alt*-maleic anhydride)* (SMAh) or a homopolymer, *poly(4-vinylpyridine)* (P4VP), containing polar groups was chosen for the block sticking to the copper layer (structures shown in Figure 8.1a). These microphase separating block copolymers<sup>[4,5]</sup> demix into a SAN block, which is strongly entangled<sup>[2]</sup> with the SAN phase in an ABS substrate, and a polar block which is free for the interaction with the applied metal coating.

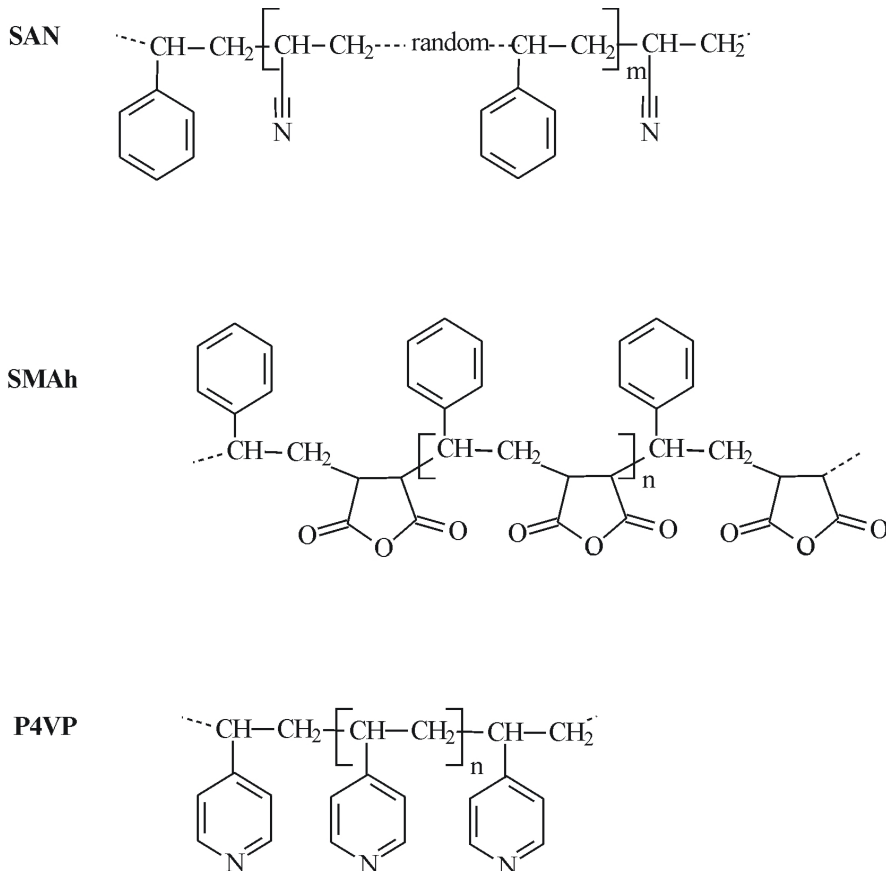


**Figure 8.1.** Structures of the copolymers used to improve the adhesion between the ABS and copper.

## 8.2 Experimental procedures \*\*\*\*

Normally used ABS substrates (for details see Section 3.1) were cut into a smaller rectangular slides referred throughout the text as ABS panels ( $10 \times 10 \times 1 \text{ mm}^3$ ). Afterwards the panels were coated with well defined copolymer and block copolymer

---

\*\*\*\* The pull off test used for adhesion quantification has been developed as a part of PhD research project of Srdjan Kisin at the Laboratory of Materials and Interface Chemistry while the synthesis and characterization of all the model copolymer and block copolymer molecules was performed at the Laboratory of Polymer Chemistry as a part of the PhD research project of Jelena Božović Vukić. The two projects have been related through the framework of Innovation Oriented research Program Surface Technology (IOP-OT) project #IOT01008.

films via spin-coating. Finally the copper coating was deposited on top of the polymer coated ABS panels using a PVD process (see Section 3.2) and the adhesion of the copper layers was tested by the pull-off test. Sample structure and the experimental settings for the pull-off test are described in detail in Section 2.2. All the measurements were repeated five times approximately 48 hours after the PVD copper deposition. Figure 8.2 shows the typical force–time curve obtained from the pull-off test and the rest of the results are presented as the detachment forces with the corresponding standard deviation values. In all the cases the fracture occurred along the Cu–ABS interface.

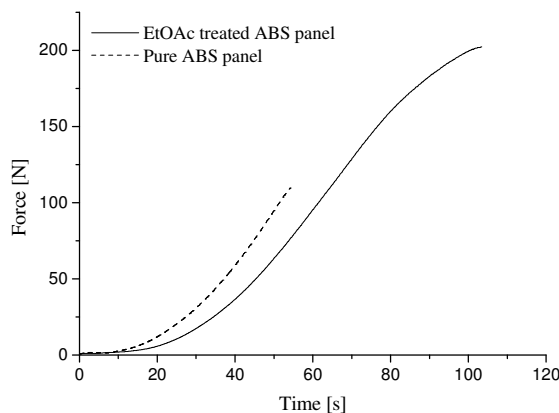


**Figure 8.2.** Typical force–time curve for the pull-off tests on copper coated pure and solvent (EtOAc) treated ABS panels.

## 8.2.1 Model copolymer synthesis and molecular characterization

### 8.2.1.1 Materials

**Monomers:** styrene (STY, Aldrich 99+%), maleic anhydride (MAh, Aldrich 99%, briquettes) and 4-vinylpyridine (4VP, Aldrich, 99%).

Initiators:  $\alpha,\alpha'$ -azobisisobutyronitrile (AIBN, Merck, > 98%), 1,1'-azobis(1-cyclohexanecarbonitrile) (ACHN, Wako, > 98%) and 4,4'-azobis(4-cyanovaleic acid) (ACVA, Fluka, > 98%).

Solvents: n-heptane (Aldrich, 99.5%), toluene (Hi-Dry<sup>TM</sup>, anhydrous, Romil Ltd.) butanone (Merck, 99%) and ethyl acetate (EtOAc, Biosolve, AR).

### 8.2.1.1 Synthesis and characterization<sup>†††††</sup>

Both copolymers, SAN<sup>[6]</sup> and SMAh<sup>[7]</sup>, were synthesized<sup>[8]</sup> via solution polymerization by a reversible addition–fragmentation chain transfer (RAFT)-mediated polymerization, using S-dodecyl-S'-(isobutyric acid) trithiocarbonate (DIBTTC), as chain transfer agent (CTA). The chain transfer agent was synthesized according to Lai *et al.*<sup>[9]</sup> recrystallized from n-heptane and dried under vacuum. The RAFT technique allows the synthesis of well defined polymers, with predetermined molar mass and narrow molar mass distributions. Molar masses of the copolymers were determined using size exclusion chromatography (SEC, Waters GPC with Waters 510 pump and 410 differential refractometer) relative to *poly(styrene)* standards and are labeled as  $M_{n,SEC}$  in Table 8.1. The molecular weight ( $\overline{M}_w$ ) of random SAN copolymer (20 wt % of AN, and  $\overline{M}_{n(SAN)}$  = 74.6 kg/mole;  $\overline{M}_w/\overline{M}_n = 1.2$ ), used in this study, is a factor 7–8 higher than the average molar mass between entanglements<sup>[10]</sup>,  $\overline{M}_{e(SAN)} \approx 10$  kg/mole<sup>[11]</sup>. The applied SMAh copolymer is an alternating copolymer, with almost equal amounts of STY and MAh and a regular chain structure. The  $\overline{M}_e$  value of the SMAh copolymer is in the order of magnitude of 18–25 kg/mole, which is higher than the molar mass of the SMAh copolymer applied in this study ( $\overline{M}_{n(SMAh)} = 14$  kg/mole,  $\overline{M}_w/\overline{M}_n = 1.1$ ).

---

<sup>†††††</sup> Completely elaborated synthetic procedure is available elsewhere<sup>[11]</sup>.

Sample name	Media	Block copolymer	SAN block	SMAh/P4V P block
		$M_{n,SEC} (\times 10^3 \text{ g/mole})$		
SAN	solution	-	74.6	-
SMAh		-	-	13.1
SMAh- <i>b</i> -SAN (High $M_n$ )	solution	151.3	138.2	13.1
SMAh- <i>b</i> -SAN (Low $M_n$ )		135.4	129.9	5.5
SMAh- <i>b</i> -SAN	latex	81.7	76.2	5.5
P4VP- <i>b</i> -SAN		48.8	47.6	1.2

**Table 8.1.** The SAN and SMAh model copolymers, and SMAh-*b*-SAN and P4VP-*b*-SAN block copolymers of different molar masses and of different SAN block lengths, used as adhesion promoting linkers.

SMAh copolymer (Table 8.1) was used as a macro-CTA for the synthesis of high  $M_n$  SMAh-*b*-SAN (Table 8.1). For this, SMAh copolymer was dissolved in a mixture of toluene and butanone (70/30 w/w) and STY and AN monomers followed by an azo-initiator AIBN or ACHN were added to the solution to reinitiate polymerization. A similar procedure was followed for synthesis of low  $M_n$  SMAh-*b*-SAN (Table 8.1), the only difference being the molecular weight of the starting macro-CTA (5.5 kg/mole in this case).

For synthesis of SMAh-*b*-SAN latex (Table 8.1), 5.5 kg/mole SMAh copolymer was used as a macro-CTA and azeotropic STY/AN mixture (63/37 mole/mole) was used for chain extension. ACVA was used as the initiator.

For latex P4VP-*b*-SAN (Table 8.1), P4VP of 1.2 kg/mole was synthesized from 4VP monomer via RAFT polymerization using DIBTTC as CTA. The polymer so obtained was then used for additional chain extension with STY/AN monomer mixture in a semi-continuous emulsion polymerization process<sup>[12]</sup>.

### 8.2.2 Polymer film formation by spin-coating and application of block copolymer latex

The ABS panels were ultrasonically treated for 15 minutes in a 10 wt. % solution of soap in water (Milli-Q). After this step the ABS substrates were washed several times with Milli-Q water and then heated up to 60 °C for 60 minutes in a vacuum oven prior to use. A thin polymer layer (~ 100 nm) was applied on the ABS substrate by spin-coating either from the polymer solution (SAN, SMAh copolymers and high and low  $M_n$  SAN-*b*-SMAh blocks in Table 8.1) or from the aqueous dispersion (latexes in Table 8.1). In the case for application from the solution, the polymers were dissolved in ethylacetate (EtOAc), at a 30 mg/mL concentration prior to spin-coating. To evaluate its influence on the adhesion, the pure EtOAc was spin-coated as well. The aqueous dispersions (referred to as latexes) were used as obtained after the emulsion polymerization reaction. The polymer solutions, the pure solvent and the aqueous dispersions were applied on the ABS panels by spin-coating, using a KarlSus, RC8 apparatus, at 2500 rpm for 45 s and with an acceleration of 1500 rpm/s. The resulting samples were dried under vacuum at 40 °C for 3 days to remove any residual solvent. It is important to mention that also the latex coated ABS panels were post-treated after the application: they were dried under vacuum at 80 °C for 4 h in order to improve the adherence to the ABS substrate before the copper coating was applied.

## 8.3 Changes in adhesion

### 8.3.1 Influence of the solvent on the ABS surface and copper-to-ABS adhesion

For application of the (block) copolymers on the ABS surface spin-coating from EtOAc solution is performed. Since ABS consists of a continuous SAN phase and since EtOAc is able to swell the pBd particles and even partially dissolve SAN, a clear influence of this solvent on the surface and on the adhesion process can be expected. To investigate this in more detail pure EtOAc was applied on the ABS panels and it was found to

change their surfaces (Figure 8.3). A comparison of Figures 8.3a and 8.3b learns that the ABS surface becomes smoother, but at the same time shows a higher number of holes upon solvent application. It is hypothesized that the generation of these holes is related to the presence of pBd rubbery particles, at or very close to the surface.

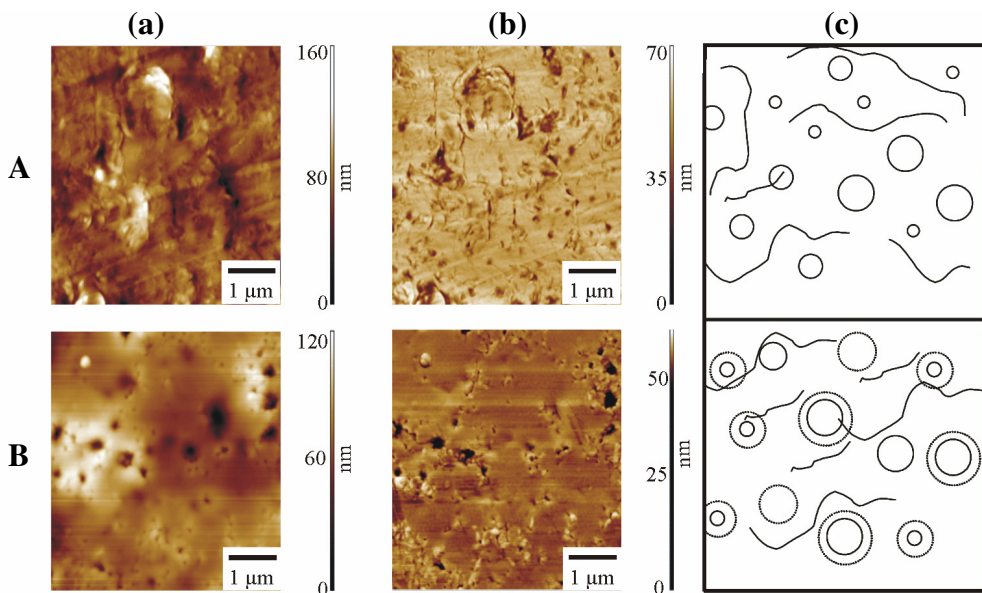


**Figure 8.3.** SFM images a) topography, b) phase images and c) schematic top view of the ABS surface. A) pure ABS substrate without any treatment and B) solvent treated ABS. Note that pictures (B) were taken after complete evaporation of solvent (ethyl acetate). In c) the lines indicate the ‘loose’ SAN molecules while the circles refer to the pBd particles (swollen state shown in dotted lines).

When the ABS substrate is exposed to the solvent, the crosslinked pBd rubber particles, containing the EtOAc soluble ‘occlusion’ SAN, will swell. Furthermore, non-grafted SAN polymer chains close to or at the surface are dissolved, pushed away from the swollen rubber particles and deposited elsewhere on the surface (see Figure 8.4 A and B). After evaporation of the solvent, the newly distributed SAN leaves a perfectly smooth surface and former irregularities and small holes have disappeared. Upon evaporation of the solvent, there is shrinkage of the pBd particles, but there is no reason why the transported loose SAN polymer chains would return to their original position. This might explain why the number of new holes seems to increase (see Figure 8.3b).

One should also take into account that the continuous SAN phase dries out faster than the occlusion SAN-containing pBd particles. After the continuous SAN phase has solidified, the pBd particles will slowly loose their EtOAc and the pBd particles will shrink inside an already solidified SAN environment. This process results in the formation of relatively large holes, much larger than the small cavities introduced by the injection molding process.

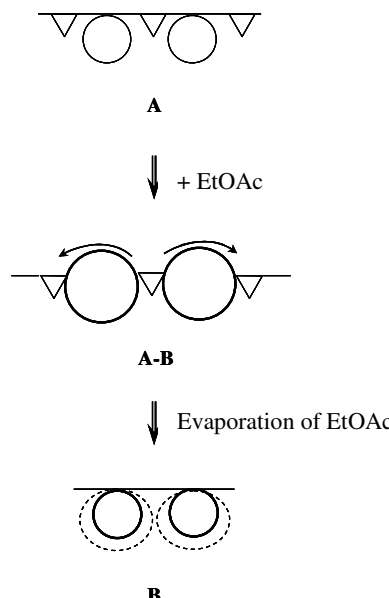


**Figure 8.4.** Side view of the ABS substrate shown in Figure 8.3c A) without any treatment, A-B) during and B) after the treatment with the ethyl acetate.

In Figures 8.2 and 8.5 one can compare the pull-off forces of a copper coated pure, non-treated ABS and a copper coated ABS which has been pretreated with EtOAc. The force required to detach the copper coating from a pure ABS substrate is approximately half of the detachment force for the EtOAc treated panel. This difference can be attributed to increased mechanical interlocking of copper and ABS, in line with the larger number of the surface holes initiated by the solvent treatment. Namely, the holes formed on the substrate surface can act as nucleation centers for the copper during the PVD process. The number of nucleation sites created on the ABS surface is thus increased, allowing for a larger number of anchoring points between the substrate and the coating. In addition to this ‘enlarged surface effect’ and mechanical interlocking, one

cannot exclude that the EtOAc treatment removes some low molar mass material, which had not been removed by the washing with the soap. This loss of low molar mass components would also enhance the adhesion.

### 8.3.2 Influence of the SAN and SMAh copolymers on the copper-to-ABS adhesion

Knowing that EtOAc itself has a large influence on the adhesion strength of copper on ABS, EtOAc treated ABS samples were used as the reference. Subsequently, the SAN and SMAh model copolymers were applied on the ABS substrate from an EtOAc solution, after which the copper was deposited. Figure 8.5 shows that the adhesion force for the SMAh-covered sample is lower, whereas for the SAN-covered sample it was the same as compared to the EtOAc-treated ABS reference sample. Nevertheless, our previous results on pure SMAh and SAN showed a stronger adhesion of copper to SMAh than to SAN<sup>[1,2]</sup>. For the SMAh-covered substrate, the low detachment force indicates that there is no strong interaction between the deposited SMAh and the SAN phase of the ABS substrate. These two phases are expected to be incompatible<sup>[12]</sup> owing to a large mismatch in their STY content (roughly 30 wt. %). The result obtained for the SAN-based sample indicates that there is no significant influence of the SAN copolymer, which was applied on the ABS substrate from an EtOAc solution, on the adhesion to the copper coating. Note that the contents of AN in the deposited SAN sample (*ca.* 20 wt. % of AN) and in the SAN of the ABS substrate (*ca.* 24 wt. % of AN) do not differ more than 4 wt%, which guarantees their good miscibility<sup>[14]</sup>. One may argue that the SAN layer, deposited on the ABS, could counteract the solvent effect, in which the pBd rubber particles play a crucial role (Figure 8.3). However, the deposited SAN layer is thinner than the diameter of the pBd spheres, which will definitely swell and shrink upon the solvent treatment and evaporation, respectively, thereby enhancing the surface roughness regardless of the presence of the additional SAN.

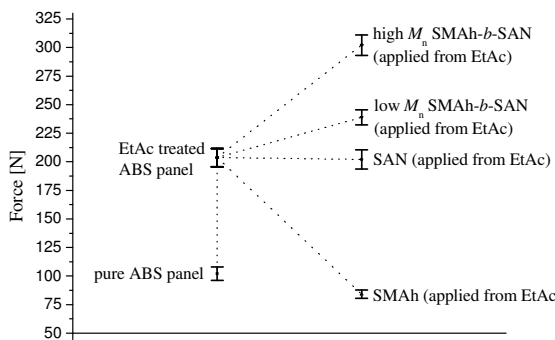


**Figure 8.5.** Detachment forces, measured by the pull-off test, for copper coated copolymer and block copolymer modified ABS panels. Note that the (block) copolymers were applied from the EtAc solution. Detachment forces for copper coated pure ABS and copper coated EtAc treated ABS panels are shown as references. Data points indicate the average of 5 measurements while the error bars indicate the sample standard deviation. The horizontal axis is not drawn as a scale.

### 8.3.3 Influence of the solvent borne SAN–b–SMAh block copolymers on the copper–to–ABS adhesion

Significantly higher forces were required to detach the copper coating from the block copolymer treated samples, as compared to the corresponding forces required for the pure ABS substrate and for the EtOAc–treated ABS substrate, as well as for the SAN–covered system (Figure 8.5). The high molecular weight block copolymer shows a higher adhesion force as compared to the sample modified with low  $M_n$  SMAh–b–SAN block copolymer. The reason could lie in a higher number of SMAh–copper bonds formed in the case of the high  $M_n$  sample as the differences between these block copolymers are restricted to the SMAh block lengths, whereas SAN block lengths are similar, ensuring the comparable degree of entanglement formation with the SAN phase of the ABS substrate.

A possible explanation for the superior adhesion observed when both the solvent and a block copolymer are used, is that the SAN polymer chains at the surface of the ABS, during the spin–coating process, are dissolved in the EtOAc, in which the block copolymer has already been dissolved. This assures an efficient entanglement formation

during evaporation of the solvent after the spin-coating process. The results obtained indicate that the presence of a block copolymer, in which SAN and SMAh blocks are covalently linked together, is crucial for obtaining good adhesion between copper and ABS. This block copolymer acts as an interface-active compound, and clearly enhances the interfacial adhesion. Note that the use of a solvent has an enormous influence on the ABS surface texture, and probably also on the indispensable entanglement formation, and consequently shows strong interference with the adhesion process.

### 8.3.4 Influence of the water borne latexes on copper-to-ABS adhesion

In addition to evaluating the influence of the solvent borne block copolymers on the copper-to-ABS adhesion, pull-off measurements were performed on samples in which water-borne block copolymer latexes were used as interface-active compounds. The results were compared to those of copper coated pure ABS substrates, since for the latex application the use of EtOAc solvent is omitted. Furthermore, a SAN copolymer free-film was applied on the ABS substrate. In this specific case, the SAN film was pre-formed by spin-coating on a glass substrate, and subsequently transferred to the ABS panel. In order to enable the deposited SAN to form entanglements with the polymer chains present in the SAN phase of the ABS substrate, the sample was annealed for 3 h at 90 °C. Note that this temperature is below, but close to the  $T_g$  of SAN (~107 °C). Anyway, the applied temperature proved to be high enough to provide a relatively strong interaction between the SAN copolymer film and the ABS substrate. Figure 8.6 shows that the adhesion force for this sample is of the same order of magnitude as the adhesion force recorded for the reference ABS sample (compare to the SAN sample applied from EtOAc solution, which gave a much stronger adhesion). The application of a free SAN copolymer film between the ABS and copper makes no essential difference to the adhesion. The higher detachment force in the case of SAN applied from EtOAc solution can be explained by the more efficient entanglement formation compared to the case where a free SAN film was applied and annealed at 90 °C.

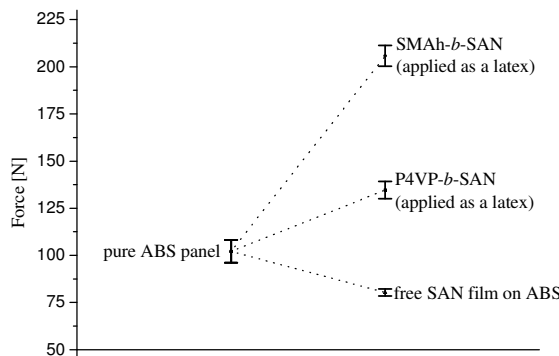


**Figure 8.6** Detachment forces, measured by the pull-off test, for copper coated P4VP-*b*-SAN and SMAh-*b*-SAN modified ABS panels and for copper coated free SAN film on ABS. Note that the block copolymers were applied from the aqueous dispersions containing block copolymer latex particles; free SAN film was annealed for 3 h at 90 °C on the ABS substrate. Detachment force for copper coated pure ABS is shown as reference. The horizontal axis is not drawn as a scale.

Furthermore, Figure 8.6 illustrates that the copper adhesion forces increase, as compared with the adhesion force of the pure ABS reference sample, when block copolymer latexes (see the corresponding symbols) were applied as interface-active compounds. The adhesion force increases with increasing length of the block interacting with the copper coating (SMAh and P4VP). Because of the different lengths of the SMAh and P4VP blocks in the corresponding block copolymers, one cannot conclude that SMAh outperforms P4VP as a copper-adhering block. The worse performance of the P4VP-*b*-SAN block copolymer may also be due to its relatively low molar mass SAN block which might result in somewhat less efficient entanglement formation. Finally, the block copolymers spin-coated from EtOAc give a slightly stronger adhesion than the spin-coated block copolymer latexes. The low molecular weight SMAh-*b*-SAN and latex SMAh-*b*-SAN have the same SMAh block length and their both SAN blocks have a sufficiently high molar mass ( $\geq 7-8 \times \overline{M}_{e(SAN)}$ , being *ca.* 10000 g/mole<sup>[10]</sup>) for efficient entanglement formation with the SAN phase of the ABS. The block copolymer, spin-coated from EtOAc, gives an adhesive force of around 240 N, whereas the block copolymer spin-coated as a latex, gives a maximum force of about 205 N. Clearly the

more efficient entanglement in the case of the sample applied from the EtOAc solution can explain this difference.

## 8.4 Conclusions

Block copolymers consisting of an SAN block and a second block containing polar groups, either maleic anhydride or 4-vinylpyridine, were investigated as adhesion promoters at the interface between ABS and copper. Pull-off adhesion measurements were performed in order to evaluate the influence of these block copolymers on the adhesive interactions.

The results obtained indicate that the application of the block copolymers results in significantly higher binding affinity between copper and ABS, the value of the adhesive force being dependent on their molecular weight. The adhesive force increases with increasing length of the polar block interacting with the copper, provided that the SAN block is long enough for an efficient entanglement formation on the ABS side. Therefore these block copolymers can be used as adhesion promoting linkers between a copper coating and an ABS substrate. There is a pronounced difference between applying these polymers from ethyl acetate solution or from an aqueous dispersion of the corresponding block copolymers, as the EtOAc itself has a strong influence on the adhesion forces. The use of the proper organic solvent, facilitating the entanglement formation between the SAN block and the SAN phase of the ABS, is crucial for obtaining good adhesion. Our best system shows a three-fold enhancement of the copper–ABS adhesion with respect to pure, non solvent-treated ABS.

## References

- [1] J. Božović, S. Hoeppener, D. A. Kozodaev, S. Kisin, B. Klumperman, U. S. Schubert, G. de With, C. E. Koning, *ChemPhysChem*, **2006**, *7*, 1912–1916.
- [2] J. Božović Vukić, *Block copolymers for adhesion improvement synthesized via RAFT-mediated polymerization*, PhD Thesis, Technische Universiteit Eindhoven, Eindhoven, **2006**.
- [3] G. Hadzioannou, S. Patel, S. Granick, M. Tirrell, *J. Am. Chem. Soc.* **1986**, *108*, 2869–2876.
- [4] F. S. Bates, *Science* **1991**, *251*, 898–905.
- [5] A. Noro, M. Iinuma, J. Suzuki, A. Takano, Y. Matsushita, *Macromolecules* **2004**, *37*, 3804–3808.
- [6] J. Chiefari, Y. K. B. Chong, F. Ercole, J. Krstina, J. Jeffery, T. P. T. Le, R. T. A. Mayadunne, G. F. Meijjs, C. L. Moad, G. Moad, E. Rizzardo, S. H. Thang, *Macromolecules* **1998**, *31*, 5559–5559.
- [7] H. D. Brouwer, M. A. J. Schellekens, B. Klumperman, M. J. Monteiro, A. L. German, *J. Polym. Sci., Part A: Polym. Chem.* **2000**, *38*, 3596–3603.
- [8] J. Bozovic, B. Klumperman, *Polym. Preprints* **2005**, *46*, 450.
- [9] J. T. Lai, D. Filla, R. Shea, *Macromolecules*, **2002**, *35*, 6754–6756.
- [10] S. Wu, *J. Polym. Sci., Part B: Polym. Phys.* **1989**, *27*, 723–741.
- [11] S. Wu, *Polymer Engineering & Science* **1992**, *32*, 823–830.
- [12] C. J. Ferguson, R. J. Hughes, D. Nguyen, B. T. T. Pham, R. G. Gilbert, A. K. Serelis, C. H. Such, B. S. Hawkett, *Macromolecules*, **2005**, *38*, 2191–2204.
- [13] C. Wastlund, H. Berndtsson, F. H. J. Maurer, *Macromolecules*, **1998**, *31*, 3322–3327.
- [14] J. Božović Vukić, J. Meuldijk, B. Klumperman, C. E. Koning, *Macromolecules*, **2006**, submitted manuscript.



# CHAPTER 9

## EPILOGUE

### 9.1 The lessons learned

Adhesion is not something constant in time, but shows significant changes with time, which are caused by different processes taking place at the interface as a result of the preparation procedure. For sputtered and galvanically strengthened copper films, the removal of galvanically introduced water from the interface causes a large increase in adhesion. The water saturated interface shows quite small values of the adhesive energy as the water separates the surfaces in contact on a molecular level. As the water disappears, the materials get into intimate contact showing a higher adhesion and subsequently start to influence each other. As the sample is stored for prolonged periods of time, structural changes of both materials near the interface take place, rearranging into energetically favorable conformation and thus increasing the adhesive energy. Parallel to the structural changes, chemical changes of the polymer start to occur. Probably due to a contact with the metallic surface and because water and electrolytes from the galvanic solution that were or are present at the interface, carbonyl functionalities develop at the polymer surface causing also an increase of the adhesive energy. The adhesive energy measured by the use of the mechanical 90° peel test showed a remarkable increase in time, from 6 initially to about 60 J/m<sup>2</sup> after approximately 1000 h storage.

To investigate in more detail the mechanism of the adhesion and estimate the thermodynamic work of adhesion, molecular dynamic simulations proved to be very useful. Using a relatively simple “single-molecule-on-a-metallic-surface” approach, it is possible to conclude that polymer molecules indeed change their conformation once in contact with the metallic surface and a strong influence of the oxygen atoms present in both interacting parts was found.

Using the work of adhesion calculated from the “single molecule” approach and a mixing rule, the work of adhesion for the used material system can be estimated. If these estimates are corrected for the local plasticity at the crack tip within the metallic film, only partial matching of the calculated values and peel test measured adhesive energies is obtained.

Knowing that polar moieties, such as carbonyl groups will influence the adhesion strongly, a block copolymer to be used as the adhesion promoting linker was tested. A microphase-separating block copolymer which demixes into a phase compatible with the substrate and a phase compatible with the metallic coating was tested. The proposed SAN-*b*-SMAh molecule showed strong adhesion promoting capabilities. The adhesion change caused by this molecule is visible on 2 length scales. On the macroscale, using the pull-off test, a significant adhesion increase was detected and on the molecular scale using molecular dynamics calculations, the block copolymer showed very high work of adhesion, provided that the metallic surface is oxidized.

## 9.2 Recommendations

From the practical point of view the influence of the galvanic deposition and storage time on the adhesion is the most important result. However, more clarification is needed here and a galvanically non-contaminated interface at different temperatures should be studied to determine the real magnitude and influence of the structural changes on the adhesion. The purity of the initially sputtered layers can be manipulated by changing the copper deposition rate and this should be looked into in more detail. The chemistry of the polymer should be monitored on the pure metal–polymer interface and on the galvanically modified interface. This will help to distinguish whether the contact with the metal, the contamination or both have a decisive influence. After all, the phenomenon could also be interesting from the point of view of the durability of interfaces (e.g. automotive coatings). Finally, on carefully chosen model systems macroscale and nanoscale measurements and the molecular dynamics calculations should be quantitatively linked.

## SUMMARY

The main goal of the project was to understand adhesion mechanism within the chosen model metal–polymer system on a fundamental level. To monitor the adhesion, the 90° peel test was chosen. A sputtered and galvanically strengthened copper coating on an ABS substrate was chosen as a model system because it is an industrially interesting material combination.

The adhesion proved to be a dynamic process with increasing adhesive energy in time. The reason for the drastic initial adhesion increase between copper and the ABS was ascribed to the removal of water introduced to the interface during the sample preparation procedure. The subsequent increase is due to structural rearrangements of the polymer near the interface as proven by *e.g.* contact angle measurements. Further study showed that not only structural changes of the polymer are taking place, but chemical changes as well. These chemical changes were identified using ATR–FTIR measurements and ascribed to initial stages of the ABS oxidation. Developed carbonyl moieties on the polymer surface, combined with the structural rearrangements caused the adhesion increase in time.

To theoretically confirm these results molecular dynamics calculations were performed. Using force field calculations, it became clear that the vicinity of the copper surface induces changes in geometry of *poly(styrene–co–acrylonitrile)* (SAN) and *poly(butadiene)* (pBd) molecules, constituents of the ABS. It was also possible to estimate the thermodynamic work of adhesion from the interaction energy and the van der Waals contact area between a single polymer molecule and the copper surface. The work of adhesion thus calculated is independent of the number of the polymer molecules present on the copper surface, the type of the copper surface and the repeat unit sequence within the polymer molecules. Oxidation of the copper surface and/or the SAN molecule resulted in the increase of the work of adhesion. To assess the influence of the oxygen present in the polymer molecule, the work of adhesion was calculated for a copolymer molecule with a high oxygen content, *poly(styrene–alt–maleic anhydride)* (SMAh) interacting with pure and oxidized copper surfaces. Indeed, of all the

combinations studied, the highest work of adhesion was found for the SMAh molecule on the oxidized copper surface.

Using the mixing rule and the work of adhesion estimated from the MD simulations the work of adhesion was estimated for the model system. The work of adhesion thus calculated was corrected for the local plasticity at the crack tip within the film and the corresponding adhesive energy was calculated. Matching of these values and the peel test measured adhesive energies was possible only for a small storage time interval.

Finally, adhesion promoting block copolymers, SAN-*b*-SMAh and SAN-*b*-P4VP, were tested. The SAN block provide a strong interaction with the ABS substrate by the entanglement formation while the polar blocks (SMAh and P4VP) have strong interactions with the copper coating.

The research has been financially supported by the Innovation Oriented research Program Surface Technology (IOP-OT) as a part of project #IOT01008.

## SAMENVATTING

Het hoofddoel van het project was het op fundamenteel niveau begrijpen van het adhesiemechanisme van het gekozen metaal-polymeer modelsysteem. De 90° peel test werd gebruikt om adhesie te meten. Het gekozen modelsysteem bestond uit een ABS substraat met een gesputterde en galvanisch versterkte koperlaag, vanwege het feit dat deze materiaalcombinatie interessant is voor de industrie.

Er is aangetoond dat de adhesie een dynamisch proces is; deze neem toe in de tijd. De oorzaak van de drastische initiële adhesietename tussen koper en ABS wordt toegeschreven aan de verwijdering van het water dat op het grensvlak aanwezig was tengevolge van de monstervoorbewerkingsprocedure. Latere toename wordt veroorzaakt door structurele harrangschikking van het polymeer aan het oppervlak, zoals aangetoond met onder andere contacthoekmeting. Verder inzicht in het systeem toont aan dat er niet alleen structurele maar ook chemische veranderingen van het polymeer plaatsvinden. De chemische veranderingen werden aangetoond met ATR-FTIR metingen en toegeschreven aan initiële stadia van ABS oxidatie. De in de tijd toenemende adhesie werd veroorzaakt door carbonyl eenheden op het polymeeroppervlak, gecombineerd met structurele harrangschikking.

Molecular dynamics simulaties (MD) werd gebruikt om dit theoretisch te bevestigen. Met behulp van een krachtveld berekening wordt duidelijk dat de nabijheid van het koperoppervlak geometrieveranderingen van *poly(styreen-co-acrylonitril)* (SAN) en *poly(butadiëen)* (pBd) moleculen induceert (componenten van ABS). We waren ook in staat om, uit de interactie-energie en het van der Waals contactoppervlak tussen een enkel polymeermolecuul en het koperoppervlak, de thermodynamische adhesiearbeit te schatten. De aldus berekende adhesiearbeit is onafhankelijk van het aantal polymeermoleculen op het koperoppervlak, het type koperoppervlak en de volgorde van de herhalingseenheid in het polymeermolecuul. Oxidatie van het koperoppervlak en/of van het SAN molecuul leidden tot een toename van de adhesiearbeit. Teneinde tot een schatting te komen van de invloed van zuurstof (in het polymeermolecule) op de adhesiearbeit, hebben we deze laatste berekend voor een co-polymeermolecuul met een hoog zuurstofgehalte, *poly(styreen-alt-maleïnezuur anhydride)* (SMAh) in contact met

een zuiver dan wel geoxideerd koperoppervlak. Inderdaad, van alle berekende combinaties bleek de hoogste adhesiearbeit gevonden te worden voor het SMAh molecuul op het geoxideerd koperoppervlak.

Gebruikmakend van de menregel en waarden voor adhesiearbeit zoals verkregen uit MD simulaties, werd de adhesiearbeit voor het modelsysteem geschat. Deze adhesiearbeit werd vervolgens gecorrigeerd voor de lokale plasticiteit bij de punt van de breuk in de film en de bijbehorende adhesie-energie werd berekend. Deze waarden bleken overeen te komen met de waarden voor adhesie-energie zoals verkregen uit “peel”-testen, zij het slechts voor korte opslagtijd-intervallen.

Tenslotte werd ook het effect van de adhesieverbeterende blokcopolymeren SAN-*b*-SMAh en SAN-*b*-P4VP onderzocht. Het SAN-blok levert een sterke interactie met het ABS substraat door warpuntvorming, terwijl de polaire blokken (SMAh en P4VP) sterke interactie met de koperdeklaag vertonen.

Het onderzoek werd financieel ondersteund door het Innovatiegerichte Onderzoeksprogramma Oppervlaktechnologie (IOP-OT) als onderdeel van project #IOT01008.

## **CURRICULUM VITAE**

Srdjan Kisin was born on 4<sup>th</sup> of August in Sombor in what was at the time Yugoslavia, now Serbia. Upon completion of his high school education in Sombor, in 1998 he started studies at the Faculty of Technology of the University of Novi Sad in Novi Sad (Serbia). After his graduation research on bulk free radical polymerization of styrene at the Charles University in Prague (Czech Republic), in November 2002 he obtained a degree of Graduated Engineer of Technology at the University of Novi Sad. In January 2003, as a PhD student, he joined the Laboratory of Materials and Interface Chemistry within the Department of Chemical Engineering and Chemistry at Eindhoven University of Technology in The Netherlands. The main results of the PhD research work, performed under the supervision of prof. dr. Bert de With and dr. ir. Paul van der Varst, are described in this thesis. In September 2006 he accepted to continue his career as a research engineer for Dow Benelux B.V.

## **ACKNOWLEDGEMENTS**

Fours years ago I would never believe that 4 years of my life could be summarized in 131 page. Since I'm currently typing the 132<sup>nd</sup>, it must have happened! Nonetheless, I will remember these four years as the most dynamic in my life, at least so far. Dynamic not only because in the thesis it was shown that the adhesion of copper to ABS is a dynamic process, not even because I did quite some molecular dynamics calculations, but mostly because of the people that I met, worked and lived with.

I would like to thank prof. Bert de With for giving me a chance to start a PhD research within his Laboratory, for his support, professional guidance, never-ending optimism and for steering and driving the research forward with his numerous ideas, the results of which are shown in the thesis. Most of the mathematical analysis, calculations and small energy considerations would probably not be in the text if I have had no help from dr. Paul van der Varst, who accepted to act as a co-promoter of the thesis. I have to say that the final outline of the thesis is the result of numerous differences in opinion that Paul and I had during the past few years. It taught me to approach any scientific result, technique or discussion with an optimal dose of criticism. I would also like to thank prof. Cor Koning for, not only accepting to be a member of the core-committee, but also for being actively involved in the project. I am grateful to prof. Sybrand van der Zwaag and prof. Jeff de Hosson for finding time to read through the manuscript and accepting to be the members of the core-committee.

I also have to express my gratitude to dr. Cor Schrauwen, for keeping the same level of enthusiasm for the project from the first to the last day. I learned a lot from Cor about metals on plastics, about the PVD deposition techniques and I am glad that he accepted to be a part of the defense committee. Also thanks to prof. Jaap den Toonder for having will and time to be a member of the defense committee.

The essential part of the study was the construction of the peel-testing device. I would like to thank the GTD of the Eindhoven University of Technology for manufacturing the device, in particular Erwin Dekkers for the design, Jos de Laat for turning the drawing into reality and Ruud de Regt for the sample preparation. For his patience and help during the initial period of the device testing, I have to thank Huub van der Palen.

Thanks to Francesca and Przemek for their help in performing the ATR-FTIR measurements and in interpreting the data, it resulted in Chapter 5. My most sincere gratitude goes to Jelena for her excellent work in block copolymer synthesis, for taking time to inspect the block copolymers I synthesized using a computer, for her constant drive to do more and better experiments and for, often, moving me away from my desk to the lab; it ensured meeting the goals set in the project, completing the Chapters 6 and 8 and resulted in a few publications. Thanks to Stephanie for all the AFM measurements she performed. To Sasha, thank for his instructions on how to use SEM, which were not completely unselfish, as I trained a significant number of students in using it during the unforgettable practicums. For teaching me how to perform and interpret the contact angle measurements, I have to thank Tamara. And, for all the discussions, support and understanding, I have to thank Olavio. Amir and Olavio, thanks a lot for the unique experiences on all the conferences we attended together. I am grateful to Imandra for all the help with filling in all sorts of forms, for all the translations from that funny language called Dutch and all the office supplies I got from her. Also, Imandra thank you very much for all your kindness during these 4 years.

When it comes to the more relaxed, non-work related, part of my four year, or 131 page (depends what is chosen as a unit of measurement), stay in Eindhoven some things have to be said as well. Today, unlike 4 years ago, I tend to talk a lot and express my opinion rather openly, thanks for the change go solely to the small lady named Audrey. Thanks to dr. Jetse Reijenga for offering me a chance to guide students in the MDP projects. I considered it a pleasure rather than work; after all, after each successful MDP project he sent me and the students to Istanbul. I am grateful to Huub, Sasha, Imandra, Francesca, Olavio, Przemek, Marco, Tamara, Christa, Ellen, Dennis and all the other SMG group members for all the enjoyable monthly borrels, my first day in Eindhoven was a Friday, the last Friday of the month. For the all the crazy parties, of which the beginnings I mostly remember (the rest of my memory had to be compensated by the memory stick of the camera), and unforgettable trips I have to say big thank you to Tamara, Francesca, Yohan, Petr, Olavio, Issam, Anka, Amandine, Przemek, Alberto and many more. In the end, thanks to all the members of the SMG group for making my stay in Eindhoven worth remembering.

Na kraju moram da kažem da ipak najviše dugujem mojoj porodici, mojoj mami i tati koji su mi i pored svih teškoca ukazali na važnost i prednosti obrazovanja i pružili mi priliku da odem na studije, što su na sve načine pokušali da me zaštite i ne opterećuju svim problemima koje su imali tokom godina mojih studija. Čini mi se da bi bez njih i njihove pomoći ipak sav moj trud bio uzaludan. Želim da se zahvalim i mojoj bakici, nesumnjivo najboljoj baki na svetu, za njen stalni optimizam i sve reci ljubavi i podrške. Moram da se zahvalim i mojoj sestri koja svojim vedrim duhom uvek uspe da me nasmeje, na svim dovitljivim SMS porukama o najnovijim dešavanjima u Somboru i naravno na svim pafremima, djindjuvama i poklončićima koje je zahtevala.